AD_____

Award Number: W81XWH-11-1-0236

TITLE: Genome-wide analysis of translational control in tuberous sclerosis complex

PRINCIPAL INVESTIGATOR: Shu-Bing Qian

CONTRACTING ORGANIZATION: Cornell University
Ithaca, NY 14850

REPORT DATE: July 2013

TYPE OF REPORT: Final

PREPARED FOR: U.S. Army Medical Research and Materiel Command
Fort Detrick, Maryland 21702-5012

DISTRIBUTION STATEMENT: Approved for Public Release;
Distribution Unlimited

REPORT DOCUMENTATION PAGE

Form Approved
OMB No. 0704-0188

1. REPORT DATE	2. REPORT TYPE	3. DATES COVERED
July 2013	Final	1 July 2011 - 30 June 2013

4. TITLE AND SUBTITLE
Genome-Wide Analysis of Translational Control in Tuberous Sclerosis Complex

5a. CONTRACT NUMBER

5b. GRANT NUMBER
W81XWH-11-1-0236

5c. PROGRAM ELEMENT NUMBER

6. AUTHOR(S)
Shu-Bing Qian

E-Mail: sq38@cornell.edu

5d. PROJECT NUMBER

5e. TASK NUMBER

5f. WORK UNIT NUMBER

7. PERFORMING ORGANIZATION NAME(S) AND ADDRESS(ES)

Cornell University
Ithaca, NY 14853

8. PERFORMING ORGANIZATION REPORT NUMBER

9. SPONSORING / MONITORING AGENCY NAME(S) AND ADDRESS(ES)
U.S. Army Medical Research and Materiel Command
Fort Detrick, Maryland 21702-5012

10. SPONSOR/MONITOR'S ACRONYM(S)

11. SPONSOR/MONITOR'S REPORT NUMBER(S)

12. DISTRIBUTION / AVAILABILITY STATEMENT
Approved for Public Release; Distribution Unlimited

13. SUPPLEMENTARY NOTES

14. ABSTRACT

The TSC1/TSC2 complex integrates multiple cues to regulate protein translation and cell growth via mammalian target of rapamycin complex I (mTORC1). Loss of TSC functions leads to constitutive activation of mTORC1 and uncontrolled mRNA translation. The goal of this research project to elucidate cis-regulatory elements and trans-acting factors in TSC-mTORC1-mediated translational regulation. We have discovered that the stress-induced preferential translation of Hsp70 mRNA is deficient in cells lacking TSC2. This finding provides a plausible mechanism about how persistent mTOR signaling favors the development of various pathologies of TSC by attenuating stress resistance. We recently discovered that TSC-mTORC1 increased the yield of protein synthesis at the expense of protein quality. By harnessing the power of ribosome profiling, we also discovered post-initiation ribosomal pausing that is subject to TSC-mTORC1 regulation. In addition, we have established a novel approach called Global Translation Initiation sequencing (GTI-seq) to investigate alternative translation. These studies are significant because TSC-mTORC1-controlled alternative translation initiation has never been defined.

15. SUBJECT TERMS
Translation; ribosome; protein homeostasis; high throughput; genome-wide

16. SECURITY CLASSIFICATION OF:			17. LIMITATION OF ABSTRACT	18. NUMBER OF PAGES	19a. NAME OF RESPONSIBLE PERSON
a. REPORT	b. ABSTRACT	c. THIS PAGE			USAMRMC
U	U	U	UU	45	19b. TELEPHONE NUMBER *(include area code)*

TABLE OF CONTENTS

INTRODUCTION

Tuberous sclerosis complex (TSC) is an autosomal dominant disease characterized by benign tumors in various tissues. The genes mutated in this disease, TSC1 and TSC2, encode tumor suppressors that are associated in a complex. The TSC1/2 complex, through its Rheb-GAP activity, is a critical negative regulator of mTORC1 under physiological conditions. Activation of mTORC1 positively stimulates cap-dependent mRNA translation via its downstream substrates S6K and 4E-BP. In our previous study, we demonstrated that TSC-mTORC1 signaling regulates the balance between cap-dependent and cap-independent translation. In this project, we aim to elucidate *cis*-regulatory elements and *trans*-acting factors in TSC-mTOR pathway-mediated translational regulation.

BODY

Task 1. Define TSC-mediated translational regulation using genome-wide ribosome profiling

1a. Elucidate the ribosome dynamics in response to TSC-mTOR pathway

- *Determine the pattern of ribosome pausing in TSC2 KO cells* A reliable measure of the translation of cellular mRNA is the degree of its association with ribosomes. Actively translated mRNAs are typically bound by several ribosomes (polysome) and can be separated from individual 40S and 60S ribosomal subunits and 80S monosomes by centrifugation through a linear sucrose gradient. Ribosome profiling, based on deep sequencing of ribosome-protected mRNA fragments (RPF), has proven to be powerful in defining ribosome positions on the entire transcriptome [1, 2]. To investigate the ribosome dynamics during mRNA translation, we have established a modified ribosome profiling technique (Ribo-seq) adapted from the previously published protocol. Direct comparison of RPFs from both monosome and polysome fractions afforded us an opportunity to dissect the transition between initiation and elongation.

1b. Determine the selection of translation initiation sites in response to TSC-mTOR pathway

- *Established the global mapping of translation initiation sites* A recent study used an initiation-specific translation inhibitor harringtonine to deplete elongating ribosomes from mRNAs, thereby halting ribosomes at the initiation codons [9]. This approach uncovered an unexpected abundance of alternative TIS codons, in particular non-AUG codons in the 5'UTR. However, these data was "noisy" and required a machine-learning algorithm to identify TIS codons. We develop global translation initiation sequencing (GTI-seq) by utilizing two related but distinct translation inhibitors to effectively differentiate ribosome initiation from elongation. While cycloheximide (CHX) freezes all translating ribosomes, the translation inhibitor lactimidomycin (LTM) preferentially acts on the initiating ribosome but not the elongating ribosome (**Fig. 1**). LTM bears several advantages over harringtonine in achieving the high resolution mapping of global TIS positions. First, LTM binds to the 80S ribosome already assembled at the initiation codon and permits the first peptide bond formation [10]. Thus, the LTM-associated RPF more likely represents physiological TIS positions. Second, LTM occupies the empty E-site of initiating ribosomes and thus completely blocks the translocation. This feature allows the TIS identification at single nucleotide resolution. Third, owing to the similar structure and the same binding site in the ribosome [10], LTM and CHX can be applied side-by-side to achieve simultaneous assessment of both initiation and elongation for the same transcript. With the high signal/noise ratio, GTI-seq offers a direct TIS identification approach with a minimal computational aid.

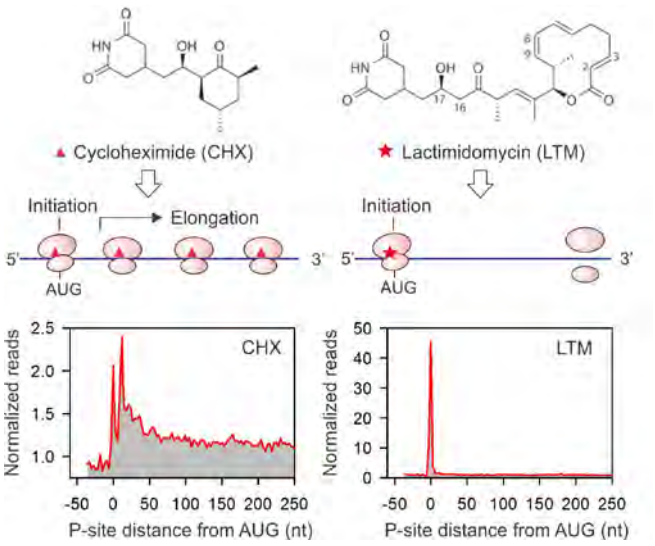

Fig. 1. Experimental Strategy of GTI-seq Using Ribosome E-site Translation Inhibitors
Pretreatment of HEK293 cells with either 100 µM CHX, or 50 µM LTM resulted in different patterns of RPFs as revealed by metagene analysis. CHX-associated RPFs are mainly located in the body of coding region. Remarkably, LTM-associated RPFs are enriched at the annotated start codon.

- *Characterize alternative translation* From 4,000 transcripts with detectable TIS peaks, we identified a total of 16,231 TIS sites. Codon composition analysis revealed that more than half of the TIS codons used AUG as the translation initiator. GTI-seq also identified a significant proportion of TIS codons employing near-cognate codons that differ from AUG by a single nucleotide, in particular CUG (16%). Remarkably, nearly half of the transcripts (42%) contained multiple TIS sites, suggesting that alternative translation prevails even under physiological conditions. In addition to validating initiation at the annotated start codon (aTIS), GTI-seq revealed 39% of the transcripts containing downstream initiation sites (dTIS) and 54% of transcripts bearing upstream TIS positions (uTIS). While dTIS codons use the conventional AUG as the main initiator, a significant fraction of uTIS codons are non-AUG with the CUG as the most frequent one. We experimentally validated different translational products initiated from alternative start codons, including non-AUG (data not shown).

Task 2. Define the impacts of TSC-mTOR pathway in protein quality and quantity control

2a. Determine how TSC-mTOR pathway the quality of newly synthesized proteins

To investigate how nutrient signaling affects the folding of nascent chains, we used firefly luciferase (Luc) as a reporter because of its high chaperone dependency and stress sensitivity [11, 12]. Cells lacking tuberous sclerosis complex 2 (TSC2) exhibit constitutively active mTORC1 signaling [13, 14]. In spite of the increased protein synthesis, we observed a much lower Luc activity in TSC2 KO cells than in wild type cells (**Fig. 2A**). Proteasome inhibition by MG132 treatment caused a significant accumulation of Luc (**Fig. 2B**), indicating the reduced stability of Luc in cells with hyperactive mTORC1 signaling. Remarkably, reducing mTORC1 signaling by specific inhibitor rapamycin was able to rescue the steady-state levels of Luc (**Fig. 2B**). The reduced protein quality in TSC2 KO cells was not limited to Luc. A significant amount of polyubiquitinated species were also accumulated in these cells after proteasome inhibition as compared to the wild type cells (**Fig. 2C**). These results strongly suggest that hyperactive mTORC1 signaling increases the yield of protein synthesis at the expense of folding quality.

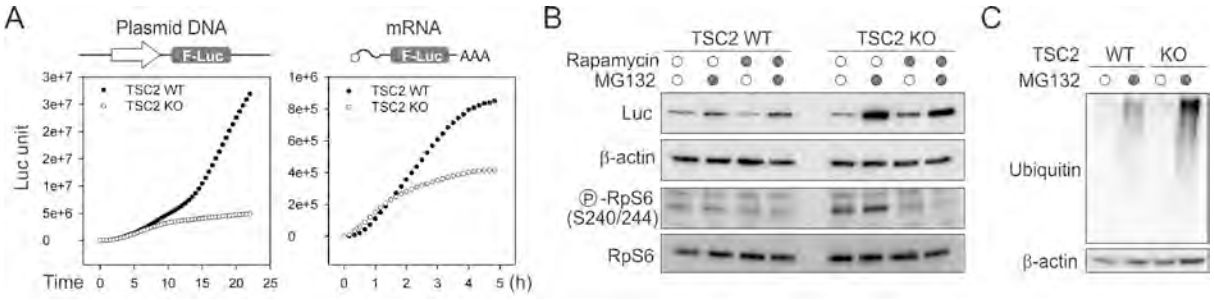

Fig 2. Hyperactive mTORC1 signaling reduces the quality of newly synthesized proteins. **(A)** TSC2 WT and TSC2 KO cells were transfected with either Luc plasmid or mRNA. Real time Luc activity was recorded immediately after transfection. **(B)** Luc-transfected TSC2 WT and TSC2 KO cells were treated with MG132 or DMSO followed by immunoblotting analysis using antibodies indicated. **(C)** Whole cell lysates of TSC2 WT and TSC2 KO cells were immunoblotted to detect ubiquin-conjugated species.

2b. Determine how TSC-mTOR pathway affects translation fidelity

Translation fidelity can be thought of a competition between the cognate and near-cognate tRNAs for a given codon. It is conceivable that the increased translation speed under hyperactive mTORC1 signaling generates more error proteins via misreading of genetic codons. We analyzed two different aspects of translation fidelity: nonsense suppression and aa-tRNA selection. To evaluate nonsense suppression we constructed a pGL3-Luc vector with a stop codon at the coding region of Luc (**Fig. 3**). To evaluate the aa-tRNA selection we made a vector in which the AGA codon of Luc at aa218 was mutated to the near-cognate AGC codon. The R218 residue is a critical amino acid for Luc activity and this mutation potently reduces the luciferase activity. Measuring the Luc activity level of R218A mutant allows us to evaluate the rate of amino acid misincorporation at this position [15]. As expected, both Fluc(Stop) and Fluc(R218A) mutants showed less than 1% of enzymatic activities of the wild type Fluc. Despite such low expression levels, TSC2 KO cells showed an increase in Fluc activity for both Fluc(Stop) and Fluc(R218A) when compared to the wild type cells (2 fold and 1.5 fold increase, respectively) (**Fig. 3**). These results suggest that the ribosomes in cells with hyperactive mTORC1 signaling have a higher rate of altered aa-tRNA selection.

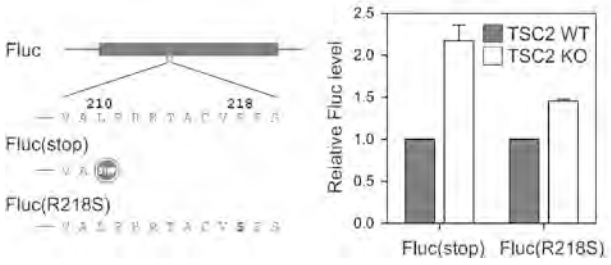

Fig 3. TSC2 WT (left panel) and KO cells (right panel) were transfected with plasmids encoding Fluc mutants as in (C). After 24 hr of transfection, cells were treated with 20nM rapamycin for 15 hr followed by measurement of Fluc activities. Relative Fluc activities were normalized using wild type Fluc (mean ± SEM; n=2).

KEY RESEARCH ACCOMPLISHMENTS

- Genome-wide ribosome profiling reveals regulated post-initiation pausing
- Role of TOP sequence in post-initiation pausing
- Global mapping of alternative translation initiation using GTI-Seq
- GTI-seq reveals prevailing alternative translation
- TSC-mTORC1 increases the yield of protein synthesis at the expense of protein quality
- TSC-mTORC1 controls translational fidelity

REPORTABLE OUTCOMES

Publications:

1. Han Y, David A, Liu B, Magadan JG, Bennink JR, Yewdell JW, and **Qian SB**. Monitoring co-translational protein folding in mammalian cells at codon resolution. *Proc Natl Acad Sci USA* 2012; 109(31):12467-72. PMID: 22802618
2. Lee S, Liu B, Lee S, Huang S, Shen B, and **Qian SB**. Global mapping of translation initiation sites in mammalian cells at single-nucleotide resolution. *Proc Natl Acad Sci USA* 2012; 109(37):E2424-32. PMID: 22927429
3. Liu B, Han Y, and **Qian SB**. Co-translational response to proteotoxic stress by elongation pausing of ribosomes. *Mol Cell* 2013; 49(3):453-463. PMID: 23290916
4. Conn CS, and **Qian SB**. mTORC1 in protein homeostasis: increase in protein quantity at the expense of quality. *Sci Signal 2013*; 6(271):ra24. PMID: 23592839

Manuscript:

1. Han Y, Gao X, Liu B, Wan J, Zhang X, and **Qian SB**. Translational pausing governed by the ribosomal exit tunnel prevents abortive translation. (in submission)
2. Zhang X, Gao X, Roots RA, Conn CS, Liu B, and **Qian SB**. Selective translation of stress proteins requires cytoplasmic function of mitochondrial ribosomal protein L18. (in submission)

Meeting Presentations:

1. Invited speaker, *Nutrient signaling in protein homeostasis: increase in protein quantity at the expense of quality.* **Gordon Research Conference**: Biology of Aging. Lucca, Italy, August, 2013
2. Selected speaker, *Linking Nutrient signaling and protein homeostasis in Growth and Aging.* **EMF Colloquium on the Biology of Aging**. Woods Hole, MA, August, 2013
3. Selected speaker, *Discovering Stress Ribosome in Mammalian Cells.* **Gordon Research Conference**: Stress Proteins in Growth, Development $ Disease. West Dover, VT, July, 2013
4. Selected speaker, *Deciphering translational re-programming using high-resolution ribosome profiling.* **Cold Spring Harbor Laboratory Meeting**: Translational Control. Cold Spring Harbor, NY, September, 2012
5. Invited speaker, *Co-translational response to proteotoxic stress by early ribosome pausing.* **2011 ASCB Annual Meeting**, Denver, CO. December, 2011
6. Selected speaker, *Co-translational response to proteotoxic stress by chaperone-controlled ribosome dynamics.* **Cold Spring Harbor Laboratory Asia Meeting**: Protein Homeostasis in Health and Diseases. Suzhou, China, September, 2011
7. Selected speaker, *Co-translational response to proteotoxic stress by chaperone-controlled ribosome dynamics.* **Gordon Research Conference**: Stress Proteins in Growth, Development and Diseases. Lucca, Italy, July, 2011

Funding Applied:

NIH R01 (AG042400-01A1)
Role: PI (1.2 calendar months) direct costs (5 years) = $ 1,025,000
Title: Linking Nutrient Signaling and Protein Homeostasis in Mammalian Aging

CONCLUSIONS

The observations described in this study have several implications. First, the critical role of TSC in ribosome dynamics and translation quality extends the molecular linkage between mTORC1 and protein homeostasis. Second, we find distinct roles for mTORC1 downstream targets in maintaining protein homeostasis. Loss of S6 kinases, but not 4E-BP family proteins, diminishes the effects of rapamycin on the quality of translational products. Third, the finding that an increase in protein synthesis is accompanied by a decrease in protein quality provides a plausible mechanism for how persistent mTORC1 signaling favors the development of age-related pathologies. With the most common feature of aging being an accumulation of misfolded proteins derived from erroneous biosynthesis and post-synthetic modification, protein homeostasis is an important mediator of rapamycin in longevity.

So this study expands our knowledge about the role of TSC-mTOR signaling in translational control of gene expression. The distinct roles for mTORC1 downstream targets in maintaining protein homeostasis reveal a mechanistic connection between mTORC1 and protein homeostasis.

REFERENCES

1. Ingolia NT, Ghaemmaghami S, Newman JR, & Weissman JS (2009) Genome-wide analysis in vivo of translation with nucleotide resolution using ribosome profiling. *Science* 324(5924):218-223.
2. Guo H, Ingolia NT, Weissman JS, & Bartel DP (2010) Mammalian microRNAs predominantly act to decrease target mRNA levels. *Nature* 466(7308):835-840.
3. Wolin SL & Walter P (1989) Signal recognition particle mediates a transient elongation arrest of preprolactin in reticulocyte lysate. *J Cell Biol* 109(6 Pt 1):2617-2622.
4. Gray NK & Hentze MW (1994) Regulation of protein synthesis by mRNA structure. *Mol Biol Rep* 19(3):195-200.
5. Cannarozzi G, Schraudolph NN, Faty M, von Rohr P, Friberg MT, Roth AC, Gonnet P, Gonnet G, & Barral Y (2010) A role for codon order in translation dynamics. *Cell* 141(2):355-367.
6. Lavner Y & Kotlar D (2005) Codon bias as a factor in regulating expression via translation rate in the human genome. *Gene* 345(1):127-138.
7. Meyuhas O (2000) Synthesis of the translational apparatus is regulated at the translational level. *Eur J Biochem* 267(21):6321-6330.
8. Hamilton TL, Stoneley M, Spriggs KA, & Bushell M (2006) TOPs and their regulation. *Biochem Soc Trans* 34(Pt 1):12-16.
9. Ingolia NT, Lareau LF, & Weissman JS (2011) Ribosome profiling of mouse embryonic stem cells reveals the complexity and dynamics of mammalian proteomes. *Cell* 147(4):789-802.
10. Schneider-Poetsch T, Ju J, Eyler DE, Dang Y, Bhat S, Merrick WC, Green R, Shen B, & Liu JO (2010) Inhibition of eukaryotic translation elongation by cycloheximide and lactimidomycin. *Nat Chem Biol* 6(3):209-217.
11. Frydman J, Erdjument-Bromage H, Tempst P, & Hartl FU (1999) Co-translational domain folding as the structural basis for the rapid de novo folding of firefly luciferase. *Nat Struct Biol* 6(7):697-705.
12. Gupta R, Kasturi P, Bracher A, Loew C, Zheng M, Villella A, Garza D, Hartl FU, & Raychaudhuri S (2011) Firefly luciferase mutants as sensors of proteome stress. *Nat Methods* 8(10):879-884.
13. Kwiatkowski DJ & Manning BD (2005) Tuberous sclerosis: a GAP at the crossroads of multiple signaling pathways. *Hum Mol Genet* 14 Spec No. 2:R251-258.
14. Huang J & Manning BD (2008) The TSC1-TSC2 complex: a molecular switchboard controlling cell growth. *Biochem J* 412(2):179-190.
15. Rakwalska M & Rospert S (2004) The ribosome-bound chaperones RAC and Ssb1/2p are required for accurate translation in Saccharomyces cerevisiae. *Mol Cell Biol* 24(20):9186-9197.

Monitoring cotranslational protein folding in mammalian cells at codon resolution

Yan Han[a], Alexandre David[b], Botao Liu[c], Javier G. Magadán[b], Jack R. Bennink[b], Jonathan W. Yewdell[b], and Shu-Bing Qian[a,c,1]

[a]Division of Nutritional Sciences, Cornell University, Ithaca, NY 14853; [b]Laboratory of Viral Diseases, National Institute of Allergy and Infectious Diseases, National Institutes of Health, Bethesda, MD 20892; and [c]Graduate Field of Genetics and Development, Cornell University, Ithaca, NY 14853

Edited by Arthur L. Horwich, Yale University School of Medicine, New Haven, CT, and approved June 20, 2012 (received for review May 14, 2012)

How the ribosome-bound nascent chain folds to assume its functional tertiary structure remains a central puzzle in biology. In contrast to refolding of a denatured protein, cotranslational folding is complicated by the vectorial nature of nascent chains, the frequent ribosome pausing, and the cellular crowdedness. Here, we present a strategy called folding-associated cotranslational sequencing that enables monitoring of the folding competency of nascent chains during elongation at codon resolution. By using an engineered multidomain fusion protein, we demonstrate an efficient cotranslational folding immediately after the emergence of the full domain sequence. We also apply folding-associated cotranslational sequencing to track cotranslational folding of hemagglutinin in influenza A virus-infected cells. In contrast to sequential formation of distinct epitopes, the receptor binding domain of hemagglutinin follows a global folding route by displaying two epitopes simultaneously when the full sequence is available. Our results provide direct evidence of domain-wise global folding that occurs cotranslationally in mammalian cells.

deep sequencing | ribosome profiling | protein quality

It is currently believed that protein folding generally begins during translation on the ribosome (1, 2). In mammalian cells, the rate of protein synthesis is approximately five residues per second, whereas folding is typically occurring on the microsecond scale (3, 4). Thus, many details of cotranslational folding pathway remain elusive. For example, what types of the structures and/or intermediates are formed in the nascent chain during cotranslational folding? How early in translation are these structures formed? In contrast to the in vitro refolding of full-length polypeptides, the cotranslational folding of emerging polypeptides is influenced by their sequential exposure from the ribosome exit tunnel to the cytosol (5). Cotranslational folding is further complicated by frequent ribosome pausing (6), as well as interactions with cellular binding partners (7).

Traditional methods of detecting cotranslational folding rely on monitoring of the enzymatic activity of model proteins synthesized in vitro (1, 2). These assays are impractical when applied to cells under physiological conditions. A few in vivo experiments supporting cotranslational folding were based on pulse-chase metabolic labeling coupled with folding-dependent cleavage analysis (8). A limitation of this approach is low resolution. Fluorescence-based techniques, such as FRET, allow detection of cotranslational folding and interactions of nascent chains with high resolution (9). However, FRET measurements require incorporation of modified amino acids and are limited to cell-free systems. None of these methods can be used for simultaneous monitoring of cotranslational folding of nascent chains with varied lengths in vivo. We developed an approach called folding-associated cotranslational sequencing (FactSeq) that overcomes many of these deficiencies. By harnessing the power of the ribosome profiling technique (10), FactSeq allows us to dissect at what point during translation the nascent chain acquires a specific conformation.

Results and Discussion

During translation elongation, the positions of ribosomes on a given mRNA, and hence the length of the synthesized polypeptide chain, can be determined by deep sequencing of the ribosome-protected mRNA fragments (RPFs) (10, 11). FactSeq is based on enriching ribosomes bearing nascent chains with recognizable structural features, followed by sequencing of the associated RPFs. Direct comparison of RPF distribution before and after ribosome enrichment provides sequence-specific structural information associated with the nascent chain. To pilot this technique, we generated a HEK293 cell line stably expressing the multidomain fusion protein Flag-FRB-GFP, in which the well-characterized FKBP12-rapamycin binding domain (FRB) was fused to the NH_2 terminus of GFP (Fig. 1). After collecting the ribosome fractions from the whole-cell lysates by using sucrose gradient sedimentation, we converted polysomes to single ribosomes by RNase I treatment to digest mRNAs not protected by the ribosome. We first enriched ribosomes bearing the NH_2-terminal Flag-tagged nascent chain by immunoprecipitation (IP) using anti-Flag mAb-coated beads. After extracting Flag tag-associated RPFs as well as total RPFs from the same sample, we constructed a cDNA library suitable for Illumina high-throughput sequencing (Fig. 1).

The sequencing results of RPFs obtained with or without Flag IP were of similar quality (Fig. S1). As expected, the majority of RPFs were approximately 30 nt in length. The 5′ end positions of RPF showed a strong 3-nt periodicity, confirming that the RPF accurately captures the ribosome movement along mRNAs. By using RPFs derived from the entire transcriptome, we built a ribosome density map on the Flag-FRB-GFP transcript (Fig. 2*A*). Consistent with the nonuniform rates of translation elongation, the transcript was punctuated with multiple ribosome pausing sites with a skewed number of reads located at the start codon region. Notably, the linker region between FRB and GFP showed the least RPF reads, possibly because of our selection of commonly used codons in creating the construct. Over four independent RPF deep-sequencing replicates, the ribosome distribution pattern on individual transcripts was highly reproducible (Fig. S2).

As the NH_2-terminal Flag tag is present at the start of the nascent chain, the Flag mAb-associated RPFs should capture nearly all the ribosome footprints during elongation. Alignment of RPF reads on Flag-FRB-GFP transcript before and after Flag IP revealed a nearly identical pattern of ribosome density except the first 50 codon region (Fig. 2*A*, *Lower*). As ~40 aa of the

Author contributions: Y.H. and S.-B.Q. designed research; Y.H., A.D., B.L., J.G.M., and S.-B.Q. performed research; J.R.B. and J.W.Y. contributed new reagents/analytic tools; Y.H., B.L., J.W.Y., and S.-B.Q. analyzed data; and S.-B.Q. wrote the paper.

The authors declare no conflict of interest.

This article is a PNAS Direct Submission.

Freely available online through the PNAS open access option.

[1]To whom correspondence should be addressed. E-mail: sq38@cornell.edu.

This article contains supporting information online at www.pnas.org/lookup/suppl/doi:10.1073/pnas.1208138109/-/DCSupplemental.

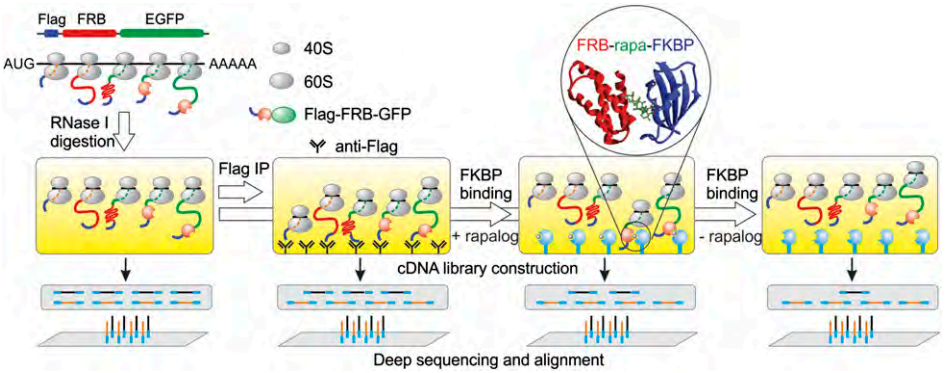

Fig. 1. Schematic for FactSeq approach. The polysomes from HEK293/Flag-FRB-GFP are converted into monosome by RNase I treatment, followed by IP using anti-Flag or recombinant FKBP in the presence or absence of rapalog. The RPFs are extracted and mixed with spike-in control before cDNA library construction. The deep sequencing results of RPFs are analyzed by transcriptome mapping. (*Inset*) Circle depicts structure of FKBP (blue, PDB 1A7X) and FRB (red, PDB 1AUE) dimerization in the presence of rapamycin (green).

growing polypeptide chain are buried within the ribosome exit tunnel, this corresponds well to the minimal length of 10 aa required for antibody binding (i.e., the full length of Flag tag). Notably, there was little reduction of Flag IP-associated RPF reads relative to total RPFs along the remaining part of the transcript, indicating that the Flag tag remains intact during the synthesis of Flag-FRB-GFP. This argues that cotranslational degradation is minimal in this multidomain fusion protein. Thus, the FactSeq approach allows tracking of the behavior of nascent chains with high accuracy and sensitivity.

We next extended the FactSeq approach to evaluate cotranslational folding of the FRB domain before the complete synthesis of GFP. To probe the folding status of FRB domain, we took advantage of its binding partner FKBP (FK506 binding protein). The dimerization of FKBP and FRB relies on their 3D structures and the presence of rapamycin or rapalog (12, 13) (Fig. 1). As expected, recombinant FKBP synthesized in *Escherichia coli* specifically pull down the Flag-FRB-GFP fusion protein in a rapalog-dependent manner (Fig. S3). Thus, FKBP-rapalog can be used as a bait to probe the folding status of FRB before the full-length fusion protein is released from the ribosome. Consistent with the high specificity of rapalog-mediated FRB–FKBP interaction, very few RPF reads were recovered in the absence of rapalog (Fig. 2*B*). By contrast, adding rapalog selectively restored a significant number of RPFs starting at the 150 codon position of the Flag-FRB-GFP transcript. Given 10 aa from the Flag tag and 40 aa buried in the ribosome tunnel, the appearance of RPF reads after 150 codon position corresponds to the minimal length of 100 aa at which the FRB domain starts to create the rapalog binding site and associate with FKBP. Thus, FRB domain is able to fold when the corresponding amino acid sequence immediately emerges from the ribosome.

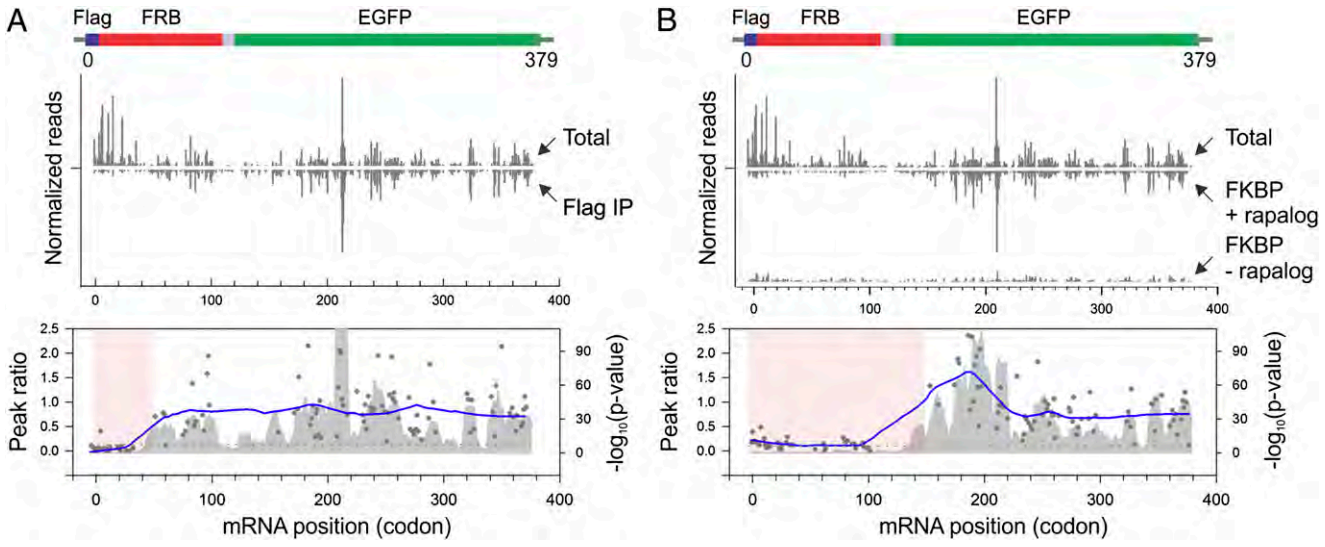

Fig. 2. Monitoring cotranslational behavior of Flag-FRB-GFP polypeptide in mammalian cells. (*A*) Comparison of RPF distribution on Flag-FRB-GFP transcript before and after anti-Flag IP. Both the total and Flag IP-associated RPFs are aligned based on the sequence position of Flag-FRB-GFP. *Lower*: Pattern analysis using single codon peak ratio (dot plot) and significance (*P* value) of RPF density vs. background in a 10-codon sliding window (field plot). The line plot represents the LOESS-smoothed trend line for single codon peak ratio (sampling proportion, 0.2). The colored areas represent regions of nascent chains that inaccessible to anti-Flag antibody. Cutoff line was set at $P = 0.001$ (green dashed line). (*B*) Comparison of RPF distribution on Flag-FRB-GFP transcript before and after FKBP affinity purification. (*Upper*) Alignment of RPFs associated with total and FKBP binding in the presence or absence of rapalog. *Lower*: Pattern analysis using single codon peak ratio (dot plot) and significance (*P* value) of RPF density vs. background in a 10-codon sliding window (field plot). The line plot represents the LOESS-smoothed trend line for single codon peak ratio (sampling proportion, 0.2). The colored areas represent regions of nascent chains inaccessible to FKBP. Cutoff line was set at $P = 0.001$ (green dashed line).

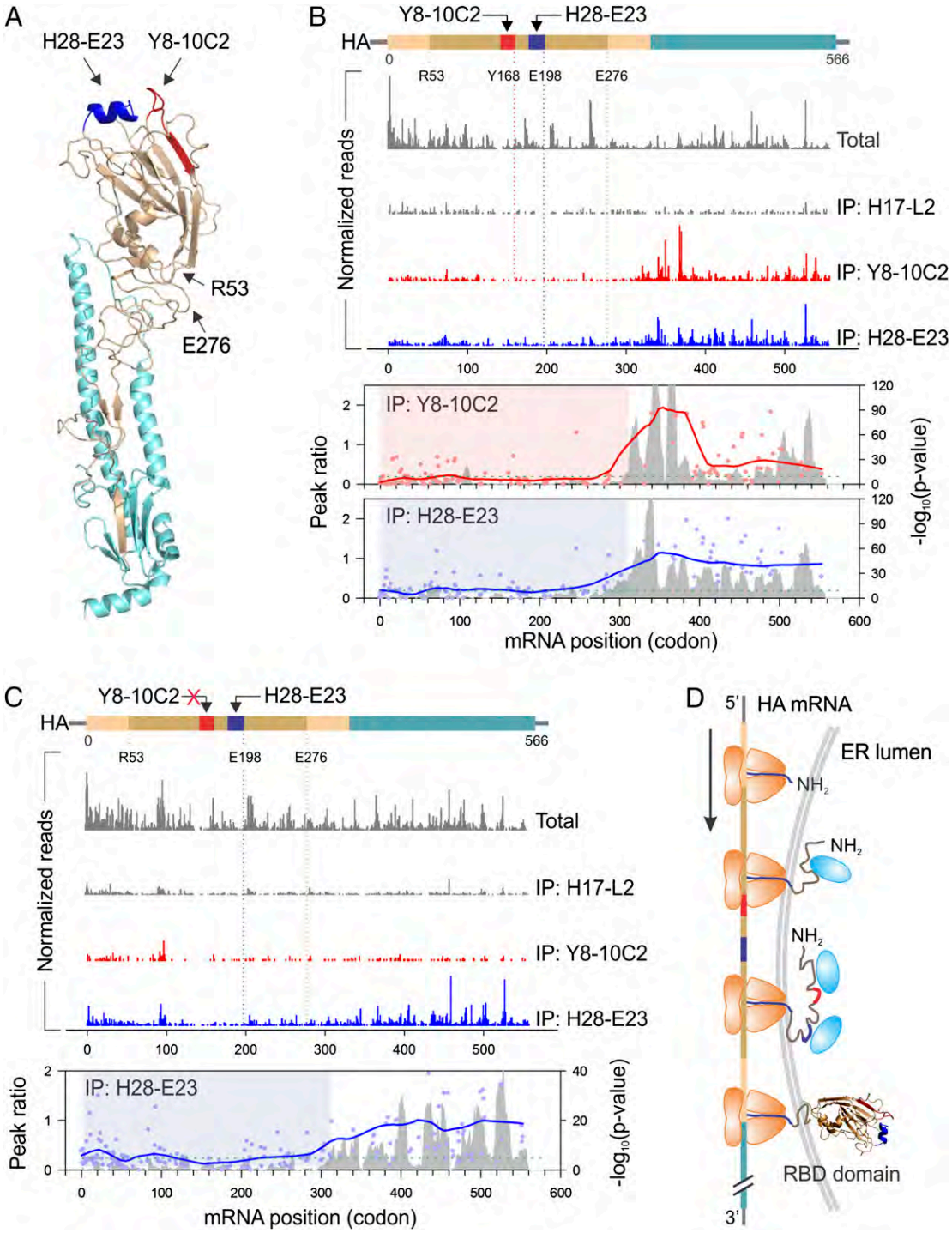

Fig. 3. Monitoring cotranslational folding of HA in influenza A-infected cells. (*A*) Epitope sites on the RBD domain of HA. The structure of monomeric HA is shown as a ball-and-stick model with HA1 in light brown and HA2 in light blue (PDB 1RU7). The Sa site recognized by Y8-10C2 is shown in red, whereas the Sb site by H28-E23 is dark blue. The RBD domain is identified from R53 to E276. (*B*) Comparison of RPF distribution on HA transcript derived from PR8 H1N1 influenza A before and after IP. Polysome fractions were prepared from influenza A-infected HeLa cells. IP was performed by using a panel of antibodies, followed by deep sequence of RPFs. *Lower*: Pattern analysis after IP with Y8-10C2 (red) and H28-E23 (blue) using single codon peak ratio (dot plot) and significance (*P* value) of RPF density vs. background in a 10-codon sliding window (field plot). The line plot represents the LOESS-smoothed trend line for single codon peak ratio (sampling proportion, 0.2). The colored areas represent regions of nascent chains inaccessible to antibodies. Cutoff line was set at $P = 0.001$ (green dashed line). (*C*) Comparison of RPF distribution on HA transcript derived from CV1 mutant that escapes the Y8-10C2 recognition. (*Lower*) Pattern analysis after IP with H28-E23 (blue) using single codon peak ratio (dot plot) and significance (*P* value) of RPF density vs. background in a 10-codon sliding window (field plot). The line plot represents the LOESS smoothed trend line for single codon peak ratio (sampling proportion, 0.2). Cutoff line was set at $P = 0.001$ (green dashed line). (*D*) A model of domain-wise global folding of the HA nascent chain attached to the ribosome. Rapid cotranslational folding occurs only after the full RBD domain sequence is available. The blue ovals represent possible binding partners of nascent chains, such as molecular chaperones.

Intriguingly, there was a significant reduction of FKBP-associated RPF reads after 200 codon position of the Flag-FRB-GFP transcript relative to total RPFs ($P = 6.256 \times 10^{-5}$; Fig. 2*B*, *Lower*). We cannot attribute this to cotranslational degradation, because the NH_2-terminal Flag tag was continuously present (Fig. 2*A*). Rather, the appearance of GFP polypeptide could partially prevent folded FRB from interacting with FKBP, possibly by associating molecular chaperones or other binding partners (5).

Having successfully monitored the cotranslational folding of FRB domain, we next applied FactSeq to evaluate the cotranslational folding process of influenza A hemagglutinin (HA). Influenza presents a serious public health challenge, and HA is a prime candidate for vaccine design and drug development (14). HA is a type I transmembrane glycoprotein with multiple folding domains. The protein is cotranslationally glycosylated in the endoplasmic reticulum. After posttransaltional trimerization, the HA trimer then traffics to the cell surface. The crystal structure of HA reveals a globular ectodomain sitting atop an extended stalk (Fig. 3*A*). The HA mediates attachment to cells via its receptor binding site in the ectodomain [i.e., receptor-binding domain (RBD)], which also contains most of the epitopes for neutralizing antibody recognition (15). All known neutralizing anti-HA mAbs recognize conformational determinants, i.e., their epitopes are formed by folding of the primary sequences. For instance, the Y8-10C2 mAb recognizes an epitope on the HA comprising residues from E158 to Y168 [Puerto Rico/8/34 (PR8)], whereas the H28-E23 epitope is principally formed by residues from N187 to E198 (16) (Fig. 3*A*). As these mAbs are capable of binding HA monomers based on local folding of their respective domains, we used them to probe cotranslational formation of distinct epitopes during the biosynthesis of HA. As a negative control, we used the H17-L2 mAb, whose binding is dependent on trimerization, as its epitope is formed by residues on each side of the trimer interface (17).

We purified ribosomes 5 h after viral infection of HeLa cells with PR8 (Fig. S4). The ribosome fractions were then immunoprecipitated using each of the mAbs followed by deep sequencing of RPFs. Total RPF reads aligned to the full length of HA transcript exhibited typical pausing sites (Fig. 3*B*). Trimer-specific H17-L2 set the background level of reads. In contrast, both Y8-10C2 and H28-E23 recovered a large number of RPFs over background. Thus, FactSeq could be used to investigate the cotranslational folding of endoplasmic reticulum proteins. Intriguingly, Y8-10C2 exhibited an almost 110-codon delay in the appearance of RPFs relative to the emergence of its epitope ending at residue Y168 from the ribosome exit tunnel (Fig. 3*B*). H28-E23 also had a lag of approximately 70 codons after the residue E198 emerged from the ribosome. Notably, both mAbs initiated simultaneous binding with the emergence of the entire globular RBD domain, which ends at residue E276 (Fig. 3*A*). These results indicate that Y8-10C2 and H28-E23 epitopes are not formed sequentially. Although we could not exclude the possibility of mAb binding-induced nascent chain folding, our previous study suggests that it is unlikely for such an event to contribute to the specific RPFs revealed by FactSeq (15). First, refolding of denatured HA by antibody binding occurs over days, not within 1 h. Second, mAb binding-induced HA folding, if rapid, would lead to continuous enrichment of mAb-associated RPFs along with elongation. However, similar to cotranslational folding of the FRB domain, the HA exhibited reduced accessibility of Y8-10C2 after its initial epitope formation. The discontinuous antibody accessibility to the continuously elongated nascent chain could represent a previously unrecognized feature of cotranslational folding pathway. Thus, the coappearance of distinct epitopes after the full ectodomain is available is consistent with a model of global folding pathway that occurs rapidly when the RBD sequence has emerged from the ribosome (Fig. 3*D*).

To validate the cotranslational folding propensity of HA revealed by FactSeq, we performed [^{35}S]methionine pulse-chase of influenza A virus-infected cells coupled with IP. Pulse-chase was performed at 20 °C to slow down elongation and trimerization of HA polypeptides. Y8-10C2 recovers HA fragments in addition to the full-length polypeptide. In contrast, HA trimer-specific antibody H17-L2 recovers only full-length HA. Y8-10C2–binding fragments completely resolve during the chase into full-length HA, demonstrating a precursor–product relationship and indicative of the ability of HA fragments to generate the Y8-10C2 conformational epitope (Fig. S5*A*). Remarkably, the pattern of HA fragments matches well with that revealed by FactSeq (Fig. S5*B*). For instance, the smallest fragment from each assay was approximately 30 kDa. Despite relatively low resolution, pulse labeling analysis confirms the discontinuous nature of mAb binding during elongation. These data support the conclusion that the high resolution pattern offered by FactSeq represents the true behavior of nascent chain synthesis.

We next asked how mutation of an epitope affects the default folding pathway of the HA globular domain. To this end, we chose a PR8 escape mutant CV1, whose single K165E substitution reduces Y8-10C2 avidity more than 100-fold (18) (Fig. S6). Only background levels of RPF reads were recovered by Y8-10C2 from CV1, providing an important confirmation of the specificity of the FactSeq method (Fig. 3*C*). Interestingly, whereas CV1 maintained the similar codon lag as WT HA in the generation of H28-E23 epitope, the full extent of epitope formation was delayed, indicating that the single K165E substitution alters the kinetics of the cotranslational folding of HA (Fig. 3 *C* and *D*).

Conclusion

It is widely believed that cotranslational folding is a universal feature of newly synthesized polypeptides (1, 2). However, monitoring this dynamic process is challenging, in particular inside mammalian cells. By harnessing the power of the ribosome profiling technique with the folding-sensitive affinity reagents, FactSeq provides a unique view of the folding competency of the nascent chain during its elongation. The acquisition of the functional FRB and the HA RBD immediately after their sequences emerge from the ribosome exit tunnel strongly favors a domain-wise global folding pathway. Despite the limitations of FactSeq in providing real-time kinetics of folding pathway, the snapshot taken by FactSeq consists of continuous frames of ribosomes with varied length of nascent chains. FactSeq also requires folding-sensitive affinity reagents to capture specific folding status of ribosome-attached nascent chains. With the increasing number of available conformation-specific antibodies or binding factors for various gene products (19), FactSeq is readily applicable to endogenous proteins thanks to the high throughput of deep sequencing that covers the entire transcriptome. In addition, taking advantage of the intrabodies that are designed to be expressed intracellularly (20, 21), FactSeq has the potential to capture cotranslational folding in live cells before cell lysis. Beyond cotranslating folding, the prototype of FactSeq can also be applied to other cotranslational events. For instance, by using an NH_2-terminal tag, the same concept can be adapted to investigate cotranslational degradation by comparing the loss, rather than the gain, of RPFs. Finally, FactSeq can also be expanded to study cotranslational chaperone interaction with nascent chains (7, 22). The applicability of FactSeq is not limited to studying cotranslational events. The basic principle can be used to design in vivo folding reporter to investigate cellular factors influencing cotranslational folding. We envision that this

approach will provide novel insights into protein triage decisions under physiological as well as pathological conditions.

Materials and Methods

Cells and Reagents. HEK293 cells stably expressing Flag-FRB-GFP were maintained in DMEM with 10% (vol/vol) FBS. Rapalog AP21967 was provided by Ariad. Anti-Flag and anti-HA antibodies were purchased from Sigma, and protein A/G beads from Santa Cruz. TRIzol reagent was purchased from Invitrogen.

Influenza A Infection. HeLa cells were infected with Influenza A/PR8 strain at a multiplicity of 20 pfu/cell in AIM medium, pH 6.6. After adsorption at 37 °C for 1 h, infected monolayers were overlaid with DMEM containing 7.5% FBS, and incubated for an additional 5 h.

Ribosome Profiling. Sucrose solutions were prepared in polysome gradient buffer [10 mM Hepes, pH 7.4, 100 mM KCl, 5 mM $MgCl_2$, 100 μg/mL cycloheximide, 5 mM DTT, and 20 U/mL SUPERase_In (Ambion)]. Sucrose density gradients [15–45% (wt/vol)] were freshly made in SW41 ultracentrifuge tubes (Fisher) using a BioComp Gradient Master (BioComp) according to the manufacturer's instructions. HEK293/Flag-FRB-GFP cells were plated to four 10-cm dishes before ribosome profiling. Cells were first treated with cycloheximide (100 μg/mL) for 3 min at 37 °C to freeze the translating ribosomes, followed by ice-cold PBS solution wash. Cells were then harvested by ice-cold polysome lysis buffer [10 mM Hepes, pH 7.4, 100 mM KCl, 5 mM $MgCl_2$, 100 μg/mL cycloheximide, 5 mM DTT, 20 U/mL SUPERase_In, and 2% (vol/vol) Triton X-100]. After centrifugation at 4 °C and 10,000 × *g* for 10 min, approximately 650 μL supernatant was loaded onto sucrose gradients, followed by centrifugation for 100 min at 38,000 rpm, 4 °C, in an SW41 rotor. Separated samples were fractionated at 0.375 mL/min by using a fractionation system (Isco) that continually monitored OD_{254} values. Fractions were collected into tubes at 1-min intervals.

Ribosome Purification. To convert the polysome into monosome, *E. coli* RNase I (Ambion) was added into the pooled polysome samples (750 U per 100 A260 units) and incubated at 4 °C for 1 h. Preclearance was conducted by incubating the ribosome samples with 30 μL protein A/G beads coated with 4% BSA for 1 h at room temperature. For IP using mAbs, 30 μL protein A/G beads were first incubated with 5 μg mAbs for 1 h at room temperature followed by blocking with 4% BSA for 1 h. The mAb-coated beads were then incubated with the precleared ribosome samples at 4 °C for 1 h, followed by washing with polysome lysis buffer for three times. For FKBP binding assay, 20 μg recombinant HA-FKBP proteins purified from *E. coli* (BL21) were first immobilized on protein A/G beads using anti-HA antibody. After blocking with 4% BSA for 1 h, the beads were then incubated with the precleared ribosome samples at 4 °C for 1 h in the absence or presence of 1 μM rapalog. After washing with polysome lysis buffer three times, total RNA extraction was performed by using TRIzol reagent.

cDNA Library Construction of Ribosome-Protected mRNA Fragments. Purified RNA samples were first mixed with 1 nM of synthetic 28-nt random RNA (5′-AUGUACACGGAGUCGACCCGCAACGCGA-3′) as the spike-in control. The mixed RNA samples were then dephosphorylated in a 15 μL reaction containing 1× T4 polynucleotide kinase buffer, 10 U SUPERase_In, and 20 U T4 polynucleotide kinase (NEB). Dephosphorylation was carried out for 1 h at 37 °C, and the enzyme was then heat-inactivated for 20 min at 65 °C. Dephosphorylated samples were mixed with 2× Novex TBE-Urea sample buffer (Invitrogen) and loaded on a Novex denaturing 15% polyacrylamide TBE-urea gel (Invitrogen). The gel was stained with SYBR Gold (Invitrogen) to visualize the RNA fragments. Gel bands containing RNA species corresponding to 28 nt were excised and physically disrupted by using centrifugation through the holes of the tube. RNA fragments were dissolved by soaking overnight in gel elution buffer (300 mM NaOAc, pH 5.5, 1 mM EDTA, 0.1 U/mL SUPERase_In). The gel debris was removed using a Spin-X column (Corning) and RNA was purified by using ethanol precipitation.

Purified RNA fragments were resuspended in 10 mM Tris (pH 8) and denatured briefly at 65 °C for 30 s Poly-(A) tailing reaction was performed in a 8 μL with 1 × poly-(A) polymerase buffer, 1 mM ATP, 0.75 U/μL SUPERase_In, and 3 U *E. coli* poly-(A) polymerase (NEB). Tailing was carried out for 45 min at 37 °C. For reverse transcription, the following oligos containing barcodes were synthesized:

MCA02, 5′-pCAGATCGTCGGACTGTAGAACTCTCAAGCAGAAGACGGCATACGATTTTTTTTTTTTTTTTTTTTTTVN-3′; LGT03, 5′-pGTGATCGTCGGACTGTAGAACTCTCAAGCAGAAGACGGCATACGATT TTTTTTTTTTTTTTTTTTVN-3′; YAG04, 5′-pAGGATCGTCGGACTGTAGAACTCTCAAGCAGAAGACGGCATACGATT TTTTTTTTTTTTTTTTTTVN-3′; HTC05, 5′-pTCGATCGTCGGACTGTAGAACTCTCAAGCAGAAGACGGCATACGATT TTTTTTTTTTTTTTTTTTVN-3′.

In brief, the tailed RNA product was mixed with 0.5 mM dNTP and 2.5 mM synthesized primer and incubated at 65 °C for 5 min, followed by incubation on ice for 5 min. The reaction mix was then added with 20 mM Tris (pH 8.4), 50 mM KCl, 5 mM MgCl, 10 mM DTT, 40 U RNaseOUT, and 200 U SuperScript III (Invitrogen). RT reaction was performed according to the manufacturer's instructions. RNA was eliminated from cDNA by adding 1.8 μL 1 M NaOH and incubating at 98 °C for 20 min. The reaction was then neutralized with1.8 μL 1 M HCl. Reverse transcription products were separated on a 10% polyacrylamide TBE-urea gel as described earlier. The extended first-strand product band was expected to be approximately 100 nt, and the corresponding region was excised. The cDNA was recovered by using DNA gel elution buffer (300 mM NaCl, 1 mM EDTA).

First-strand cDNA was circularized in 20 μL of reaction containing 1× CircLigase buffer, 2.5 mM $MnCl_2$, 1 M Betaine, and 100 U CircLigase II (Epicentre). Circularization was performed at 60 °C for 1 h, and the reaction was heat-inactivated at 80 °C for 10 min. Circular single-strand DNA was relinearized with 20 mM Tris-acetate, 50 mM potassium acetate, 10 mM magnesium acetate, 1 mM DTT, and 7.5 U APE 1 (NEB). The reaction was carried out at 37 °C for 1 h. The linearized single-strand DNA was separated on a Novex 10% polyacrylamide TBE-urea gel (Invitrogen) as described earlier. The expected 100-nt product bands were excised and recovered as described earlier.

Deep Sequencing. Single-stranded template was amplified by PCR by using the Phusion High-Fidelity enzyme (NEB) according to the manufacturer's instructions. The oligonucleotide primers qNTI200 (5′-CAAGCAGAAGACGGCATA-3′) and qNTI201 (5′-AATGATACGGCGACCACCG ACAGGTTCAGAGTTCTACAGTCCGACG-3′) were used to create DNA suitable for sequencing, i.e., DNA with Illumina cluster generation sequences on each end and a sequencing primer binding site. The PCR contains 1× HF buffer, 0.2 mM dNTP, 0.5 μM oligonucleotide primers, and 0.5 U Phusion polymerase. PCR was carried out with an initial 30 s denaturation at 98 °C, followed by 12 cycles of 10 s denaturation at 98 °C, 20 s annealing at 60 °C, and 10 s extension at 72 °C. PCR products were separated on a nondenaturing 8% polyacrylamide TBE gel as described earlier. Expected DNA at 120 bp was excised and recovered as described earlier. After quantification by Agilent BioAnalyzer DNA 1000 assay, equal amount of barcoded samples were pooled into one sample. Approximately 3–5 pM mixed DNA samples were used for cluster generation followed by sequencing by using sequencing primer 5′-CGACAGGTTCAGAGTTC TACAGTCCGACGATC-3′ (Illumina Genome Analyzer 2 or HiSeq).

Data Analysis. The deep sequencing data of ribosome footprints was processed and analyzed by using a collection of custom Perl scripts. The barcoded multiplex sequencing output files were separated into individual sample datasets according to the first 2-nt barcodes. Second, the 3′ polyA tails allowing one mismatch were identified and removed. After that, the high-quality reads of length ranging from 25 to 35 nt were retained whereas other reads were excluded from the downstream analysis. The sequences of the longest transcript isoform for each human gene were downloaded from the Ensembl database to construct a human transcriptome reference. In addition, the sequence of HA (NC_002017) from the National Center for Biotechnology Information database and the plasmid sequence of Flag-FRB-GFP were used as the reference. The trimmed reads were aligned to the corresponding reference transcripts by SOAP 2.0, allowing as many as two mismatches, and only unique mapping hits were retained. Last, the 5′ end positions of aligned reads were mapped into the coding frame and the number of reads was counted at each codon ranging from −20 codon 5′ UTR to the stop codon for the downstream analysis.

The reproducibility of the RPF distribution on individual transcripts was evaluated by Pearson correlation. The replicates were clustered by Cluster 3.0, and heat maps were produced by Treeview. To compare the RPF distribution on transcript before and after the affinity purification, the reads in the first 30-codon window were considered as the background because the polypeptides are still buried within the ribosome exit tunnel and cannot be accessed by binding partners. The significance (i.e., *P* value) of the RPF density vs. background within a 10-codon sliding window in the pull-down sample was calculated by Fisher exact test across the transcripts compared with the total sample. The first position at which the *P* value was less than 0.001 was considered as the folding start point. Based on the number of reads after the folding start point, the total and pull-down data were normalized to the same scale. To decrease the counting error, only the positions with reads above the mean reads density in the total sample were treated as comparable sites. Subsequently, the single codon peak ratio was calculated by dividing the normalized reads of pull-down sample to those of total

sample at the same codon. The trend line of the single codon peak ratio was determined by locally estimated scatterplot smoothing (LOESS)by using SigmaPlot 11.0 (Systat).

ACKNOWLEDGMENTS. The authors thank the Cornell University Life Sciences Core Laboratory Center for performing deep sequencing and Dr. Yuxin Mao for help in preparing the hemagglutinin structure shown in Fig. 3*A*. This work was supported by the National Institute of Allergy and Infectious Diseases Division of Intramural Research (A.D., J.R.B., and J.W.Y.), National Institutes of Health Grant 1DP2 OD006449-01 (to S.-B.Q.), Ellison Medical Foundation Grant AG-NS-0605-09 (to S.-B.Q.), and US Department of Defense Exploration-Hypothesis Development Award TS10078 (to S.-B.Q.).

1. Fedorov AN, Baldwin TO (1997) Cotranslational protein folding. *J Biol Chem* 272: 32715–32718.
2. Komar AA (2009) A pause for thought along the co-translational folding pathway. *Trends Biochem Sci* 34:16–24.
3. Ingolia NT, Lareau LF, Weissman JS (2011) Ribosome profiling of mouse embryonic stem cells reveals the complexity and dynamics of mammalian proteomes. *Cell* 147: 789–802.
4. Sosnick TR, Barrick D (2011) The folding of single domain proteins—have we reached a consensus? *Curr Opin Struct Biol* 21:12–24.
5. Kramer G, Boehringer D, Ban N, Bukau B (2009) The ribosome as a platform for co-translational processing, folding and targeting of newly synthesized proteins. *Nat Struct Mol Biol* 16:589–597.
6. Buchan JR, Stansfield I (2007) Halting a cellular production line: Responses to ribosomal pausing during translation. *Biol Cell* 99:475–487.
7. Frydman J (2001) Folding of newly translated proteins in vivo: The role of molecular chaperones. *Annu Rev Biochem* 70:603–647.
8. Nicola AV, Chen W, Helenius A (1999) Co-translational folding of an alphavirus capsid protein in the cytosol of living cells. *Nat Cell Biol* 1:341–345.
9. Johnson AE (2005) The co-translational folding and interactions of nascent protein chains: A new approach using fluorescence resonance energy transfer. *FEBS Lett* 579: 916–920.
10. Ingolia NT, Ghaemmaghami S, Newman JR, Weissman JS (2009) Genome-wide analysis in vivo of translation with nucleotide resolution using ribosome profiling. *Science* 324:218–223.
11. Guo H, Ingolia NT, Weissman JS, Bartel DP (2010) Mammalian microRNAs predominantly act to decrease target mRNA levels. *Nature* 466:835–840.
12. Choi J, Chen J, Schreiber SL, Clardy J (1996) Structure of the FKBP12-rapamycin complex interacting with the binding domain of human FRAP. *Science* 273:239–242.
13. Qian SB, et al. (2009) Engineering a ubiquitin ligase reveals conformational flexibility required for ubiquitin transfer. *J Biol Chem* 284:26797–26802.
14. Skehel JJ, Wiley DC (2000) Receptor binding and membrane fusion in virus entry: the influenza hemagglutinin. *Annu Rev Biochem* 69:531–569.
15. Yewdell JW (2010) Monoclonal antibodies specific for discontinuous epitopes direct refolding of influenza A virus hemagglutinin. *Mol Immunol* 47:1132–1136.
16. Yewdell JW, et al. (1993) Mutations in or near the fusion peptide of the influenza virus hemagglutinin affect an antigenic site in the globular region. *J Virol* 67:933–942.
17. Yewdell JW, Yellen A, Bächi T (1988) Monoclonal antibodies localize events in the folding, assembly, and intracellular transport of the influenza virus hemagglutinin glycoprotein. *Cell* 52:843–852.
18. Gerhard W, Yewdell J, Frankel ME, Webster R (1981) Antigenic structure of influenza virus haemagglutinin defined by hybridoma antibodies. *Nature* 290:713–717.
19. Clark PL, King J (2001) A newly synthesized, ribosome-bound polypeptide chain adopts conformations dissimilar from early in vitro refolding intermediates. *J Biol Chem* 276:25411–25420.
20. Lobato MN, Rabbitts TH (2003) Intracellular antibodies and challenges facing their use as therapeutic agents. *Trends Mol Med* 9:390–396.
21. Stocks MR (2004) Intrabodies: production and promise. *Drug Discov Today* 9:960–966.
22. Oh E, et al. (2011) Selective ribosome profiling reveals the cotranslational chaperone action of trigger factor in vivo. *Cell* 147:1295–1308.

Global mapping of translation initiation sites in mammalian cells at single-nucleotide resolution

Soonchel Lee[a,1,2], Botao Liu[b,1], Soohyun Lee[c,1,3], Sheng-Xiong Huang[d], Ben Shen[d,e], and Shu-Bing Qian[a,b,4]

[a]Division of Nutritional Sciences and [b]Graduate Field of Genetics, Genomics and Development, Cornell University, Ithaca, NY 14853; [c]Proboco Informatics, Ithaca, NY 14850; [d]Department of Chemistry and [e]Department of Molecular Therapeutics, The Scripps Research Institute, Jupiter, FL 33458

Edited* by Jonathan S. Weissman, University of California, San Francisco, CA, and approved July 24, 2012 (received for review May 9, 2012)

Understanding translational control in gene expression relies on precise and comprehensive determination of translation initiation sites (TIS) across the entire transcriptome. The recently developed ribosome-profiling technique enables global translation analysis, providing a wealth of information about both the position and the density of ribosomes on mRNAs. Here we present an approach, global translation initiation sequencing, applying in parallel the ribosome E-site translation inhibitors lactimidomycin and cycloheximide to achieve simultaneous detection of both initiation and elongation events on a genome-wide scale. This approach provides a view of alternative translation initiation in mammalian cells with single-nucleotide resolution. Systemic analysis of TIS positions supports the ribosome linear-scanning mechanism in TIS selection. The alternative TIS positions and the associated ORFs identified by global translation initiation sequencing are conserved between human and mouse cells, implying physiological significance of alternative translation. Our study establishes a practical platform for uncovering the hidden coding potential of the transcriptome and offers a greater understanding of the complexity of translation initiation.

genome wide | high throughput | leaky scanning | start codon

Protein synthesis is the final step in the flow of genetic information and lies at the heart of cellular metabolism. Translation is regulated principally at the initiation stage, and during the last decade significant progress has been made in dissecting the role of initiation factors (eIFs) in the assembly of elongation-competent 80S ribosomes (1–3). However, mechanisms underlying start codon recognition are not fully understood. Proper selection of the translation initiation site (TIS) on mRNAs is crucial for the production of desired protein products. A fundamental and long-sought goal in understanding translational regulation is the precise determination of TIS codons across the entire transcriptome.

In eukaryotes, ribosomal scanning is a well-accepted model for start codon selection (4). During cap-dependent translation initiation, the small ribosome subunit (40S) is recruited to the 5′ end of mRNA (the m^7G cap) in the form of a 43S preinitiation complex (PIC). The PIC is thought to scan along the message in search of the start codon. It is commonly assumed that the first AUG codon that the scanning PIC encounters serves as the start site for translation. However, many factors influence the start codon selection. For instance, the initiator AUG triplet usually is in an optimal context, with a purine at position −3 and a guanine at position +4 (5). The presence of an mRNA secondary structure at or near the TIS position also influences the efficiency of recognition (6). In addition to these *cis* sequence elements, the stringency of TIS selection also is subject to regulation by *trans- acting* factors such as eIF1 and eIF1A (7, 8). Inefficient recognition of an initiator codon results in a portion of 43S PIC continuing to scan and initiating translation at a downstream site, a process known as "leaky scanning" (4). However, little is known about the frequency of leaky scanning events at the transcriptome level.

Many recent studies have uncovered a surprising variety of potential translation start sites upstream of the annotated coding sequence (CDS) (9, 10). It has been estimated that about 50% of mammalian transcripts contain at least one upstream ORF (uORF) (11, 12). Intriguingly, many non-AUG triplets have been reported to act as alternative start codons for initiating uORF translation (13). Because there is no reliable way to predict non-AUG codons as potential initiators from *in silico* sequence analysis, there is an urgent need to develop experimental approaches for genome-wide TIS identification.

Ribosome profiling, based on deep sequencing of ribosome-protected mRNA fragments (RPF), has proven to be powerful in defining ribosome positions on the entire transcriptome (14, 15). However, the standard ribosome profiling is not suitable for identifying TIS. Elevated ribosome density near the beginning of CDS is not sufficient for unambiguous identification of alternative TIS positions, in particular the TIS positions associated with overlapping ORFs. To overcome this problem, a recent study used an initiation-specific translation inhibitor, harringtonine, to deplete elongating ribosomes from mRNAs (16). This approach uncovered an unexpected abundance of alternative TIS codons, in particular non-AUG codons in the 5′ UTR. However, because the inhibitory mechanism of harringtonine on the initiating ribosome is unclear, whether the harringtonine-marked TIS codons truly represent physiological TIS remains to be confirmed.

We developed a technique, global translation initiation sequencing (GTI-seq), that uses two related but distinct translation inhibitors to differentiate ribosome initiation from elongation effectively. GTI-seq has the potential to reveal a comprehensive and unambiguous set of TIS codons at nearly single-nucleotide resolution. The resulting TIS maps provide a remarkable display of alternative translation initiators that vividly delineates the variation in start codon selection. This technique allows a more complete assessment of the underlying principles that specify start codon use in vivo.

Results

Experimental Design. Cycloheximide (CHX) has been widely used in ribosome profiling of eukaryotic cells because of its potency in stabilizing ribosomes on mRNAs. Both biochemical (17) and structural studies (18) revealed that CHX binds to the exit (E)-

Author contributions: Soonchel Lee, B.L., and S.-B.Q. designed research; Soonchel Lee and B.L. performed research; S.-X.H. and B.S. contributed new reagents/analytic tools; Soonchel Lee, Soohyun Lee, and S.-B.Q. analyzed data; and Soohyun Lee and S.-B.Q. wrote the paper.

The authors declare no conflict of interest.

*This Direct Submission article had a prearranged editor.

Freely available online through the PNAS open access option.

Data deposition: The sequences reported in this work have been deposited in the Sequence Read Archive database (accession no. SRA056377).

[1]Soonchel Lee, B.L., and Soohyun Lee contributed equally to this work.

[2]Present address: Cancer Center, Massachusetts General Hospital, Harvard Medical School, Boston, MA 02115.

[3]Present address: Center for Biomedical Informatics, Harvard Medical School, Boston, MA 02115.

[4]To whom correspondence should be addressed. E-mail: sq38@cornell.edu.

See Author Summary on page 14728 (volume 109, number 37).

This article contains supporting information online at www.pnas.org/lookup/suppl/doi:10.1073/pnas.1207846109/-/DCSupplemental.

site of the large ribosomal subunit, close to the position where the 3′ hydroxyl group of the deacylated transfer RNA (tRNA) normally binds. CHX thus prevents the release of deacylated tRNA from the E-site and blocks subsequent ribosomal translocation (Fig. 1*A*, *Left*). Recently, a family of CHX-like natural products isolated from *Streptomyces* was characterized, including lactimidomycin (LTM) (19, 20). Acting as a potent protein synthesis inhibitor, LTM uses a mechanism similar but not identical to that used by CHX (17). With its 12-member macrocycle, LTM is significantly larger in size than CHX (Fig. 1*A*). As a result, LTM cannot bind to the E-site when a deacylated tRNA is present. Only during the initiation step, in which the initiator tRNA enters the peptidyl (P)-site directly (21), is the empty E-site accessible to LTM. Thus, LTM acts preferentially on the initiating ribosome but not on the elongating ribosome. We reasoned that ribosome profiling using LTM in a side-by-side comparison with CHX should allow a complete segregation of the ribosome stalled at the start codon from the one in active elongation (Fig. 1*B*).

We designed an integrated GTI-seq approach and performed the ribosome profiling in HEK293 cells pretreated with either LTM or CHX. Although CHX stabilized the polysomes slightly compared with the no-drug treatment (DMSO), 30 min of LTM treatment led to a large increase in monosomes accompanied by a depletion of polysomes (Fig. S1). This result is in agreement with the notion that LTM halts translation initiation while allowing elongating ribosomes to run off (17). After RNase I digestion of the ribosome fractions, the purified RPFs were subjected to deep sequencing. As expected, CHX treatment resulted in an excess of RPFs at the beginning of ORFs in addition to the body of the CDS (Fig. 1*C*). Remarkably, LTM treatment led to a pronounced single peak located at the −12-nt position relative to the annotated start codon. This position corresponds to the ribosome P-site at the AUG codon when an offset of 12 nt is considered (14, 15). LTM treatment also eliminated the excess of ribosomes seen at the stop codon in untreated cells or in the presence of CHX. Therefore, LTM efficiently stalls the 80S ribosome at the start codons.

During the course of our study, Ingolia et al. (16) reported a similar TIS mapping approach using harringtonine, a different translation initiation inhibitor. One key difference between harringtonine and LTM is that the former drug binds to free 60S subunits (22), whereas LTM binds to the 80S complexes already assembled at the start codon (17). We compared the pattern of RPF density surrounding the annotated start codon in the published datasets (16) and the LTM results (Fig. S2). It appears that a considerable amount of harringtonine-associated RPFs are not located exactly at the annotated start codon. To compare the accuracy of TIS mapping accuracy by LTM and harringtonine directly, we performed ribosome profiling in HEK293 cells treated with harringtonine using the same protocol as in LTM treatment. As in the previous study, harringtonine treatment caused a substantial fraction of RPFs to accumulate in regions downstream of the start codon (Fig. 1*D*). The relaxed positioning of harringtonine-associated RPFs after prolonged treatment leaves uncertainty in TIS mapping. In contrast, GTI-seq using LTM largely overcomes this deficiency and offers high precision in global TIS mapping with single-nucleotide resolution (Fig. 1*D*).

Global TIS Identification by GTI-seq. One of the advantages of GTI-seq is its ability to analyze LTM data in parallel with CHX. Because of the structural similarity between these two translation inhibitors, the LTM background reads resembled the pattern of CHX-associated RPFs (Fig. 2*A*). This feature allows us to reduce the background noise of LTM-associated RPFs further by subtracting the normalized density of CHX reads at every nucleotide position from the density of LTM reads at that position. A TIS peak then is called at a position in which the adjusted LTM reads density is well above the background (red asterisk in Fig. 2*A*; see *Materials and Methods* for details). From ∼10,000 transcripts with

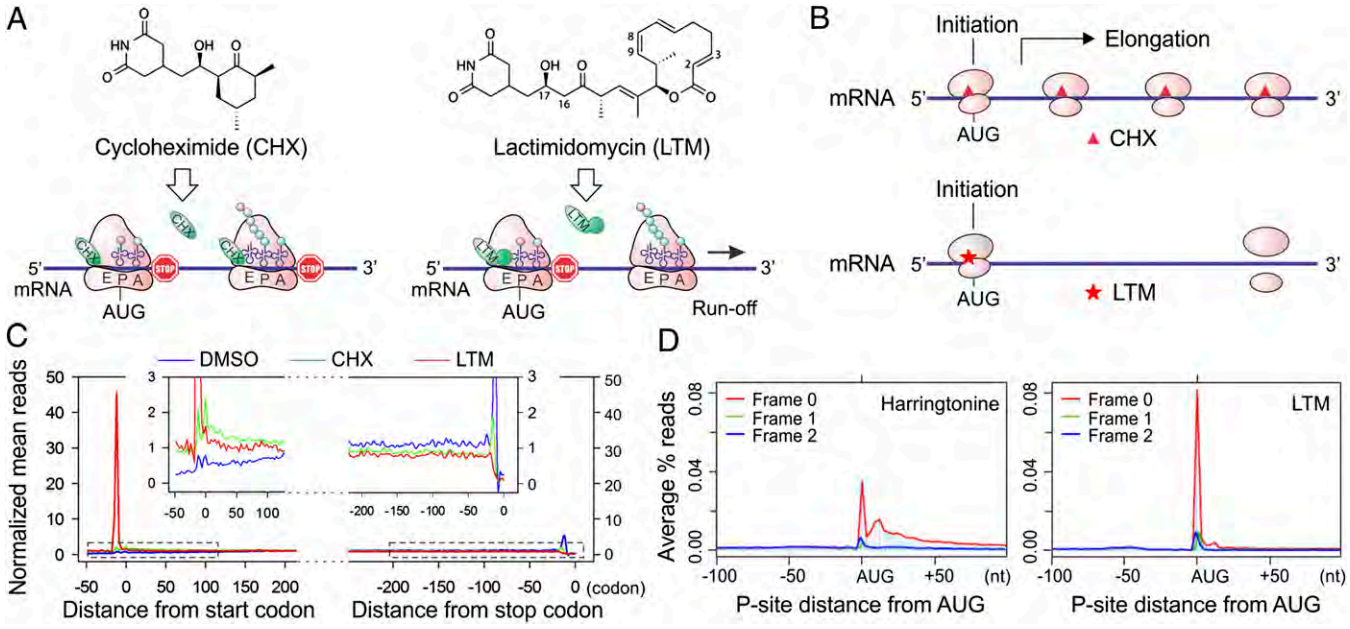

Fig. 1. Experimental strategy of GTI-seq using ribosome E-site translation inhibitors. (*A*) Schematic diagram of the experimental design for GTI-seq. Translation inhibitors CHX and LTM bind to the ribosome E-site, resulting in inhibition of translocation. CHX binds to all translating ribosomes (*Left*), but LTM preferentially incorporates into the initiating ribosomes when the E-site is free of tRNA (*Right*). (*B*) Ribosome profiling using CHX and LTM side by side allows the initiating ribosome to be distinguished from the elongating one. (*C*) HEK293 cells were treated with DMSO, 100 μM CHX, or 50 μM LTM for 30 min before ribosome profiling. Normalized RPF reads are averaged across the entire transcriptome, aligned at either their start site or stop codon from the 5′ end of RPFs. (*D*) Metagene analysis of RPFs obtained from HEK293 cells treated with harringtonine (*Left*) or LTM (*Right*). All mapped reads are aligned at the annotated start codon AUG, and the density of reads at each nucleotide position is averaged using the P-site of RPFs.

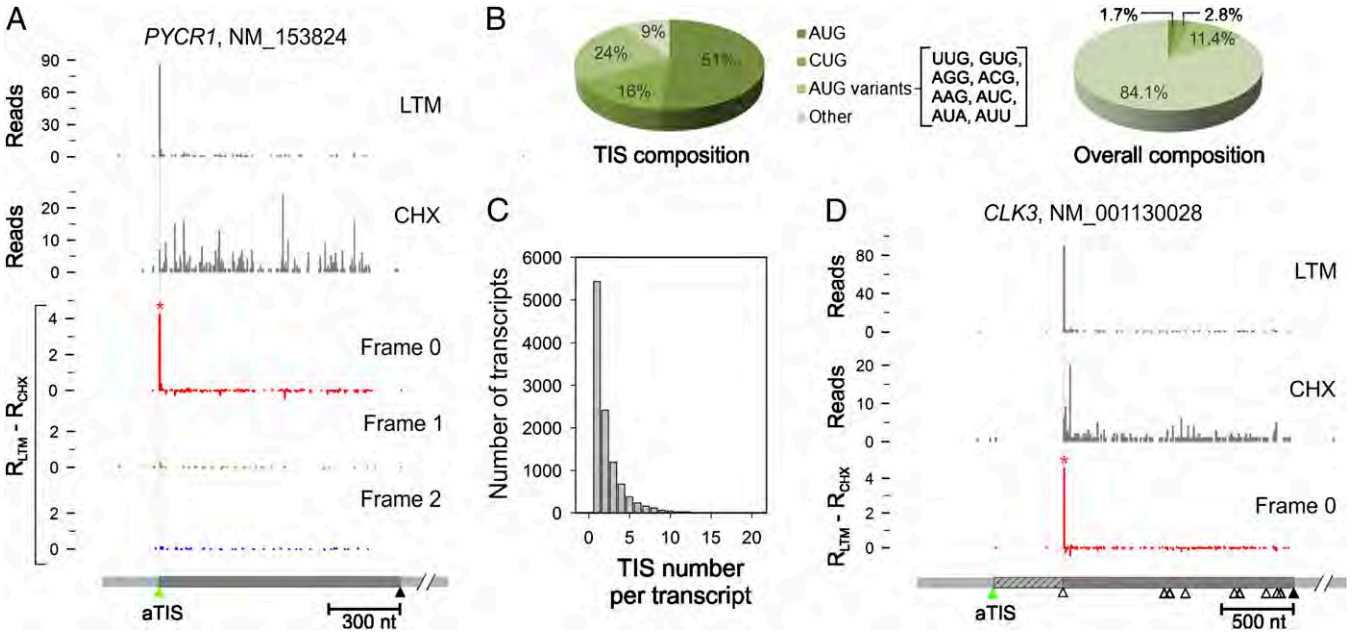

Fig. 2. Global identification of TIS by GTI-seq. (*A*) TIS identification on the *PYCR1* transcript. LTM and CHX reads are plotted as gray bar graphs. TIS identification is based on normalized density of LTM reads minus the density of CHX reads. The three reading frames are separated and presented as distinct colors. The identified TIS position is marked by a red asterisk and highlighted by a vertical line color-coded by the corresponding reading frame. The annotated coding region is indicated by a green triangle (start codon) and a black triangle (stop codon). (*B*) Codon composition of all TIS codons identified by GTI-seq (*Left*) is shown in comparison with the overall codon distribution over the entire transcriptome (*Right*). (*C*) Histogram showing the overall distribution of TIS numbers identified on each transcript. (*D*) Misannotation of the start codon on the *CLK3* transcript. The annotated coding region is indicated by the green (start codon) and black (stop codon) triangles. AUG codons on the body of the coding region are also shown as open triangles. For clarity, only one reading frame is shown.

detectable TIS peaks, we identified a total of 16,863 TIS sites (Dataset S1). Codon composition analysis revealed that more than half the TIS codons used AUG as the translation initiator (Fig. 2*B*). GTI-seq also identified a significant proportion of TIS codons using near-cognate codons that differ from AUG by a single nucleotide, in particular CUG (16%). Remarkably, nearly half the transcripts (49.6%) contained multiple TIS sites (Fig. 2*C*), suggesting that alternative translation prevails even under physiological conditions. Surprisingly, over a third of the transcripts (42.3%) showed no TIS peaks at the annotated TIS position (aTIS) despite clear evidence of translation (Dataset S1). Although some could be false negatives resulting from the stringent threshold cutoff for TIS identification (Fig. S3), others were attributed to alternative translation initiation (see below). However, it is possible that some cases represent misannotation. For instance, the translation of *CLK3* clearly starts from the second AUG, although the first AUG was annotated as the initiator in the current database (Fig. 2*D*). We found 50 transcripts that have possible misannotation in their start codons (Dataset S2). However, some mRNAs might have alternative transcript processing. In addition, we could not exclude the possibility that some of these genes might have tissue-specific TIS.

Characterization of Downstream Initiators. In addition to validating initiation at the annotated start codon, GTI-seq revealed clear evidence of downstream initiation on 27% of the analyzed transcripts with TIS peaks (Dataset S1). As a typical example, *AIMP1* showed three TIS peaks exactly at the first three AUG codons in the same reading frame (Fig. 3*A*). Thus, the same transcript generates three isoforms of AIMP1 with varied NH_2 termini, a finding that is consistent with the previous report (23). Of the total TIS positions identified by GTI-seq, 22% (3,741/16,863) were located downstream of aTIS codons; we termed these positions "dTIS." Nearly half of the identified dTIS codons used AUG as the initiator (Fig. 3*B*).

What are the possible factors influencing downstream start codon selection? We classified genes with multiple TIS codons into three groups based on the Kozak consensus sequence of the first AUG. The relative leakiness of the first AUG codon was estimated by measuring the fraction of LTM reads at the first AUG over the total reads recovered on and after this position. The AUG codon with a strong Kozak sequence context showed higher initiation efficiency (or lower leakiness) than a codon with a weak or no consensus sequence ($P = 1.12 \times 10^{-142}$) (Fig. 3*C*). These results indicate the critical role of sequence context in start codon recognition. To substantiate this conclusion further, we performed a reciprocal analysis by grouping genes according to whether an initiation peak was identified at the aTIS or dTIS positions on their transcripts (Fig. 3*D*). A survey of the sequences flanking the aTIS revealed a clear preference of Kozak sequence context for different gene groups. We observed the strongest Kozak consensus sequence in the gene group with aTIS initiation but no detectable dTIS, (Fig. 3*D*, *Bottom*). This sequence context was largely absent in the group of genes lacking detectable translation initiation at the aTIS (Fig. 3*D*, *Top*). Thus, ribosome leaky scanning tends to occur when the context for an aTIS is suboptimal.

Cells use the leaky scanning mechanism to generate protein isoforms with changed subcellular localizations or altered functionality from the same transcript (24). GTI-seq revealed many more genes that produce protein isoforms via leaky scanning than had been previously reported (Dataset S1). For independent validation of the dTIS positions identified by GTI-seq, we cloned the gene *CCDC124* whose transcript showed several initiation peaks above the background (Fig. 3*E*). One dTIS is in the same reading frame as the aTIS, allowing us to use a COOH-terminal tag to detect different translational products in transfected cells. Immunoblotting of transfected HEK293 cells showed two clear bands

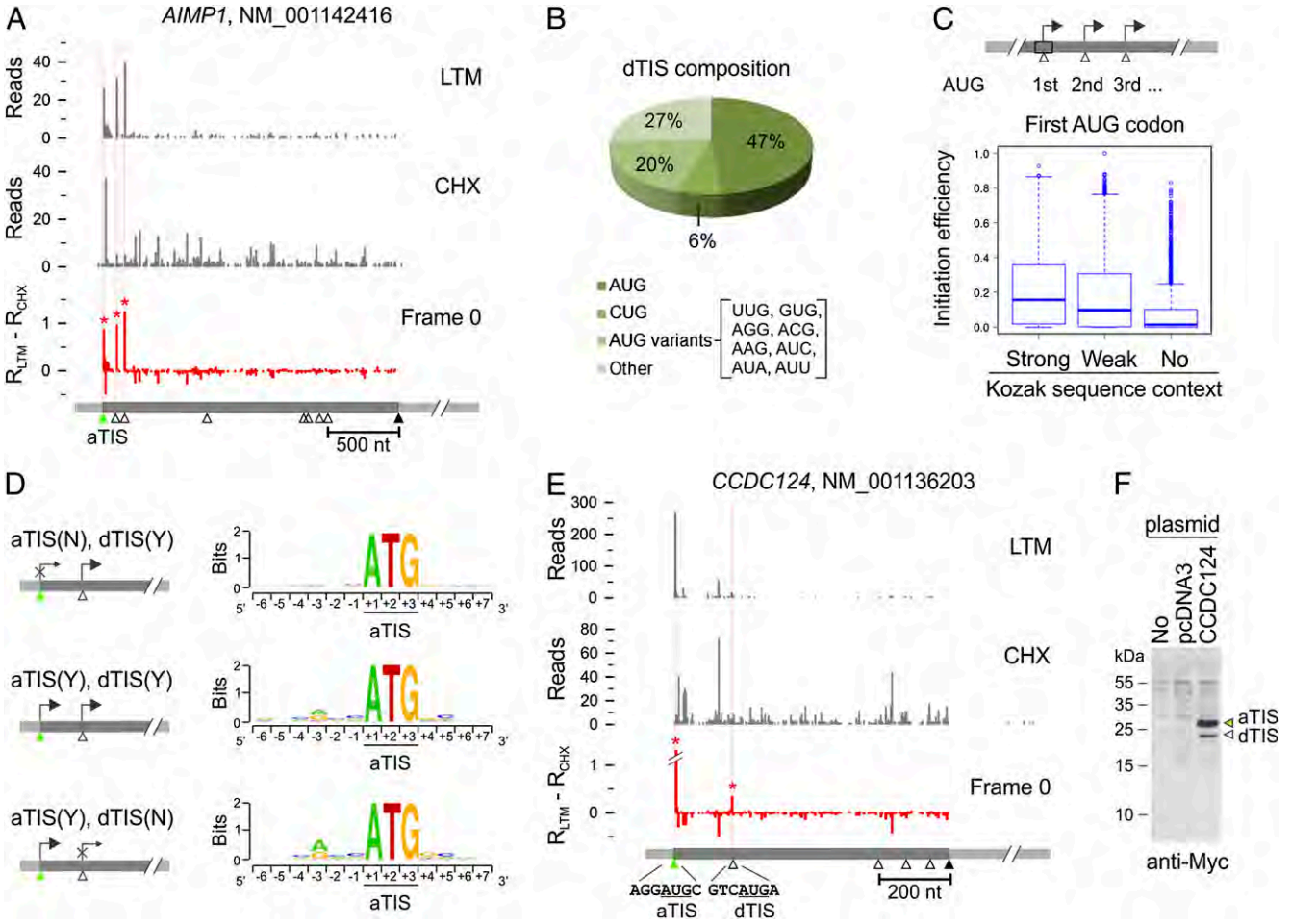

Fig. 3. Characterization of dTIS. (*A*) Identification of multiple TIS codons on the *AIMP1* transcript. For clarity, only one reading frame is shown. (*B*) Codon composition of total dTIS codons identified by GTI-seq. (*C*) Relative efficiency of initiation at the first AUG codon with different Kozak sequence contexts (one-tailed Wilcoxon rank sum test: strong vs. weak: $P = 7.92 \times 10^{-24}$; weak vs. no Kozak context: $P = 1.34 \times 10^{-75}$). (*D*) Genes are grouped according to the identified initiation at an aTIS, at a dTIS, or at both. The sequence context surrounding the aTIS is shown as sequence logos. χ^2 test, $P = 2.57 \times 10^{-100}$ for the −3 position and $P = 3.95 \times 10^{-18}$ for the +4 position. (*E*) Identification of multiple TIS codons on the *CCDC124* transcript. (*F*) Validation of *CCDC124* TIS codons by immunoblotting. The DNA fragment encompassing both the 5′ UTR and the CDS of *CCDC124* was cloned and transfected into HEK 293 cells. Whole-cell lysates were immunoblotted using *c-myc* antibody.

whose molecular masses correspond to full-length CCDC124 (28.9 kDa) and the NH_2-terminally truncated isoform (23.7 kDa), respectively. Intriguingly, the relative abundance of both isoforms matched well to the density of corresponding LTM reads, suggesting that GTI-seq might provide quantitative assessment of translation initiation.

Characterization of Upstream Initiators. Sequence-based computational analyses predicted that about 50% of mammalian transcripts contain at least one uORF (11, 12). In agreement with this notion, GTI-seq revealed that 54% of transcripts bear one or more TIS positions upstream of the annotated start codon (Dataset S1). These upstream TIS (uTIS) codons, when outside the aTIS reading frame, often are associated with short ORFs. A classic example is *ATF4*, whose translation is controlled predominantly by several uORFs (25–27). This feature was clearly captured by GTI-seq (Fig. 4*A*). As expected, the presence of these uORFs efficiently repressed the initiation at the aTIS, as evidenced by few CHX reads along the CDS of *ATF4*.

Nearly half of the total TIS positions identified by GTI-seq were uTIS (7,936/16,863). In contrast to the dTIS, which used AUG as the primary start codon (Fig. 3*B*), the majority of uTIS (74.4%) were non-AUG codons (Fig. 4*B*). CUG was the most prominent of these AUG variants, with a frequency even higher than that of AUG (30.3% vs. 25.6%). In a few well-documented examples, the CUG triplet was reported to serve as an alternative initiator (13). To confirm experimentally the alternative initiators identified by GTI-seq, we cloned the gene *RND3* that showed a clear initiation peak at a CUG codon in addition to the aTIS (Fig. 4*C*). The two initiators are in the same reading frame without a stop codon between them, thus permitting us to detect different translational products using an antibody against the fused COOH-terminal tag. Immunoblotting of transfected HEK293 cells showed two protein bands corresponding to the CUG-initiated long isoform (34 kDa) and the main product (31 kDa) (Fig. 4*C*). Once again, the levels of both isoforms were in accordance with the relative densities of LTM reads, further supporting the quantitative feature of GTI-seq in TIS mapping.

Global Impacts of uORFs on Translational Efficiency. Initiation from an uTIS and the subsequent translation of the short uORF negatively influence the main ORF translation (10, 11). To find possible factors governing the alternative TIS selection in the 5′ UTR, we categorized uTIS-bearing transcripts into two groups according to whether initiation occurs at the aTIS and compared the sequence context of uTIS codons (Fig. 5*A*). For transcripts with initiation at

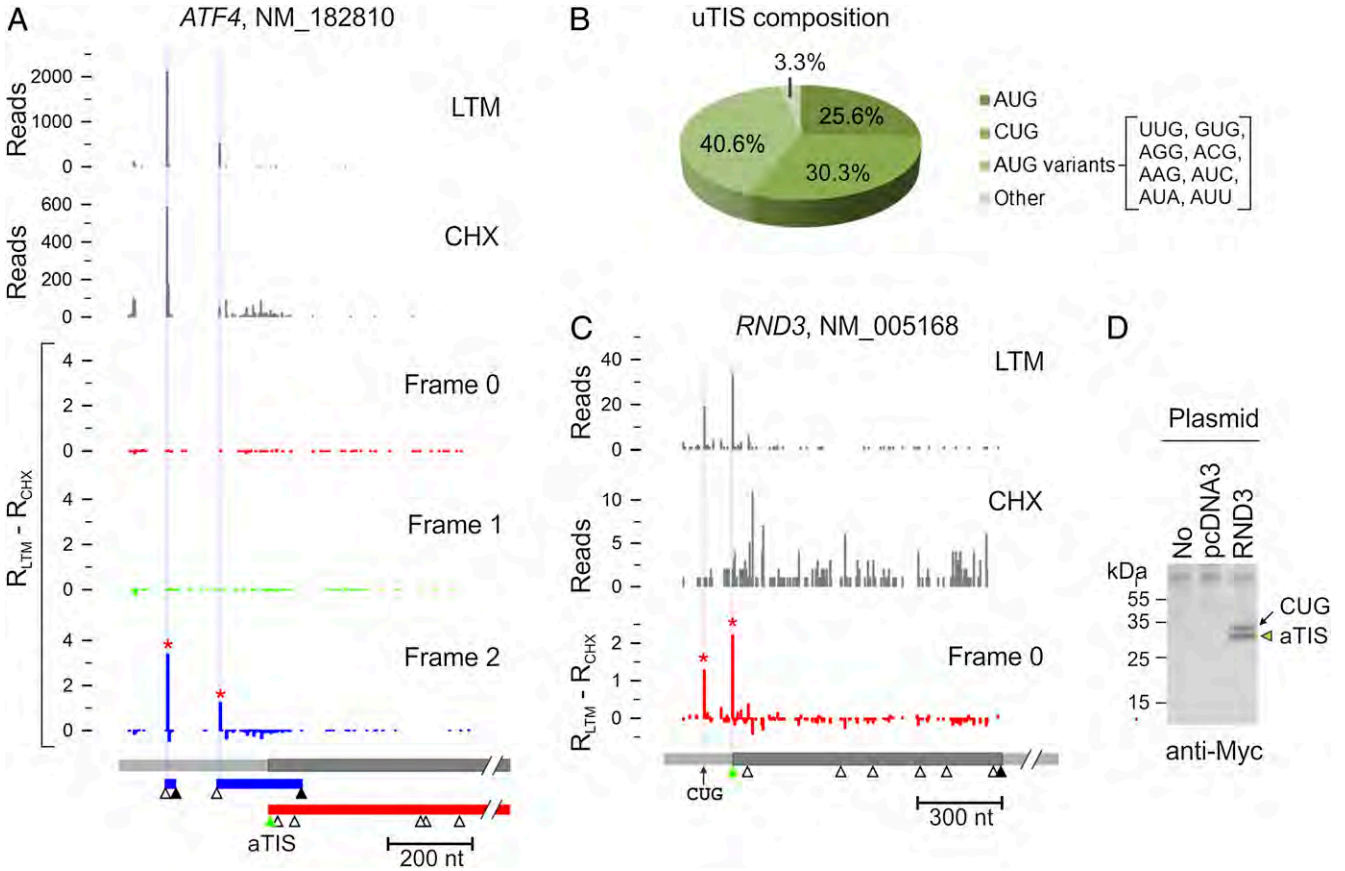

Fig. 4. Characterization of uTIS. (*A*) Identification of multiple TIS codons on the *ATF4* transcript. *Inset* shows a region of frame 0 with the *y* axis enlarged 10-fold, showing the LTM peak at the annotated start codon AUG. Different ORFs are shown in boxes color-coded for the different reading frames. (*B*) Codon composition of total uTIS codons identified by GTI-seq. (*C*) Identification of multiple TIS codons on the *RND3* transcript. (*D*) Validation of *RND3* TIS codons by immunoblotting. The DNA fragment encompassing both the 5′ UTR and the CDS of *RND3* was cloned and transfected into HEK 293 cells. Whole-cell lysates were immunoblotted using c-*myc* antibody.

both uTIS and aTIS positions [aTIS(Y)], the uTIS codons were preferentially composed of nonoptimal AUG variants. In contrast, the uTIS codons identified on transcripts with repressed aTIS initiation [aTIS(N)] showed a higher percentage of AUG with Kozak consensus sequences ($P = 1.74 \times 10^{-80}$). These results are in agreement with the notion that the accessibility of an aTIS to the ribosome for initiation depends on the context of uTIS codons.

Recent work showed a correlation between secondary structure stability of local mRNA sequences near the start codon and the efficiency of mRNA translation (28–30). To examine whether the uTIS initiation also is influenced by local mRNA structures, we computed the free energy associated with secondary structures from regions surrounding the uTIS position (Fig. 5*B*). We observed an increased folding stability of the region shortly after the uTIS in transcripts with repressed aTIS initiation (Fig. 5*B*, blue line). In particular, more stable mRNA secondary structures were present on transcripts with less optimal uTIS codons (Fig. 5*B*, *Center* and *Right*). Therefore, when the consensus sequence is absent from the start codon, the local mRNA secondary structure has a stronger correlation with the TIS selection.

Depending on the uTIS positions, the associated uORF can be separated from or overlap the main ORF. These different types of uORF could use different mechanisms to control the main ORF translation. For instance, when the uORF is short and separated from the main ORF, the 40S subunit can remain associated with the mRNA after termination at the uORF stop codon and can resume scanning, a process called "reinitiation" (2). When the uORF overlaps the main ORF, the aTIS initiation relies solely on the leaky scanning mechanism. We sought to dissect the respective contributions of reinitiation and leaky scanning to the regulation of aTIS initiation. Interestingly, we found a higher percentage of separated uORFs in aTIS(N) transcripts (Fig. 5*C*, $P = 3.52 \times 10^{-41}$). This result suggests that the reinitiation generally is less efficient than leaky scanning and is consistent with the negative role of uORFs in translation of main ORFs.

Cross-Species Conservation of Alternative Translation Initiators. The prevalence of alternative translation reshapes the proteome landscape by increasing the protein diversity or by modulating translation efficiency. The biological significance of alternative initiators could be preserved across species if they are of potential fitness benefit. We applied GTI-seq to a mouse embryonic fibroblast (MEF) cell line and identified TIS positions, including uTIS and dTIS, across the mouse transcriptome (Dataset S3). MEF cells showed remarkable similarity to HEK293 cells in overall TIS features (Fig. S4). For example, uTIS codons used non-AUG, especially CUG, as the dominant initiator. Additionally, about half the transcripts in MEF cells exhibited multiple initiators. Thus, the general features of alternative translation are well conserved between human and mouse cells.

To analyze the conservation of individual alternative TIS position on each transcript, we chose a total of 12,949 human/mouse orthologous mRNA pairs. We analyzed the 5′ UTR and CDS regions separately to measure the conservation of uTIS and dTIS positions, respectively (Fig. 6*A*). Each group was classified into two subgroups based on their sequence similarity. For genes with high

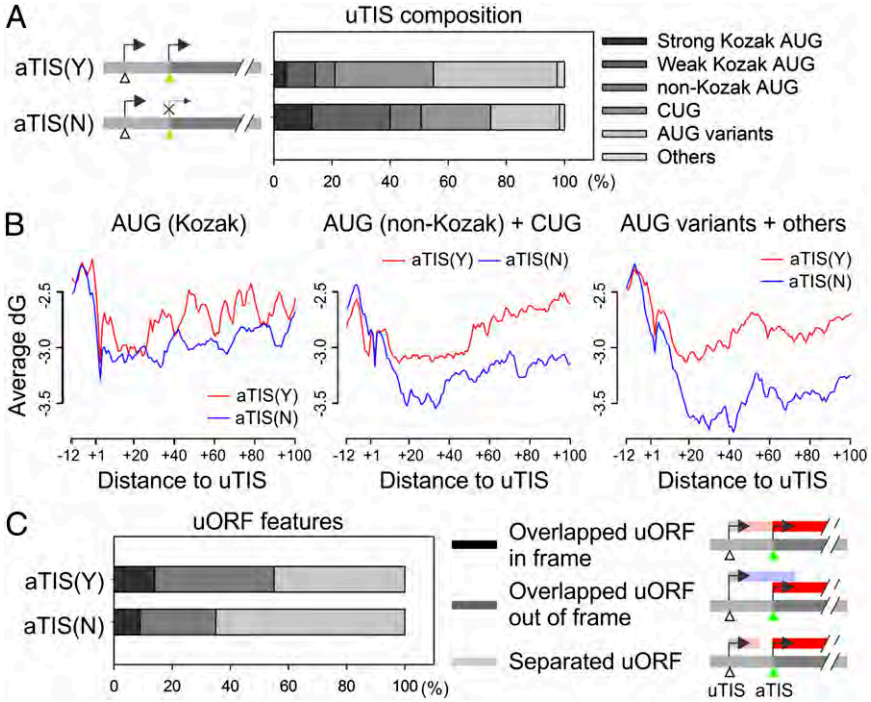

Fig. 5. Impact of uORF features on translational regulation. (*A*) The sequence composition of uTIS codons for genes with [aTIS(Y)] or without [aTIS(N)] aTIS initiation. Genes are classified into two groups based on aTIS initiation, and the uTIS sequence composition is categorized based on the consensus features shown on the right. (*B*) The contribution of mRNA secondary structure to TIS selection. Genes are grouped based on uTIS codon features listed in *A*. For each group, the transcripts with (red line) or without (blue line) aTIS initiation are analyzed for the averaged Gibbs free energy (ΔG) value in regions surrounding the identified uTIS codons. (*C*) The composition of uORFs in gene groups with or without aTIS initiation on their transcripts. Different ORF features are shown on the right.

sequence similarity, 85% of the uTIS and 60% of dTIS positions were conserved between human and mouse cells. Some of these alternative TIS codons were located at the same positions on the aligned sequences (Fig. S5). For example, *RNF10* in HEK293 cells showed three uTIS positions, which also were found at the identical positions on the aligned 5′ UTR sequence of the mouse homolog in MEF cells (Fig. 6*B*). Remarkably, genes with low sequence similarity also displayed high TIS conservation across the two species (Fig. 6*A*). For instance, the 5′ UTR of the *CTTN* gene has low sequence identity between human and mouse homologs (alignment score = 40.3) (Fig. 6*C*). However, a clear uTIS was identified at the same position on the aligned region in both cells. Notably, the majority of alternative ORFs conserved between human and mouse cells were of the same type, i.e., either separated from or overlapping the main ORF (Fig. 6*A* and Fig. S5). The evolutionary conservation of those TIS positions and the associated ORFs is a strong indication of the functional significance of alternative translation in regulating gene expression.

Characterization of Non-Protein Coding RNA Translation. The mammalian transcriptome contains many non–protein-coding RNAs (ncRNAs) (31). ncRNAs have gained much attention recently because of increasing recognition of their role in a variety of cellular processes, including embryogenesis and development (32). Motivated by the recent report of the possible translation of large intergenic ncRNAs (16), we sought to explore the possible translation, or at least ribosome association, of ncRNAs in HEK293 cells. We selected RPFs uniquely mapped to ncRNA sequences to exclude the possibility of spurious mapping of reads originated from mRNAs. Of 5,763 ncRNAs annotated in RefSeq (http://www.ncbi.nlm.nih.gov/RefSeq/), we identified 228 ncRNAs (about 4%) that were associated with RPFs marked by both CHX and LTM (Fig. 6*D* and Dataset S4). Compared with protein-coding mRNAs, most ORFs recovered from ncRNAs were very short, with a median length of 54 nt (Fig. 6*E*). Several ncRNAs also showed alternative initiation at non-AUG start codons, as exemplified by *LOC100506233* (Fig. 6*F*).

Comparative genomics reveals that the coding regions often are evolutionarily conserved elements (33). We retrieved the PhastCons scores (http://genome.ucsc.edu) for both coding and noncoding regions of ncRNAs and found that the ORF regions identified by GTI-seq indeed showed a higher conservation (Fig. 6*G*). Some ncRNAs showed a clear enrichment of highly conserved bases within the ORFs marked by both LTM and CHX reads (Fig. S6). Despite the apparent engagement by the protein synthesis machinery, the physiological functions of the coding capacity of these ncRNAs remain to be determined.

Discussion

The mechanisms of eukaryotic translation initiation have received increasing attention because of their central importance in diverse biological processes (1). The use of multiple initiation codons in a single mRNA contributes to protein diversity by expressing several protein isoforms from a single transcript. Distinct ORFs defined by alternative TIS codons also could serve as regulatory elements in controlling the translation of the main ORF (10, 11). Although we have some understanding of how ribosomes determine where and when to start initiation, our knowledge is far from complete. GTI-seq provides a comprehensive and high-resolution view of TIS positions across the entire transcriptome. The precise TIS mapping offers insights into the mechanisms of start codon recognition.

Global TIS Mapping at Single-Nucleotide Resolution by GTI-seq. Traditional toeprinting analysis showed heavy ribosome pausing at both the initiation and the termination codons of mRNAs (34,

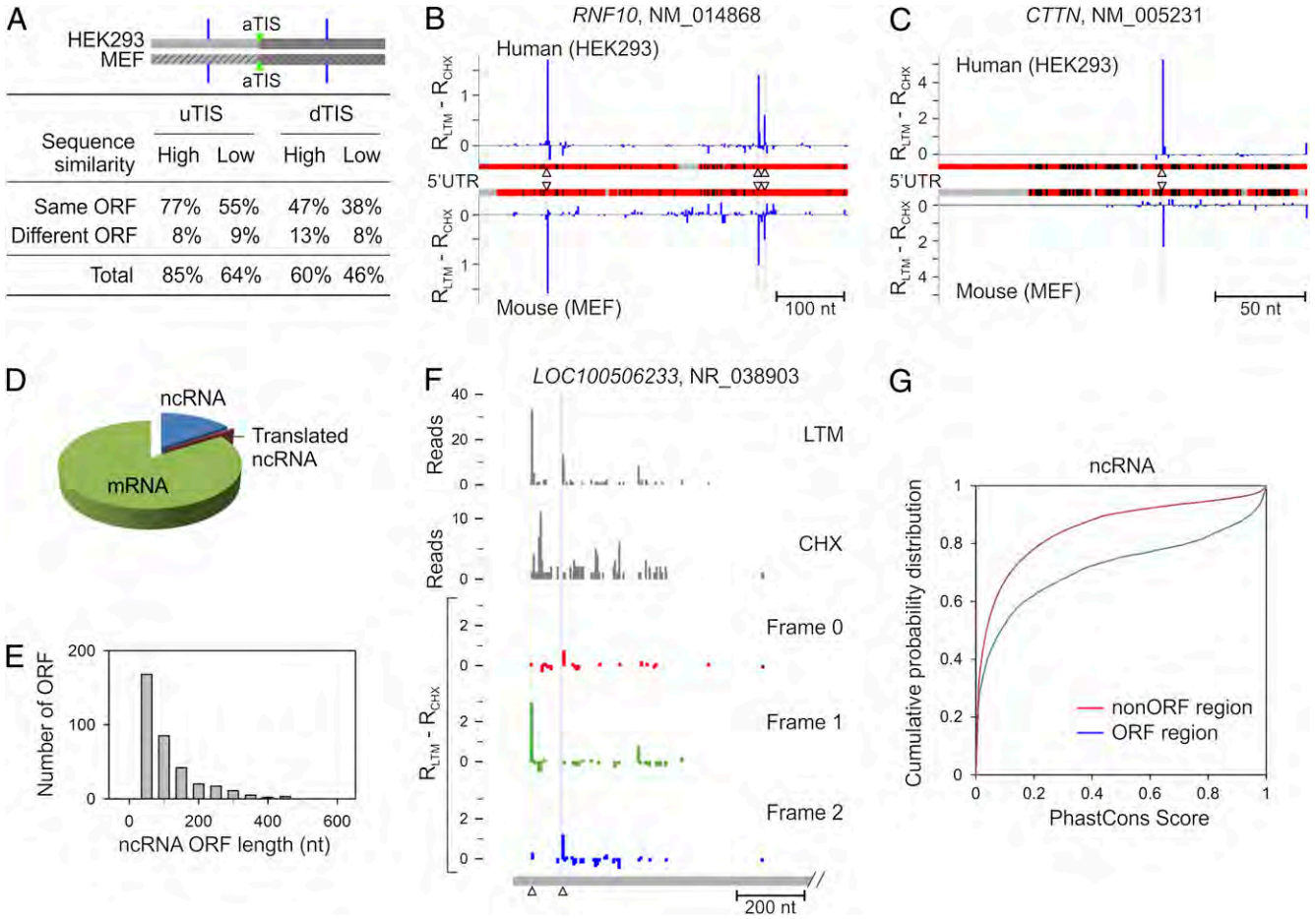

Fig. 6. Cross-species conservation of alternative TIS positions and identification of translated ncRNA. (*A*) Evolutionary conservation of alternative TIS positions identified by GTI-seq in HEK293 and MEF cells. Alternative uTIS and dTIS positions identified on human-mouse ortholog mRNA pairs are each classified into two subsets according to the alignment score of relevant sequences (5′ UTR for uTIS and CDS for dTIS). Each subset is divided further based on types of alternative ORFs. Percentage values are presented in the table. (*B*) Conservation of uTIS positions on the *RNF10* transcript with high 5′ UTR sequence similarity between HEK293 and MEF cells. Red regions indicate matched sequences, black regions indicate mismatched sequences, and gray regions indicate sequence gaps. Identified uTIS positions are indicated by triangles. (*C*) Conservation of uTIS positions on the *CTTN* transcript with low sequence similarity of 5′ UTR between HEK293 and MEF cells. (*D*) Pie chart showing the relative percentage of mRNA, ncRNA and translated ncRNA identified by GTI-seq. (*E*) Histogram showing the overall length distribution of ORFs identified in ncRNAs. (*F*) Identification of multiple TIS positions on the ncRNA *LOC100506233*. (*G*) Evolutionary conservation of the ORF region on ncRNAs identified by GTI-seq. PhastCons scores are retrieved from the primate genome sequence alignment.

35). Consistently, deep sequencing-based ribosome profiling also revealed higher RPF density at both the start and the stop codons (14, 15). Although this feature enables approximate determination of decoded mRNA regions, it does not allow unambiguous identification of TIS positions, especially when multiple initiators are used. Translation inhibitors acting specifically on the first round of peptide bond formation allow the run-off of elongating ribosomes, thereby specifically halting ribosomes at the initiation codon. Indeed, harringtonine treatment caused a profound accumulation of RPFs in the beginning of CDS (16). A caveat regarding the use of harringtonine is that this drug binds to free 60S subunits, and the inhibitory mechanism is unclear. In particular, it is not known whether harringtonine completely blocks the initiation step. We observed that a significant fraction of ribosomes still passed over the start codon in the presence of harringtonine.

The translation inhibitor LTM has several features that contribute to the high resolution of global TIS identification. First, LTM binds to the 80S ribosome already assembled at the initiation codon and permits the formation of the first peptide bond (17). Thus, the LTM-associated RPF more likely represents physiological TIS positions. Second, LTM occupies the empty E-site of initiating ribosomes and thus completely blocks the translocation. This feature allows TIS identification at single-nucleotide resolution. With this precision, different reading frames become unambiguous, thereby revealing different types of ORFs within each transcript. Third, because of their similar structure and the use of the same binding site in the ribosome, LTM and CHX can be applied side by side to achieve simultaneous assessment of both initiation and elongation for the same transcript. With the high signal/noise ratio, GTI-seq offers a direct approach to TIS identification with minimal computational aid. From our analysis, the uncovering of alternative initiators allows us to explore the mechanisms of TIS selection. We also experimentally validated different translational products initiated from alternative start codons, including non-AUG codons. Further confirming the accuracy of GTI-seq, a sizable fraction of alternative start codons identified by GTI-seq exhibited high conservation across species. The evolutionary conservation strongly suggests a physiological significance of alternative translation in gene expression.

Diversity and Complexity of Alternative Start Codons. GTI-seq revealed that the majority of identified TIS positions belong to alternative start codons. The prevailing alternative translation was corroborated by the finding that nearly half the transcripts

contained multiple TIS codons. Although dTIS codons use the conventional AUG as the main initiator, a significant fraction of uTIS codons are non-AUG, with CUG being the most frequent one. In a few well-documented cases, including *FGF2* (36), *VEGF* (37), and *Myc* (38), the CUG triplet was reported to serve as the non-AUG start codon. With the high-resolution TIS map across the entire transcriptome, GTI-seq greatly expanded the list of mRNAs with hidden coding potential not visible by sequence-based *in silico* analysis.

By what mechanisms are alternative start codons selected? GTI-seq revealed several lines of evidence supporting the linear-scanning mechanism for start codon selection. First, the uTIS context, such as the Kozak consensus sequence and the secondary structure, largely influenced the frequency of aTIS initiation. Second, the stringency of an aTIS codon negatively regulated the dTIS efficiency. Third, the leaky potential at the first AUG was inversely correlated with the strength of its sequence context. Because it is less likely that a preinitiation complex will bypass a strong initiator to select a suboptimal one downstream, it is not surprising that most uTIS codons are not canonical, whereas the dTIS codons are mostly conventional AUG. In addition to the leaky scanning mechanism for alternative translation initiation, ribosomes could translate a short uORF and reinitiate at downstream ORFs (2). After termination of a uORF is completed, it was assumed that some translation factors remain associated with the ribosome, facilitating the reinitiation process (39). However, this mechanism is widely considered to be inefficient. From the GTI-seq data set, about half the uORFs were separated from the main ORFs. Compared with transcripts with overlapping uORFs that must rely on leaky scanning to mediate the downstream translation, we observed repressed aTIS initiation in transcripts containing separated uORFs. It is likely that the ribosome reinitiation mechanism plays a more important role in selective translation under stress conditions (27).

Biological Impacts of Alternative Translation Initiation. One expected consequence of alternative translation initiation is an expanded proteome diversity that has not been and could not be predicted by *in silico* analysis of AUG-mediated main ORFs. Indeed, many eukaryotic proteins exhibit a feature of NH_2-terminal heterogeneity presumably caused by alternative translation. Protein isoforms localized in different cellular compartments are typical examples, because most localization signals are within the NH_2-terminal segment (40, 41). Alternative TIS selection also could produce functionally distinct protein isoforms. One well-established example is C/EBP, a family of transcription factors that regulate the expression of tissue-specific genes during differentiation (42).

When an alternative TIS codon is not in the same frame as the aTIS, it is conceivable that the same mRNA will generate unrelated proteins. This production could be particularly important for the function of uORFs, which often are separated from the main ORF and encode short polypeptides. Some of these uORF peptide products control ribosome behavior directly, thereby regulating the translation of the main ORF. For instance, the translation of *S*-adenosylmethionine decarboxylase is subject to regulation by the six-amino acid product of its uORF (43). The alternative translational products also could function as biologically active peptides. A striking example is the discovery of short ORFs in noncoding RNAs of *Drosophila* that produce functional small peptides during development (44). However, both computational prediction and experimental validation of peptide-encoding short ORFs within the genome are challenging. Our study using GTI-seq represents a potential addition to the expanding ORF catalog by including ORFs from ncRNAs.

Perspective. The enormous biological breadth of translational regulation has led to an enhanced appreciation of its complexities. However, current endeavors aiming to understand protein translation have been hindered by technological limitations. Comprehensive cataloging of global TIS and the associated ORFs is just the beginning step in unveiling the role of translational control in gene expression. More focused studies will be needed to decipher the function and regulatory mechanism of novel ORFs individually. A systematic, high-throughput method like GTI-seq offers a top-down approach, in which one can identify a set of candidate genes for intensive study. GTI-seq is readily applicable to broad fields of fundamental biology. For instance, applications of GTI-seq in different tissues will facilitate the elucidation of the tissue-specific translational control. The illustration of altered TIS selection under different growth conditions will set the stage for future investigation of translational reprogramming during organismal development as well as in human diseases.

Materials and Methods

HEK293 or MEF cells were treated with 100 μM CHX, 50 μM LTM, 2 μg/mL harringtonine, or DMSO at 37 °C for 30 min. Cells were lysed in polysome buffer, and cleared lysates were separated by sedimentation through sucrose gradients. Collected polysome fractions were digested with RNase I, and the RPF fragments were size selected and purified by gel extraction. After the construction of the sequencing library from these fragments, deep sequencing was performed using Illumina HiSEQ. The trimmed RPF reads with final lengths of 26–29 nt were aligned to the RefSeq transcript sequences by Bowtie-0.12.7, allowing one mismatch. A TIS position on an individual transcript was called if the normalized density of LTM reads at the every nucleotide position minus the density of CHX reads at that position was well above the background. In the analysis of noncoding RNA, only reads unique to single ncRNA were used. To validate the identified TIS codons experimentally, specific genes encompassing both the 5′ UTR and the CDS were amplified by RT-PCR from total cellular RNAs extracted from HEK293 cells. The resultant cDNAs were cloned into pcDNA3.1 containing a c-*myc* tag at the COOH terminus. After transfection into HEK293 cells, whole-cell lysates were used for immunoblotting using anti-*myc* antibody. Full methods are available in *SI Materials and Methods*.

ACKNOWLEDGMENTS. We thank S.-B.Q. laboratory members for helpful discussions during the course of this study; Drs. Chaolin Zhang (Rockefeller University) and Adam Siepel (Cornell University) for critical reading of the manuscript; and the Cornell University Life Sciences Core Laboratory Center for performing deep sequencing. This work was supported by National Institutes of Health (NIH) Grants CA106150 (to B.S.) and 1 DP2 OD006449-01, Ellison Medical Foundation Grant AG-NS-0605-09, and Department of Defense Exploration-Hypothesis Development Award W81XWH-11-1-02368 (to S.-B.Q.).

1. Sonenberg N, Hinnebusch AG (2009) Regulation of translation initiation in eukaryotes: Mechanisms and biological targets. *Cell* 136:731–745.
2. Jackson RJ, Hellen CU, Pestova TV (2010) The mechanism of eukaryotic translation initiation and principles of its regulation. *Nat Rev Mol Cell Biol* 11:113–127.
3. Gray NK, Wickens M (1998) Control of translation initiation in animals. *Annu Rev Cell Dev Biol* 14:399–458.
4. Kozak M (2002) Pushing the limits of the scanning mechanism for initiation of translation. *Gene* 299:1–34.
5. Kozak M (1991) Structural features in eukaryotic mRNAs that modulate the initiation of translation. *J Biol Chem* 266:19867–19870.
6. Kozak M (1990) Downstream secondary structure facilitates recognition of initiator codons by eukaryotic ribosomes. *Proc Natl Acad Sci USA* 87:8301–8305.
7. Maag D, Fekete CA, Gryczynski Z, Lorsch JR (2005) A conformational change in the eukaryotic translation preinitiation complex and release of eIF1 signal recognition of the start codon. *Mol Cell* 17:265–275.
8. Martin-Marcos P, Cheung YN, Hinnebusch AG (2011) Functional elements in initiation factors 1, 1A, and 2β discriminate against poor AUG context and non-AUG start codons. *Mol Cell Biol* 31:4814–4831.
9. Iacono M, Mignone F, Pesole G (2005) uAUG and uORFs in human and rodent 5′untranslated mRNAs. *Gene* 349:97–105.
10. Morris DR, Geballe AP (2000) Upstream open reading frames as regulators of mRNA translation. *Mol Cell Biol* 20:8635–8642.
11. Calvo SE, Pagliarini DJ, Mootha VK (2009) Upstream open reading frames cause widespread reduction of protein expression and are polymorphic among humans. *Proc Natl Acad Sci USA* 106:7507–7512.

12. Resch AM, Ogurtsov AY, Rogozin IB, Shabalina SA, Koonin EV (2009) Evolution of alternative and constitutive regions of mammalian 5′UTRs. *BMC Genomics* 10:162.
13. Touriol C, et al. (2003) Generation of protein isoform diversity by alternative initiation of translation at non-AUG codons. *Biol Cell* 95:169–178.
14. Ingolia NT, Ghaemmaghami S, Newman JR, Weissman JS (2009) Genome-wide analysis in vivo of translation with nucleotide resolution using ribosome profiling. *Science* 324:218–223.
15. Guo H, Ingolia NT, Weissman JS, Bartel DP (2010) Mammalian microRNAs predominantly act to decrease target mRNA levels. *Nature* 466:835–840.
16. Ingolia NT, Lareau LF, Weissman JS (2011) Ribosome profiling of mouse embryonic stem cells reveals the complexity and dynamics of mammalian proteomes. *Cell* 147: 789–802.
17. Schneider-Poetsch T, et al. (2010) Inhibition of eukaryotic translation elongation by cycloheximide and lactimidomycin. *Nat Chem Biol* 6:209–217.
18. Klinge S, Voigts-Hoffmann F, Leibundgut M, Arpagaus S, Ban N (2011) Crystal structure of the eukaryotic 60S ribosomal subunit in complex with initiation factor 6. *Science* 334:941–948.
19. Ju J, et al. (2009) Lactimidomycin, iso-migrastatin and related glutarimide-containing 12-membered macrolides are extremely potent inhibitors of cell migration. *J Am Chem Soc* 131:1370–1371.
20. Sugawara K, et al. (1992) Lactimidomycin, a new glutarimide group antibiotic. Production, isolation, structure and biological activity. *J Antibiot (Tokyo)* 45: 1433–1441.
21. Steitz TA (2008) A structural understanding of the dynamic ribosome machine. *Nat Rev Mol Cell Biol* 9:242–253.
22. Fresno M, Jiménez A, Vázquez D (1977) Inhibition of translation in eukaryotic systems by harringtonine. *Eur J Biochem* 72:323–330.
23. Shalak V, Kaminska M, Mirande M (2009) Translation initiation from two in-frame AUGs generates mitochondrial and cytoplasmic forms of the p43 component of the multisynthetase complex. *Biochemistry* 48:9959–9968.
24. Kochetov AV (2008) Alternative translation start sites and hidden coding potential of eukaryotic mRNAs. *Bioessays* 30:683–691.
25. Spriggs KA, Bushell M, Willis AE (2010) Translational regulation of gene expression during conditions of cell stress. *Mol Cell* 40:228–237.
26. Harding HP, Calfon M, Urano F, Novoa I, Ron D (2002) Transcriptional and translational control in the Mammalian unfolded protein response. *Annu Rev Cell Dev Biol* 18:575–599.
27. Vattem KM, Wek RC (2004) Reinitiation involving upstream ORFs regulates ATF4 mRNA translation in mammalian cells. *Proc Natl Acad Sci USA* 101:11269–11274.
28. Kudla G, Murray AW, Tollervey D, Plotkin JB (2009) Coding-sequence determinants of gene expression in Escherichia coli. *Science* 324:255–258.
29. Kochetov AV, et al. (2007) AUG_hairpin: Prediction of a downstream secondary structure influencing the recognition of a translation start site. *BMC Bioinformatics* 8:318.
30. Kertesz M, et al. (2010) Genome-wide measurement of RNA secondary structure in yeast. *Nature* 467:103–107.
31. Mattick JS (2005) The functional genomics of noncoding RNA. *Science* 309:1527–1528.
32. Pauli A, Rinn JL, Schier AF (2011) Non-coding RNAs as regulators of embryogenesis. *Nat Rev Genet* 12:136–149.
33. Siepel A, et al. (2005) Evolutionarily conserved elements in vertebrate, insect, worm, and yeast genomes. *Genome Res* 15:1034–1050.
34. Wolin SL, Walter P (1989) Signal recognition particle mediates a transient elongation arrest of preprolactin in reticulocyte lysate. *J Cell Biol* 109:2617–2622.
35. Sachs MS, et al. (2002) Toeprint analysis of the positioning of translation apparatus components at initiation and termination codons of fungal mRNAs. *Methods* 26: 105–114.
36. Vagner S, et al. (1996) Translation of CUG- but not AUG-initiated forms of human fibroblast growth factor 2 is activated in transformed and stressed cells. *J Cell Biol* 135:1391–1402.
37. Meiron M, Anunu R, Scheinman EJ, Hashmueli S, Levi BZ (2001) New isoforms of VEGF are translated from alternative initiation CUG codons located in its 5′UTR. *Biochem Biophys Res Commun* 282:1053–1060.
38. Hann SR, King MW, Bentley DL, Anderson CW, Eisenman RN (1988) A non-AUG translational initiation in c-myc exon 1 generates an N-terminally distinct protein whose synthesis is disrupted in Burkitt's lymphomas. *Cell* 52:185–195.
39. Pöyry TA, Kaminski A, Jackson RJ (2004) What determines whether mammalian ribosomes resume scanning after translation of a short upstream open reading frame? *Genes Dev* 18:62–75.
40. Chang KJ, Wang CC (2004) Translation initiation from a naturally occurring non-AUG codon in Saccharomyces cerevisiae. *J Biol Chem* 279:13778–13785.
41. Porras P, Padilla CA, Krayl M, Voos W, Bárcena JA (2006) One single in-frame AUG codon is responsible for a diversity of subcellular localizations of glutaredoxin 2 in Saccharomyces cerevisiae. *J Biol Chem* 281:16551–16562.
42. Descombes P, Schibler U (1991) A liver-enriched transcriptional activator protein, LAP, and a transcriptional inhibitory protein, LIP, are translated from the same mRNA. *Cell* 67:569–579.
43. Hill JR, Morris DR (1993) Cell-specific translational regulation of S-adenosylmethionine decarboxylase mRNA. Dependence on translation and coding capacity of the cis-acting upstream open reading frame. *J Biol Chem* 268:726–731.
44. Kondo T, et al. (2010) Small peptides switch the transcriptional activity of Shavenbaby during Drosophila embryogenesis. *Science* 329:336–339.

Molecular Cell
Article

Cotranslational Response to Proteotoxic Stress by Elongation Pausing of Ribosomes

Botao Liu,[1,4] Yan Han,[2,3,4] and Shu-Bing Qian[1,2,*]
[1]Graduate Field of Genetics, Genomics & Development
[2]Division of Nutritional Sciences
Cornell University, Ithaca, NY 14853, USA
[3]Department of Infectious Diseases, Ruijin Hospital, Shanghai Jiaotong University School of Medicine, Shanghai 20005, China
[4]These authors contributed equally to this work
*Correspondence: sq38@cornell.edu
http://dx.doi.org/10.1016/j.molcel.2012.12.001

SUMMARY

Translational control permits cells to respond swiftly to a changing environment. Rapid attenuation of global protein synthesis under stress conditions has been largely ascribed to the inhibition of translation initiation. Here we report that intracellular proteotoxic stress reduces global protein synthesis by halting ribosomes on transcripts during elongation. Deep sequencing of ribosome-protected messenger RNA (mRNA) fragments reveals an early elongation pausing, roughly at the site where nascent polypeptide chains emerge from the ribosomal exit tunnel. Inhibiting endogenous chaperone molecules by a dominant-negative mutant or chemical inhibitors recapitulates the early elongation pausing, suggesting a dual role of molecular chaperones in facilitating polypeptide elongation and cotranslational folding. Our results further support the chaperone "trapping" mechanism in promoting the passage of nascent chains. Our study reveals that translating ribosomes fine tune the elongation rate by sensing the intracellular folding environment. The early elongation pausing represents a cotranslational stress response to maintain the intracellular protein homeostasis.

INTRODUCTION

Protein misfolding imposes a major risk to the health of cells and organisms. An elaborate protein quality control (PQC) system has been laid down during evolution to maintain protein homeostasis—a delicate balance between protein synthesis, folding, and degradation (Bukau et al., 2006; Frydman, 2001; Hartl et al., 2011). Molecular chaperones are "cellular lifeguards" that govern the integrity of the proteome. By interacting with different cochaperones and cofactors, Hsp70 family proteins actively participate in protein triage decisions from folding and degradation to aggregation (McClellan et al., 2005; Zhang and Qian, 2011). Most recent studies highlighted the robust network of chaperones acting cotranslationally on nascent chains in eukaryotic (del Alamo et al., 2011) as well as prokaryotic cells (Oh et al., 2011). Interestingly, prokaryotes and eukaryotes have evolved distinct ribosome-associated chaperone systems (Kramer et al., 2009). In *S. cerevisiae*, two ribosome-associated systems interact with newly synthesized polypeptides, the nascent chain-associated complex (NAC) and the Hsp70-based Ssb/Ssz/Zuo triad system (Kampinga and Craig, 2010). Both systems are physically located in close proximity at the peptide exit tunnel of ribosomes. The ribosome-associated chaperone system also exists in mammals, although its functionality is not fully understood (Jaiswal et al., 2011). Despite the wide appreciation of the impact that this chaperone system may have on cotranslational folding, little is known about how the ribosome-associated chaperone system regulates the process of translation per se.

Messenger RNA (mRNA) translation can be divided into three stages: initiation, elongation, and termination. Regulation of translation occurs predominantly during the initiation phase (Sonenberg and Hinnebusch, 2009; Spriggs et al., 2010). The initiation is a complex multistep process governed by a large number of protein factors and involves mRNA 5′-cap recognition, scanning, and start codon recognition (Gray and Wickens, 1998; Jackson et al., 2010). Much attention has been focused on the role of translation initiation factors (eIFs) in the assembly of elongation-competent ribosome complexes. However, after the commitment of polypeptide synthesis, the regulatory steps during elongation remain poorly understood.

Given the fact that translation consumes a lion's share of energy, cells often reduce global protein synthesis under most, if not all, types of adverse conditions. The global repression of protein synthesis not only saves the cellular energy but also relieves the burden of the PQC system due to the decreased protein production (Holcik and Sonenberg, 2005). Current models for the mechanism governing this translational attenuation are largely limited to the initiation stage. For instance, eIF4F-complex-mediated cap recognition and eIF2-controlled ternary complex formation are key initiation targets in controlling global mRNA translation (Ma and Blenis, 2009; Ron and Walter, 2007). In response to stresses, the shutdown of protein synthesis is, in general, mediated by the inhibition of 43S complex loading to the 5′ end cap and/or reducing the amount of ternary complex that is available. Despite the

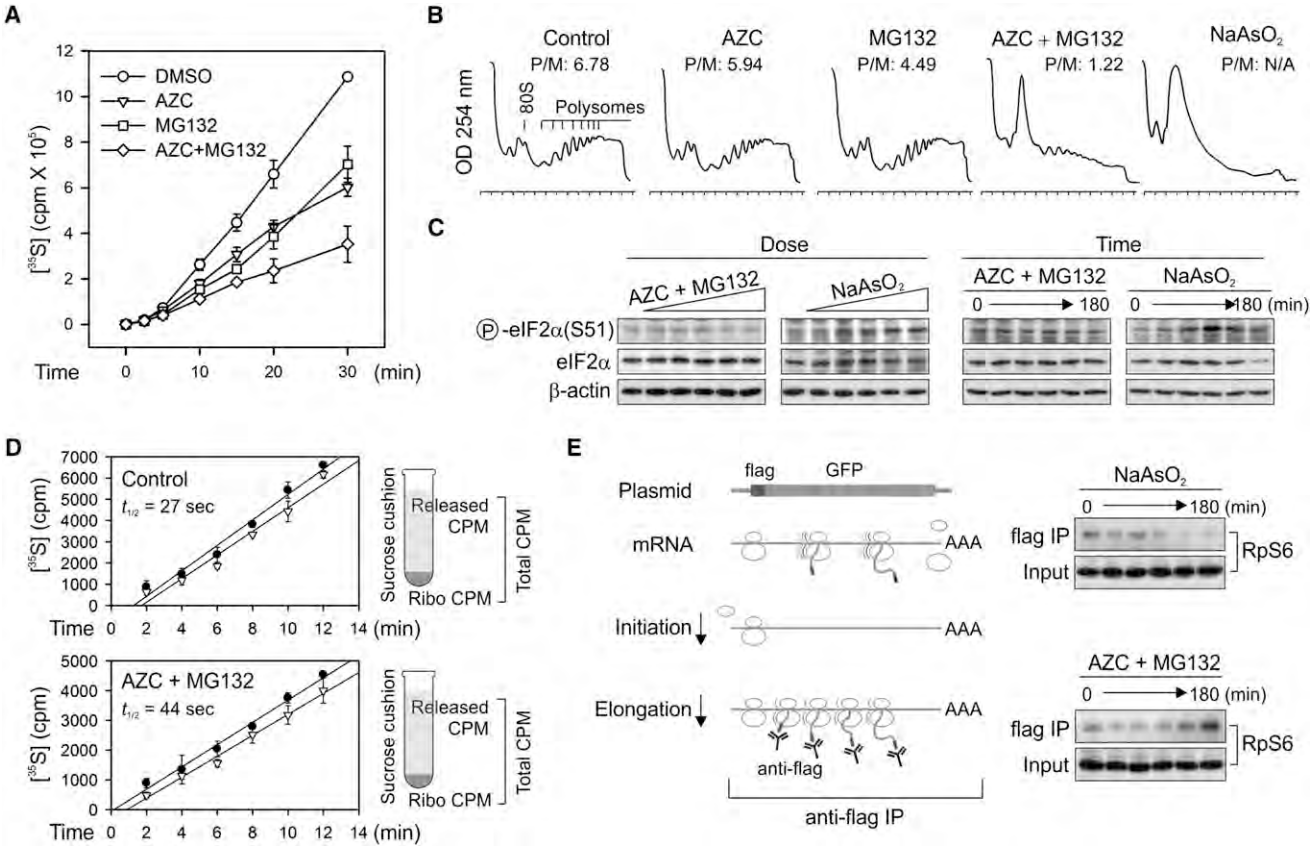

Figure 1. Proteotoxic Stress Attenuates Protein Synthesis by Affecting Translation Elongation

(A) Global protein synthesis in HEK293 cells treated with 10 mM AZC, 20 μM MG132, or both. [^{35}S] radioactivity of trichloroacetic acid (TCA)-insoluble material was measured at given times. Means ± SEM of four experiments are shown.

(B) Polysome profiles were determined using sucrose gradient sedimentation. HEK293 cells were pre-treated with 10 mM AZC, 20 μM MG132, or both for 60 min followed by polysome preparation. p:m ratio was calculated by comparing areas under the polysome and 80S peak.

(C) HEK293 cells were treated with increasing doses of AZC (from 0 to 25 mM with 5-fold dilution) in the presence of 20 μM MG132 for 60 min, or increasing doses of $NaAsO_2$ (from 0 to 1 mM with 2-fold dilution) for 60 min (left two panels), followed by immunoblotting using antibodies as indicated. The right two panels show the immunoblotting results of cells treated with 10 mM AZC and 20 μM MG132 or 500 μM $NaAsO_2$ for various times (0, 10, 30, 60, 120, and 180 min).

(D) The ribosomal half-transit time was determined in the absence or presence of 10 mM AZC and 20 μM MG132. Fitting lines of [^{35}S] incorporation into total (filled circle) and completed (open triangle) protein synthesis were obtained by linear regression. Means ± SEM of three experiments are shown.

(E) Schematic for nascent chain immunoprecipitation assay to differentiate elongation defect from initiation deficiency (left panel). HEK293 cells expressing Flag-GFP were pretreated with 10 mM AZC and 20 μM MG132 or 500 μM $NaAsO_2$ for various times (0, 10, 30, 60, 120, and 180 min). Immunoprecipitation was performed using anti-Flag-antibody-coated beads followed by immunoblotting with anti-RpS6 antibody. The 0 time point serves as the control condition without any drug treatment. See also Figure S1.

well-documented role of these initiation regulators, it remains surprisingly obscure whether the 80S ribosome, once assembled on the mRNA, maintains the responsiveness to protein misfolding during elongation.

Here we report that proteotoxic stress triggers ribosomal pausing during elongation. Remarkably, the pausing occurs primarily near the site where nascent polypeptide chains emerge from the ribosomal exit tunnel. We demonstrate that the early elongation pausing is induced by the sequestration of chaperone molecules by misfolded proteins. Our results expand the critical role of chaperone molecules from cotranslational folding to polypeptide elongation. The early elongation pausing of ribosomes thus represents a mechanism of cotranslational stress response to maintain intracellular protein homeostasis.

RESULTS

Proteotoxic Stress Attenuates Global Protein Synthesis

Intracellular accumulation of misfolded proteins is a common feature of a variety of stress conditions. To induce misfolding of newly synthesized polypeptides without massively perturbing cellular functions, we used an amino acid analog, L-azetidine-2-carboxylic acid (AZC), that competes with proline during amino acid incorporation (Goldberg and Dice, 1974). Once incorporated into proteins in place of proline, AZC potently induces protein misfolding and degradation (Qian et al., 2010; Trotter et al., 2002). Pre-exposure of HEK293 cells to 10 mM AZC resulted in a marked reduction of [^{35}S] incorporation (Figure 1A). In agreement with the enhanced degradation

of AZC-incorporated polypeptides, pulse-chase analysis showed an increased turnover of [^{35}S] labeled proteins in the presence of AZC (Figure S1A). We asked whether proteasome inhibition would prevent the loss of [^{35}S] incorporation by blocking the degradation. To our surprise, adding proteasome inhibitor MG132 further decreased the total amount of [^{35}S] incorporation (Figure 1A). This was not due to the side effects of MG132 because adding this inhibitor alone only partially reduced the level of [^{35}S] incorporation. Since the AZC-induced misfolded polypeptides progressively accumulate under proteasome inhibition, it appears that the intracellular proteotoxic stress triggers a rapid attenuation of translation. To substantiate this finding further, we analyzed the polysome profiles by velocity sedimentation of lysates in sucrose gradients. Treatment with either AZC or MG132 alone had minor effects on the polysome formation (Figure 1B). In contrast, the presence of both AZC and MG132 markedly disassembled the polysomes with an approximately 5-fold decrease in the polysome/monosome (p:m) ratio.

Proteotoxic Stress Affects Primarily Translation Elongation

To investigate the mechanisms underlying the proteotoxic stress-induced translational attenuation, we examined the phosphorylation status of eIF2α, a prominent initiation regulator in the unfolded protein response (Ron and Walter, 2007). In contrast to sodium arsenite ($NaAsO_2$), a known inducer of eIF2α phosphorylation, treating cells with both AZC and MG132 at increasing doses and for extended times had little effect on eIF2α phosphorylation (Figure 1C). Additionally, we observed no change in the phosphorylation of S6 and its kinase S6K1, one of the downstream targets of mammalian target of rapamycin complex 1 (mTORC1) (Jackson et al., 2010; Ma and Blenis, 2009) (Figure S1B). Thus, the intracellular proteotoxic stress does not primarily affect the translation initiation regulators, at least in the early stage.

We next examined whether proteotoxic stress inhibits protein synthesis by interfering with postinitiation events, such as elongation. One way to distinguish elongation from initiation is the formation of stress granules (SGs). Inhibiting translation initiation triggers SG formation, whereas blocking translation elongation prevents this process (Buchan and Parker, 2009; Kedersha et al., 2000). Unlike sodium arsenite treatment, which induced an evident SG formation, adding both AZC and MG132 to cells failed to induce any discernible SG formation (Figure S1C). Thus proteotoxic stress probably affects translation elongation rather than initiation. To assess independently whether the reduced protein synthesis under proteotoxic stress was primarily due to defective elongation, we determined ribosomal transit times in these cells. The ribosomal transit time refers to the time required for a ribosome, after initiation, to traverse an average-sized mRNA and release the completed polypeptide chain (Nielsen and McConkey, 1980). The estimated half-transit time ($t_{1/2}$) in the presence of both AZC and MG132 (44 s) was ~1.6-fold longer than that in control cells (27 s) (Figure 1D), confirming that proteotoxic stress significantly reduced the elongation rate of polypeptide synthesis. Additionally, we conducted an elongation chase experiment using a synthesized *firefly* luciferase (Fluc) mRNA in lysates programmed from cells with or without proteotoxic stress. Compared to the control, the stressed cell lysates showed a delayed accumulation of Fluc activity (Figure S1D), further indicating a slowdown of elongation process under proteotoxic stress.

To examine whether the stalled ribosome during elongation was still associated with the newly synthesized polypeptide, we performed nascent chain immunoprecipitation followed by detection of ribosomal small subunit S6 (RpS6). We established a HEK293 cell line stably expressing a green fluorescent protein (GFP) reporter with an NH_2-terminal Flag-tag (Figure 1E). We enriched the ribosome complexes bearing the partially synthesized GFP by anti-Flag immunoprecipitation. Arsenite treatment led to a progressive loss of the associated RpS6 in a time-course-dependent manner (Figure 1E, right top panel), which is consistent with the inhibition of translation initiation. Remarkably, treating cells with both AZC and MG132 resulted in an accumulation of RpS6 in the anti-Flag precipitates, clear evidence of paused ribosomes on the mRNA during elongation. The prolonged ribosome association with the nascent chain persists in the polysome fractions of these cells (Figures S1E and S1F). Taken together, our results strongly indicate that proteotoxic stress acts at the level of translation elongation to suppress protein synthesis.

Proteotoxic Stress Triggers Early Elongation Pausing of Ribosomes

A defective translation elongation should result in slower ribosome run-off and the retention of polysomes (Saini et al., 2009). It is surprising to find that the polysomes were largely disassembled in cells treated with both AZC and MG132 (Figure 1B). We considered the possibility that proteotoxic stress primarily induced ribosomal pausing at the early stage of elongation, thereby creating a road block for following ribosomes. To provide a definitive assessment of ribosome positions on mRNAs under proteotoxic stress, we isolated the ribosome-protected mRNA fragments (RPFs) and performed deep sequencing using methods reported previously (Ingolia et al., 2009). RPF reads obtained from cells with or without proteotoxic stress were of equal quality as evidenced by the similar size distribution and strong 3nt periodicity after alignment. Notably, AZC and MG132 treatment did not result in global variation in overall ribosome density along each transcript ($r = 0.9825$) (Figure 2A). To directly visualize the pattern of RPF distribution on individual transcripts, we built a ribosome density map across the entire transcriptome (Figure 2B). Compared to control cells, the presence of both AZC and MG132 led to a clear enrichment of RPF density at the 5′ end of coding sequences (CDSs) on the vast majority of mRNAs. Metagene analysis revealed a pronounced accumulation of RPF reads within the first 50 codon region of transcripts in cells treated with both AZC and MG132 (Figure 2C). We defined the ribosome pausing index (PI) of individual transcripts by calculating the normalized ribosome density within a 50 codon window from the start codon (5′ PI) or stop codon (3′ PI), respectively. In cells under proteotoxic stress, the median 5′ PI showed more than a 2-fold increase as compared to control cells (Figure 2D). Intriguingly, proteotoxic stress also caused an elevation of RPF density in the 5′ untranslated region (5′ UTR) (Figure 2C),

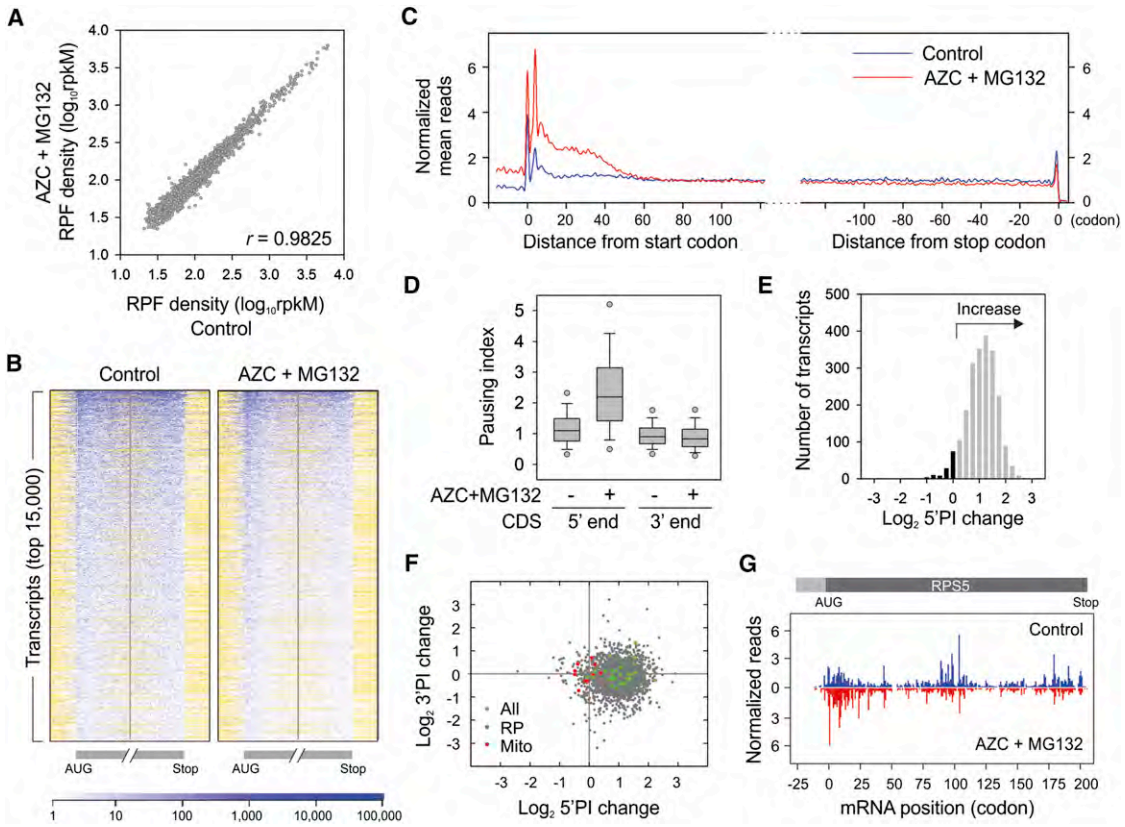

Figure 2. Intracellular proteotoxic stress triggers early elongation pausing of ribosomes.

(A) HEK293cells were treated with 10 mM AZC and 20 μM MG132 for 60 min before ribosome profiling. Ribosome densities of cells with or without treatment are plotted for comparison. The density in reads per kilobase of coding sequence per million mapped reads (rpkM) is a measure of overall translation along each transcript.

(B) Ribosome density heat-maps of cells with or without treatment. The entire transcriptome is sorted based on total RPF reads and the top 15,000 transcripts are aligned in row. Both the first and last 160 codon regions of CDS are shown, together with flanking 40 codon untranslated regions. Read density is represented in blue. White indicates regions without reads, whereas yellow indicates regions without sequence. A short 5′ UTR has yellow region before the AUG, whereas a short 3′ UTR has yellow region after the stop codon.

(C) Metagene analysis of early ribosome pausing of cells with or without treatment. Normalized RPF reads are averaged across the entire transcriptome, aligned at either their start (left panel) or stop (right panel) codon, and plotted as smoothed lines.

(D) Ribosome pausing index (PI) is determined in a 50 codon window at the beginning (5′ end) and end (3′ end) of CDS, respectively. Both the 5′ and 3′ PI of each transcript in cells with or without treatment are shown in box plots with single dots as 5th and 95th percentile.

(E) Distribution of 5′PI changes in cells with proteotoxic stress. The $\log_2$ change of 5′PI after AZC and MG132 treatment is plotted, with the increase shown in gray bar and the decrease in black.

(F) Changes of 5′PI and 3′PI after AZC and MG132 treatment. The $\log_2$ change is computed across the entire transcriptome, and presented as a scatter plot with green dots for genes encoding ribosome subunits (RP) and red dots for mitochondria-encoded genes (Mito).

(G) A typical example of early elongation pausing under proteotoxic stress. RPF reads density is shown on the CDS of *RPS5* with or without AZC and MG132 treatment. See also Figure S2–S4.

an indication of wide-spread alternative initiation under stress conditions.

A large portion of mRNAs showed an increased 5′ PI in response to proteotoxic stress (Figure 2E, gray bar). However, a small group of transcripts showed less change or even decreased 5′ PI (Figure 2E, black bar). At the transcriptome level, neither the CDS length nor the overall translation had any strong correlation with the changes of 5′ PI (Figures S2A and S2B). Gene ontology (GO) analysis revealed that genes involving ATP synthesis (e.g., mitochondria-encoded genes) were enriched in the group with decreased 5′ PI in response to proteotoxic stress (Figures S2C, S2D, and 2F). In contrast, genes with increased 5′ PI were involved in cellular processes like RNA metabolism and translation (e.g., ribosomal proteins). As a typical example, proteotoxic stress led to a clear ribosome accumulation near the beginning of the RPS5 CDS region (Figure 2G).

Through an independent biological replicate, we confirmed the early elongation pausing of ribosomes in response to proteotoxic stress (Figure S3). The global RPF distribution was highly reproducible across the replicates (Figure S3E). Notably, treatment with either AZC or MG132 alone had little effect on the ribosome dynamics (Figures S4A and S4B). In particular, we saw no

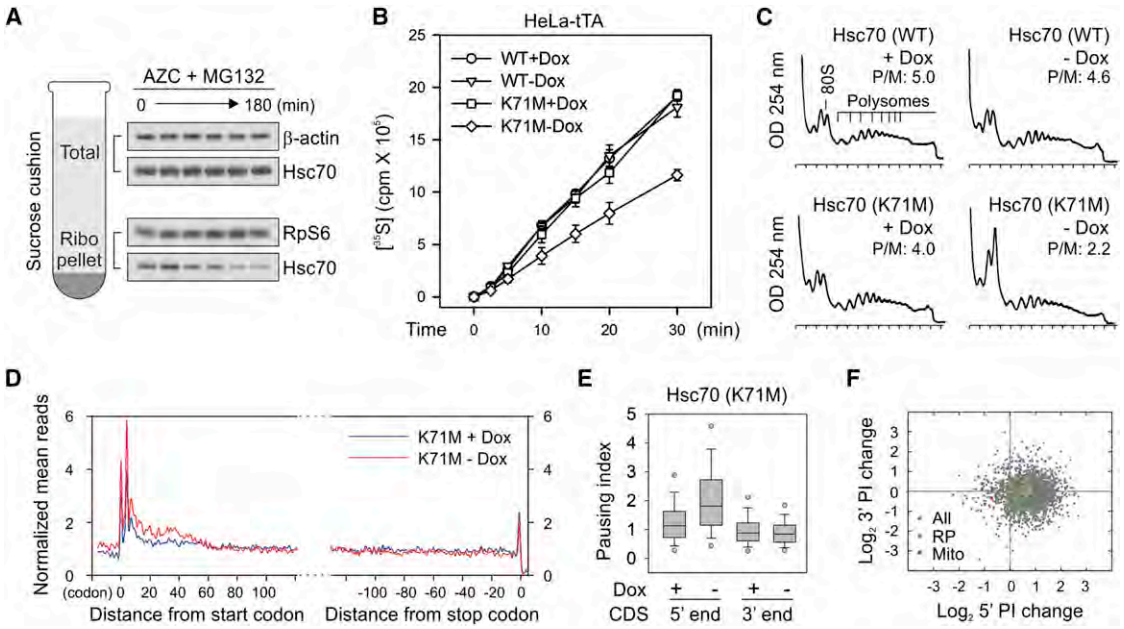

Figure 3. Disrupting Endogenous Hsc70 Recapitulates the Effects of Proteotoxic Stress on Early Elongation Pausing

(A) Sucrose cushion analysis of ribosome-associated Hsc70 along with AZC and MG132 treatment. Both the total and ribosome pellet were immunoblotted using antibodies as indicated.

(B) Global protein synthesis was analyzed in HeLa-tTA cells infected with adenoviruses expressing Hsc70(WT) and Hsc70(K71M). Transgene expression was induced by 12 hr Dox removal. [^{35}S] radioactivity of TCA-insoluble material was measured at given times. Means ± SEM of three experiments are shown.

(C) Polysome profiles were determined from cells as in (B) using sucrose gradient sedimentation.

(D) Metagene analysis for early elongation pausing in cells with or without Hsc70(K71M) expression. Normalized RPF reads are averaged across the entire transcriptome, aligned at either their start (left panel) or stop (right panel) codon.

(E) Both the 5′ and 3′ PI of each transcript in cells with or without Hsc70(K71M) expression are shown in box plots.

(F) Changes of 5′ PI and 3′ PI after Hsc70(K71M) expression. The $\log_2$ change is computed across the entire transcriptome and presented as a scatter plot with green dots for genes encoding ribosome subunits and red dots for mitochondria-encoded genes. See also Figure S5.

unique pausing sites at individual codons in the presence of AZC (Figure S4C). These results argue that the presence of AZC-charged transfer RNA (tRNA) neither perturbs the intracellular pool of amino acids nor alters the behavior of translating ribosomes. Therefore, it is the accumulation of misfolded proteins that triggers the early elongation pausing.

A Dominant-Negative Hsc70 Mutant Induces Early Elongation Pausing of Ribosomes

The approximate 50 codon region where the elongation pausing occurs under proteotoxic stress corresponds remarkably well to the length of polypeptide needed to fill the exit tunnel of the ribosome (approximately 30–40 amino acids in extended conformation) (Kramer et al., 2009). This raises an intriguing possibility that the changing environment of nascent polypeptides from the ribosome tunnel to the cytosol might influence the dynamics of translating ribosomes. Within the cellular environment, the emerging nascent chains interact with molecular chaperones that guide their folding process. At the forefront is Hsc/Hsp70, which transiently associates with a large fraction of nascent chains (Frydman, 2001; Hansen et al., 1999; Kampinga and Craig, 2010). This led us to hypothesize that the accumulated misfolded proteins titrate out the intracellular chaperone pool and the lack of chaperone association might prevent nascent chains from protruding out of the ribosome exit tunnel. The elongation slowdown at this position probably causes ribosomes to pile up over the first 50 codon region. Supporting the notion that proteotoxic stress sequesters intracellular chaperone molecules, we observed a progressive loss of ribosome-associated Hsc70 along with AZC and MG132 treatment (Figure 3A). To test the hypothesis that reduced chaperone availability leads to an early elongation pausing, we first used a dominant-negative mutant Hsc70 (K71M), which sequesters and inactivates the endogenous Hsc70 molecules (Newmyer and Schmid, 2001). The integrated ''tet-off'' system allows a rapid induction of the transgene expression in HeLa-tTA cells after removal of doxycycline (Dox) (Figure S5A). After 12 hr of transgene induction by removal of Dox, [^{35}S] metabolic labeling revealed an ~40% decrease of the global protein synthesis (Figure 3B). Similar to cells treated with both AZC and MG132, Hsc70(K71M) expression caused disassembly of polysomes with a concomitant increase of 80S peak (Figure 3C).

To evaluate whether Hsc70(K71M) expression leads to an early elongation pausing, we performed deep sequencing of RPFs extracted from the polysomes of HeLa-tTA cells with or without transgene induction. Metagene analysis revealed a modest excess (~1.6-fold) in density over the initial 50 codons after Hsc70(K71M) expression (Figure 3D and 3E). This is similar

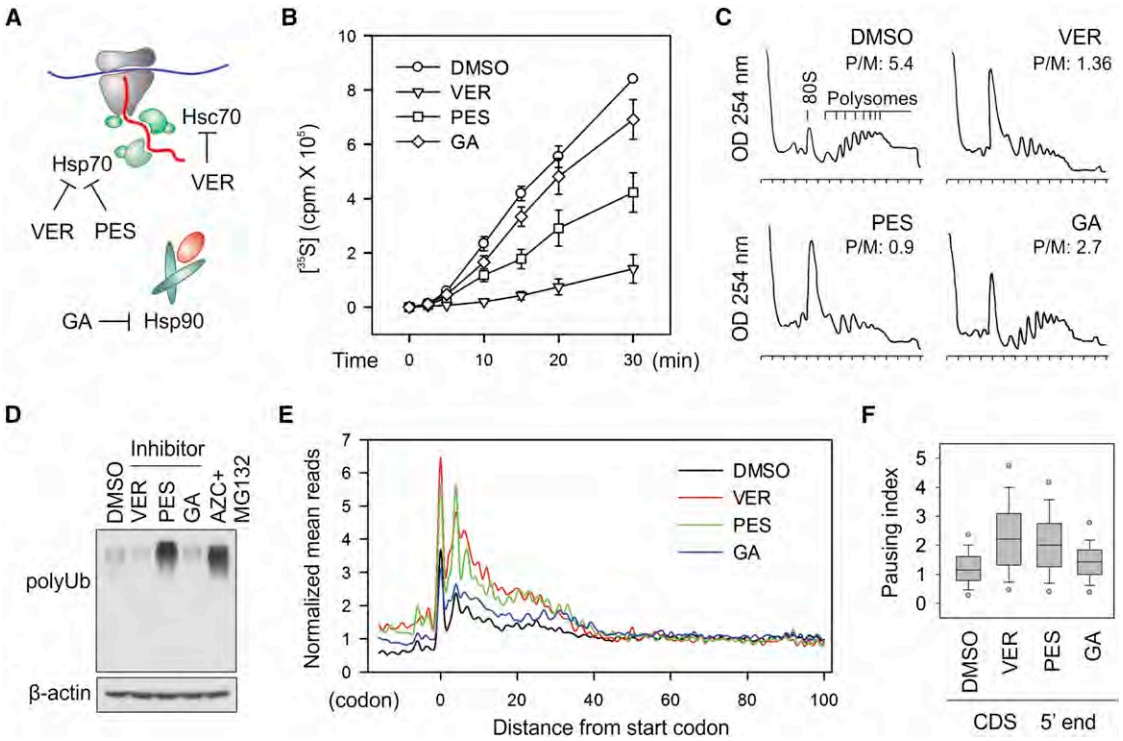

Figure 4. Direct Hsc/Hsp70 Inhibition Induces Early Elongation Pausing of Ribosomes

(A) Schematic for chaperone targets of small-molecule inhibitors. VER inhibits Hsc70, Hsp70, and Grp78 (not shown) and PES selectively inhibits Hsp70, whereas GA is a specific inhibitor of Hsp90.

(B) Global protein synthesis was analyzed in HEK293 cells treated with 100 μM VER, 50 μM PES, or 1 μM GA for 60 min. [^{35}S] radioactivity of TCA-insoluble material was measured at given times. Means ± SEM of three experiments are shown.

(C) Polysome profiles were determined from cells treated with chaperone inhibitors as in (B) using sucrose gradient sedimentation.

(D) Immunoblotting of whole-cell lysates from cells treated with chaperone inhibitors as in (B).

(E) Metagene analysis for early elongation pausing in cells treated with chaperone inhibitors as in (B). Normalized RPF reads are averaged across the entire transcriptome, aligned at their start codon.

(F) The 5′ PI of each transcript in cells treated with chaperone inhibitors as in (B) are shown in box plots. See also Figure S6.

in pattern to, but of smaller magnitude than, the early elongation pausing seen in cells treated with both AZC and MG132 (Figure 2B). We repeated the experiment and obtained the similar extent of elongation pausing in the presence of Hsc70(K71M) (Figure S5). Similar to AZC and MG132 treatment, there was an evident separation between genes encoding ribosome subunits and mitochondria proteins in response to the Hsc70(K71M) expression (Figure 3F). The 5′ PI changes also showed a good correlation between the two conditions (r = 0.65), although different cell lines were used (Figure S5F). Thus, interfering with endogenous Hsc70 recapitulates the effects of the proteotoxic stress in triggering early elongation pausing.

Direct Hsc/Hsp70 Inhibition Induces Early Elongation Pausing of Ribosomes

The dominant-negative Hsc70(K71M) mutant induced a rather weak elongation pausing when compared to AZC and MG132 treatment. It was probably due to an adaptive stress response under 12 hr of Hsc70(K71M) expression, in which the subsequent induction of Hsp70 compromised the early elongation pausing (Figure S5A). In contrast, 60 min of AZC and MG132 treatment did not yet trigger Hsp70 expression due to the time lag. Additionally, the continuous presence of the analog prevents the production of functional chaperones, if any. To address whether chaperones play a direct role in translation elongation, we applied several specific chaperone inhibitors to HEK293 cells and monitored global protein synthesis (Figure 4A). VER-155008 (VER) is a potent inhibitor of the Hsp70 family chaperones (Massey et al., 2010), whereas 2-phenylethyenesulfo-namide (PES) acts as a direct inhibitor of stress-inducible Hsp70 (Leu et al., 2011). We also included a specific Hsp90 inhibitor geldanamycin (GA) to examine the role of different chaperones in ribosome behavior. To minimize the compensatory stress response, we only treated cells with these inhibitors for 60 min. This short treatment allows us to capture direct effects of chaperone inhibition without inducing massive accumulation of misfolded proteins.

Metabolic radiolabeling analysis revealed that both VER and PES potently inhibited [^{35}S] incorporation, whereas the Hsp90 inhibitor GA slightly reduced the level of global protein synthesis (Figure 4B). The extent of translation repression was also reflected in the pattern of polysome profile, in which the inhibitors of Hsp70 family protein, but not Hsp90, disassembled the

polysome (Figure 4C). Despite the most severe inhibition of protein synthesis, 60 min treatment of VER resulted in little accumulation of ubiquitin-conjugated species in cells (Figure 4D). In addition, the steady-state chaperone levels remained unchanged in the presence of these inhibitors (Figure S6), suggesting that the stress response after 60 min of chaperone inhibition was minimal. We next performed deep sequencing of RPFs derived from the cells treated with these chaperone inhibitors. Metagene analysis revealed a prominent excess of ribosome density over the first 50 codon region in cells treated with either VER or PES (Figures 4E and 4F). Only a minor effect was observed after GA-mediated Hsp90 inhibition. Collectively, these results indicate that direct inhibition of Hsp70 family proteins triggers early elongation pausing of ribosomes.

Cotranslational Interaction of Nascent Chains Influences Elongation Rate

Hsp70 family proteins, including BiP of the endoplasmic reticulum (ER) and mtHsp70 of the mitochondrion, are essential for protein translocation across the membrane via unidirectional pulling (Jensen and Johnson, 1999). It is likely that the cytosol Hsc/Hsp70 uses the similar mechanism to pull the emerging polypeptide out of the ribosome exit tunnel. Two models have been proposed to describe how Hsp70 can generate such driving force: "trapping" and "power stroking" (Goloubinoff and De Los Rios, 2007). While both models rely on direct interactions, the latter requires ATP hydrolysis. We hypothesize that the Hsc/Hsp70 "trapping" might be sufficient to exert an entropy pulling force because most nascent chains emerging the exit tunnel are unfolded. To investigate whether cotranslational protein interaction would generate the "pulling" force for the ribosome-bound nascent chain, we utilized the heterodimerization property of FKBP12-rapamycin binding domain (FRB) and FK506 binding protein (FKBP), whose high-affinity binding can be induced by the small molecule rapamycin (Choi et al., 1996; Qian et al., 2009). We constructed a fusion protein, FRB-GFP, in order to evaluate whether the association of the NH_2-terminal FRB domain with the added FKBP protein during translation would affect the elongation rate of the carboxyl terminal GFP. In an in vitro translation system based on rabbit reticulocyte lysate (RRL), we compared the translation efficiency of FRB-GFP after supplementation with the recombinant FKBP protein. Remarkably, upon addition of 1 μM rapamycin to the RRL, the kinetics of FRB-GFP completion showed a significant acceleration (Figure 5A, left panel). We observed similar effects after swapping the FRB and FKBP domains (Figure 5A, right panel). Thus, cotranslational interaction between nascent chains and specific binding partners promotes the elongation of emerging polypeptides.

In order to extend these findings from RRL to mammalian cells, we utilized a well-characterized rapamycin analog AP21967 (rapalog) and a mutant FRB domain (FRB*) to avoid interfering with the endogenous mTOR function (Klemm et al., 1998). A HEK293 cell line stably expressing FRB*-GFP was transfected with plasmid-borne FKBP. After 60 min of pre-incubation with rapalog, polysome fractions were isolated followed by deep sequencing of RPFs. Notably, the presence of rapalog had little effect on the pattern of RPFs across the entire transcriptome (Figure S7). However, the FRB*-GFP transcript exhibited an altered distribution of RPF reads after rapalog treatment (Figure 5B). When the total reads mapped to the FRB* domain were normalized to be equal, rapalog treatment resulted in a 34% decrease of the average RPF density in the coding region of GFP (Figure 5B, bottom panel). Single-codon comparison revealed that the reduction of RPF reads mainly occurred at the ribosome pausing sites of GFP. Since the RPF density on a given codon is proportional to the average ribosome dwell time there, the reduced ribosome density after cotranslational interaction between FRB* and FKBP suggests an accelerated elongation for the remaining polypeptide.

Increasing Chaperone Availability Restores Translation Efficiency

The functional connection between chaperone availability and translation elongation underscores the central role of chaperones in protein homeostasis. Based on our results, we expected that chaperone overexpression might prevent the translation inhibition under proteotoxic stress. However, it is inherently difficult to alter the chaperone levels in cells because the chaperone concentration is controlled closely by the heat shock transcription factor 1 (HSF1) (Morimoto, 2008). Overexpression of exogenous chaperone genes inevitably suppresses the endogenous chaperone expression. To circumvent this limitation, we established an in vitro translation system programmed from cells with or without proteotoxic stress (Figure 5C, left panel). We first examined the translation efficiency using a synthesized bicistronic mRNA containing the polio internal ribosome entry site (IRES) between *Renilla* luciferase (Rluc) and Fluc. While the synthesis of Fluc is cap dependent, translation of Rluc is driven by IRES via a cap-independent mechanism (Sun et al., 2011). In lysates derived from stressed cells, the synthesis of both Rluc and Fluc was equally reduced in comparison with the control cell lysates (Figure 5C, right panel). This result further supports the notion that proteotoxic stress does not primarily inhibit cap-dependent initiation.

Next we monitored the translation efficiency of a synthesized Fluc mRNA in cell lysates supplemented with recombinant chaperone molecules. Adding recombinant Hsc70, but not bovine serum albumin, increased the Fluc activities in a dose-dependent manner (Figure 5D). Cotranslational folding of Fluc has been shown to be quite efficient (Kolb et al., 2000), so the translation rate is likely to be the major determinant of luciferase activity in the in vitro translation system. Notably, the chaperone-mediated rescue effect was more dramatic in the system derived from the stressed cells than the control. Therefore, increasing chaperone availability restores the translation efficiency.

DISCUSSION

The journey of a nascent polypeptide starts in the pepetidyl transferase center of the ribosome, from where it then traverses the peptide exit tunnel. Once the nascent chain begins to emerge from the exit tunnel, it faces a drastic environmental change. Surprisingly, most recent ribosome profiling data did not show any specific pausing sites corresponding to this turning point

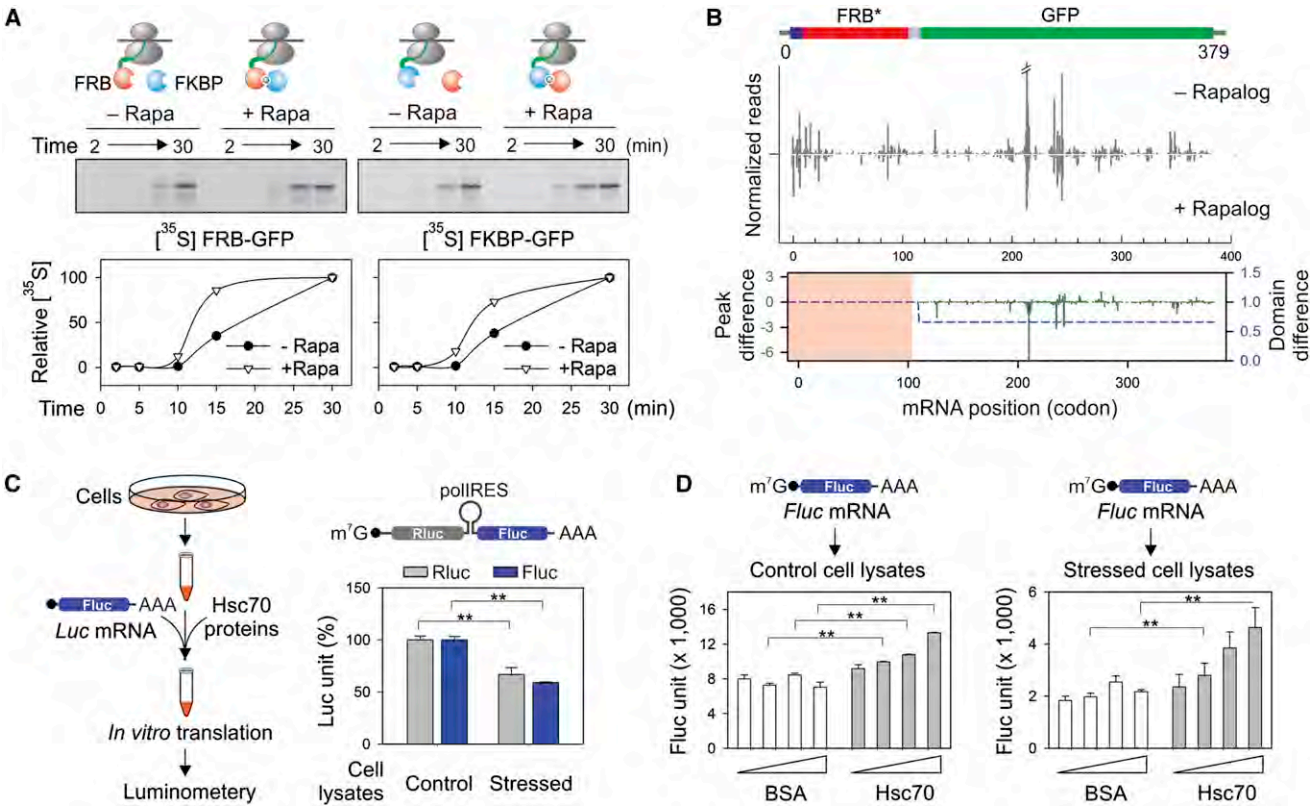

Figure 5. Cotranslational Interaction of Nascent Chains Facilitates the Elongation of Polypeptides

(A) Effects of FKBP (blue ball) on the in vitro translation of FRB-GFP (red ball) in the absence or presence of 1 μM rapamycin (left panel). The right panel shows the effects of FRB (red ball) on the in vitro translation of FKBP-GFP (blue ball) in the absence or presence of 1 μM rapamycin. Autoradiography of full-length GFP fusion protein is quantitated and plotted as a function of time.

(B) HEK293-expressing FRB*-GFP was transfected with the plasmid encoding FKBP. Cells were pretreated with 1 μM rapalog for 60 min before polysome profiling. The RPF density profiles are shown for the transgene FRB*-GFP with and without rapalog treatment. The RPF reads density is normalized based on the FRB* domain. The average change of RPF density over the entire GFP region (blue dot line) and single-codon change (green line) are plotted together (Wilcoxon signed-rank test, $p = 3 \times 10^{-4}$). See also Figure S7.

(C) Schematic of experimental design using recombinant Hsc70 protein to restore translation efficiency using an in vitro translation system programmed from cells with or without proteotoxic stress. The right panel shows the relative translation efficiency of a synthesized bicistronic mRNA containing a polio IRES element between Rluc and Fluc. Error bar: SEM. **$p < 0.001$.

(D) The in vitro translation system as (C) was used to translate a synthesized Fluc mRNA in the absence or presence of recombinant Hsc70. Error bar: SEM. **$p < 0.01$.

(Guo et al., 2010; Ingolia et al., 2011). The smooth transition from the inside of the tunnel to the outside ribosome surface is probably due to the presence of ribosome-associated chaperone systems (Kramer et al., 2009). Our study provides strong evidence that the Hsc/Hsp70 family protein plays a crucial role in the passage of nascent chains upon emerging from the ribosome exit tunnel. Reducing chaperone availability by proteotoxic stress or chemical inhibitors unequivocally caused a pileup of ribosomes on the first 50 codon region of transcripts. Notably, we did not observe any specific RPF spikes at specific codon positions, suggesting that the lack of chaperone association slows down rather than stops the elongation. The feature of ribosome stacking at the 5′ end of the CDS further indicates that the stress-induced elongation pausing precedes the suppression of translation initiation.

mRNA translation proceeds not at a constant rate but rather in a stop-and-go traffic manner (Fredrick and Ibba, 2010). Variations of elongation speed may result from local stable mRNA structure (Gray and Hentze, 1994) or the presence of rare codons (Elf et al., 2003; Lavner and Kotlar, 2005). Interestingly, nascent chains could also induce translational pausing in a sequence-specific manner (Kramer et al., 2009). Our results uncover an additional layer of elongation regulation mediated by the ribosome-associated chaperone system. The Hsc/Hsp70 family protein, like the ER and mitochondrion counterparts, not only assists cotranslational folding but also accelerates the elongation of nascent polypeptides primarily at the site where the nascent polypeptide emerges from the ribosome exit tunnel. Early studies in *S. cerevisiae* reported a similar function for Ssb, although identifying the elongation pausing sites was beyond the technical ability at that time (Nelson et al., 1992). Since multiple factors constitute the chaperone network linked to protein synthesis (Albanèse et al., 2006), it will be intriguing to determine whether interfering specific chaperone or

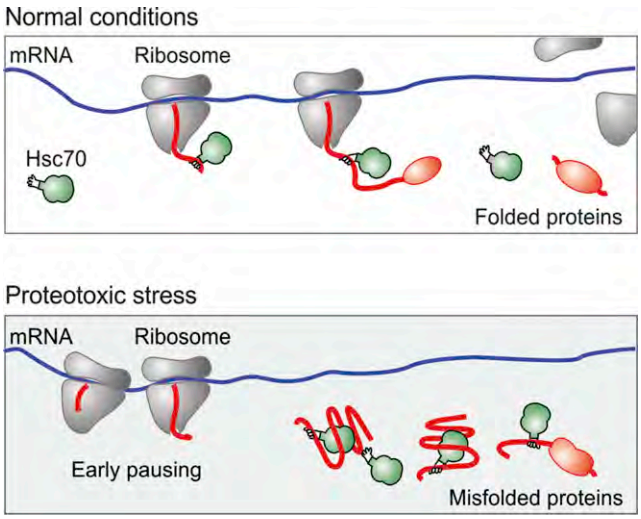

Figure 6. A Model for Cotranslational Stress Response via Early Ribosome Pausing

The cytosolic chaperone molecules, such as Hsc70 (green), not only assist the cotranslational folding, but also facilitate the elongation of emerging polypeptides (red). Under the condition of proteotoxic stress, the accumulation of misfolded proteins titrates out molecular chaperones. The lack of cotranslational interaction of chaperone molecules leads to early elongation pausing and rapid suppression of global protein synthesis.

cochaperone molecules cause selective elongation pausing on a subset of transcripts.

Despite the apparent abundance of chaperone molecules in cells, their concentration is titrated closely to the folding requirements within a specific cell type (Morimoto, 2008). Cells exploit chaperone availability as a sensing mechanism to induce stress response. At the level of transcription, reduced chaperone availability triggers the activation of HSF1 (Morimoto, 1998). As a result, more chaperone molecules will be produced to restore the protein homeostasis. The functional connection between chaperone availability and translation elongation offers an intriguing mode of regulation in response to stress conditions (Figure 6). Intracellular accumulation of misfolded proteins, a common feature of a variety of stress conditions, sequesters molecular chaperones, and the lack of chaperone association with the ribosome delays nascent chains from emerging. Our data suggest that the ribosome fine tunes the elongation rate based on the chaperone availability to match protein production with the intracellular folding capacity. This level of control allows a rapid change in the complement of proteins prior to transcriptional regulation. The early elongation pausing under proteotoxic stress thus represents the very first line of protective response for cells to maintain intracellular protein homeostasis.

EXPERIMENTAL PROCEDURES

Ribosome Profiling and Data Analysis

Ribosome profiling was performed based on the reported protocol (Ingolia et al., 2009) with minor modifications. Cells were lysed in polysome lysis buffer (10 mM HEPES, 100 mM KCl, 5 mM $MgCl_2$, 100 μg/ml cycloheximide, and 2% Triton X-100 [pH 7.4]) and cleared lysates were separated by sedimentation through sucrose gradients. Separated samples were fractionated and OD254 values were continually monitored. Collected polysome fractions were digested with ribonuclease I and the RPF fragments were size-selected and purified by gel extraction. After the library construction, deep sequencing was performed using Illumina HiSEQ2000. The trimmed RPF reads were aligned to Ensembl human transcriptome reference by SOAP 2.0 allowing two mismatches. The metagene analysis was carried out by calculating the normalized mean reads density at each codon position. The ribosome pausing index (5′ PI) was defined as the ratio between the read density in the first 50 codon window and the immediate following 100 codon region. Additional details are available in Supplemental Experimental Procedures.

[^{35}S] Pulse Assay and Ribosomal Half-Transit Time

After the treatment as indicated, cells were metabolically labeled in pulsing medium containing 10 μCi [^{35}S] mix (Perkin Elmer). An aliquot of cells was withdrawn at each time point and mixed with stop medium. Cells were lysed with polysome lysis buffer and lysates were cleared by centrifugation. For the measurement of ribosomal half-transit time, 100 μl lysates was mixed with 350 μl polysome buffer and 450 μl 0.14M sucrose in polysome buffer. A 400 μl mixture was saved for measurement of total [^{35}S] incorporation. Ribosomes were pelleted from the remaining 500 μl mixture by centrifugation at 60,000 rpm for 15 min at 4°C using a Beckman TLA-100.4 rotor. Four hundred micro liters of supernatant was taken to measure the [^{35}S] incorporation into the completed polypeptide. Proteins were precipitated with 10% Trichloroacetic acid (Sigma). The precipitates were collected on GF/C filter membrane (Watman) and the [^{35}S] incorporation was measured by scintillation counting (Beckman).

Immunoprecipitation

Cells were pretreated with 100 μg/ml cycloheximide at 37°C for 3 min to stabilize the ribosome-nascent chain complex and then scraped extensively in polysome lysis buffer supplemented with EDTA-free cocktail protease inhibitor (Roche). After clearance by centrifugation, the supernatant was collected and incubated with anti-Flag M2 affinity gel (Sigma) at 4°C for 60 min. The beads were extensively washed three times with polysome lysis buffer, and the associated proteins were eluted by heating for 10 min in the sample buffer.

In Vitro Translation

Fluc mRNA was synthesized through in vitro transcription using mMESSAGE mMACHINE T7 ULTRA Kit (Ambion). Programmed in vitro translation was performed following the published protocol (Rakotondrafara and Hentze, 2011). Cell extracts were prepared from HEK293 cells with or without 60 min treatment of 10 mM AZC and 20 μM MG132. Control and stressed cell lysates were adjusted to be equal based on protein concentration. In vitro translation was incubated at 37°C for 2 hr, and luciferase substrate (Promega) was added to measure the Fluc activity by luminometry. For in vitro translation of FRB or FKBP assay, TNT Quick Coupled Translation /Transcription system (Promega) was used. pcDNA3 plasmid encoding FRB-GFP or FKBP-GFP was mixed with RRL supplemented with [^{35}S] L-methionine and recombinant proteins as indicated. In vitro translation was performed in the presence or absence of 1 μM rapamycin. The products at different time points were collected and resolved on SDS-PAGE. The gel was dried and viewed by phosphor imaging screen (HE healthcare) and the band intensity was quantified using ImageQuant 5.2.

ACCESSION NUMBERS

Sequencing data were deposited in the SRA database with the accession number SRA061778.

SUPPLEMENTAL INFORMATION

Supplemental Information includes Supplemental Experimental Procedures and seven figures and can be found with this article online at http://dx.doi.org/10.1016/j.molcel.2012.12.001.

ACKNOWLEDGMENTS

We would like to thank Qian lab members for helpful discussion and Drs. Patsy Brannon and William Brown for critical reading of the manuscript. We also thank Jonathan Yewdell (NIH) for providing adenoviruses expressing Hsc70(WT) and Hsc70(K71M), as well as Cornell University Life Sciences Core Laboratory Center for performing deep sequencing. This work was supported by grants to S.-B.Q. from National Institutes of Health (1 DP2 OD006449-01), Ellison Medical Foundation (AG-NS-0605-09), and DOD Exploration-Hypothesis Development Award (TS10078).

Received: April 5, 2012
Revised: June 25, 2012
Accepted: November 30, 2012
Published: January 3, 2013

REFERENCES

Albanèse, V., Yam, A.Y., Baughman, J., Parnot, C., and Frydman, J. (2006). Systems analyses reveal two chaperone networks with distinct functions in eukaryotic cells. Cell *124*, 75–88.

Buchan, J.R., and Parker, R. (2009). Eukaryotic stress granules: the ins and outs of translation. Mol. Cell *36*, 932–941.

Bukau, B., Weissman, J., and Horwich, A. (2006). Molecular chaperones and protein quality control. Cell *125*, 443–451.

Choi, J., Chen, J., Schreiber, S.L., and Clardy, J. (1996). Structure of the FKBP12-rapamycin complex interacting with the binding domain of human FRAP. Science *273*, 239–242.

del Alamo, M., Hogan, D.J., Pechmann, S., Albanese, V., Brown, P.O., and Frydman, J. (2011). Defining the specificity of cotranslationally acting chaperones by systematic analysis of mRNAs associated with ribosome-nascent chain complexes. PLoS Biol. *9*, e1001100.

Elf, J., Nilsson, D., Tenson, T., and Ehrenberg, M. (2003). Selective charging of tRNA isoacceptors explains patterns of codon usage. Science *300*, 1718–1722.

Fredrick, K., and Ibba, M. (2010). How the sequence of a gene can tune its translation. Cell *141*, 227–229.

Frydman, J. (2001). Folding of newly translated proteins in vivo: the role of molecular chaperones. Annu. Rev. Biochem. *70*, 603–647.

Goldberg, A.L., and Dice, J.F. (1974). Intracellular protein degradation in mammalian and bacterial cells. Annu. Rev. Biochem. *43*, 835–869.

Goloubinoff, P., and De Los Rios, P. (2007). The mechanism of Hsp70 chaperones: (entropic) pulling the models together. Trends Biochem. Sci. *32*, 372–380.

Gray, N.K., and Hentze, M.W. (1994). Regulation of protein synthesis by mRNA structure. Mol. Biol. Rep. *19*, 195–200.

Gray, N.K., and Wickens, M. (1998). Control of translation initiation in animals. Annu. Rev. Cell Dev. Biol. *14*, 399–458.

Guo, H., Ingolia, N.T., Weissman, J.S., and Bartel, D.P. (2010). Mammalian microRNAs predominantly act to decrease target mRNA levels. Nature *466*, 835–840.

Hansen, W.J., Cowan, N.J., and Welch, W.J. (1999). Prefoldin-nascent chain complexes in the folding of cytoskeletal proteins. J. Cell Biol. *145*, 265–277.

Hartl, F.U., Bracher, A., and Hayer-Hartl, M. (2011). Molecular chaperones in protein folding and proteostasis. Nature *475*, 324–332.

Holcik, M., and Sonenberg, N. (2005). Translational control in stress and apoptosis. Nat. Rev. Mol. Cell Biol. *6*, 318–327.

Ingolia, N.T., Ghaemmaghami, S., Newman, J.R., and Weissman, J.S. (2009). Genome-wide analysis in vivo of translation with nucleotide resolution using ribosome profiling. Science *324*, 218–223.

Ingolia, N.T., Lareau, L.F., and Weissman, J.S. (2011). Ribosome profiling of mouse embryonic stem cells reveals the complexity and dynamics of mammalian proteomes. Cell *147*, 789–802.

Jackson, R.J., Hellen, C.U., and Pestova, T.V. (2010). The mechanism of eukaryotic translation initiation and principles of its regulation. Nat. Rev. Mol. Cell Biol. *11*, 113–127.

Jaiswal, H., Conz, C., Otto, H., Wölfle, T., Fitzke, E., Mayer, M.P., and Rospert, S. (2011). The chaperone network connected to human ribosome-associated complex. Mol. Cell. Biol. *31*, 1160–1173.

Jensen, R.E., and Johnson, A.E. (1999). Protein translocation: is Hsp70 pulling my chain? Curr. Biol. *9*, R779–R782.

Kampinga, H.H., and Craig, E.A. (2010). The HSP70 chaperone machinery: J proteins as drivers of functional specificity. Nat. Rev. Mol. Cell Biol. *11*, 579–592.

Kedersha, N., Cho, M.R., Li, W., Yacono, P.W., Chen, S., Gilks, N., Golan, D.E., and Anderson, P. (2000). Dynamic shuttling of TIA-1 accompanies the recruitment of mRNA to mammalian stress granules. J. Cell Biol. *151*, 1257–1268.

Klemm, J.D., Schreiber, S.L., and Crabtree, G.R. (1998). Dimerization as a regulatory mechanism in signal transduction. Annu. Rev. Immunol. *16*, 569–592.

Kolb, V.A., Makeyev, E.V., and Spirin, A.S. (2000). Co-translational folding of an eukaryotic multidomain protein in a prokaryotic translation system. J. Biol. Chem. *275*, 16597–16601.

Kramer, G., Boehringer, D., Ban, N., and Bukau, B. (2009). The ribosome as a platform for co-translational processing, folding and targeting of newly synthesized proteins. Nat. Struct. Mol. Biol. *16*, 589–597.

Lavner, Y., and Kotlar, D. (2005). Codon bias as a factor in regulating expression via translation rate in the human genome. Gene *345*, 127–138.

Leu, J.I., Pimkina, J., Pandey, P., Murphy, M.E., and George, D.L. (2011). HSP70 inhibition by the small-molecule 2-phenylethynesulfonamide impairs protein clearance pathways in tumor cells. Mol. Cancer Res. *9*, 936–947.

Ma, X.M., and Blenis, J. (2009). Molecular mechanisms of mTOR-mediated translational control. Nat. Rev. Mol. Cell Biol. *10*, 307–318.

Massey, A.J., Williamson, D.S., Browne, H., Murray, J.B., Dokurno, P., Shaw, T., Macias, A.T., Daniels, Z., Geoffroy, S., Dopson, M., et al. (2010). A novel, small molecule inhibitor of Hsc70/Hsp70 potentiates Hsp90 inhibitor induced apoptosis in HCT116 colon carcinoma cells. Cancer Chemother. Pharmacol. *66*, 535–545.

McClellan, A.J., Tam, S., Kaganovich, D., and Frydman, J. (2005). Protein quality control: chaperones culling corrupt conformations. Nat. Cell Biol. *7*, 736–741.

Morimoto, R.I. (1998). Regulation of the heat shock transcriptional response: cross talk between a family of heat shock factors, molecular chaperones, and negative regulators. Genes Dev. *12*, 3788–3796.

Morimoto, R.I. (2008). Proteotoxic stress and inducible chaperone networks in neurodegenerative disease and aging. Genes Dev. *22*, 1427–1438.

Nelson, R.J., Ziegelhoffer, T., Nicolet, C., Werner-Washburne, M., and Craig, E.A. (1992). The translation machinery and 70 kd heat shock protein cooperate in protein synthesis. Cell *71*, 97–105.

Newmyer, S.L., and Schmid, S.L. (2001). Dominant-interfering Hsc70 mutants disrupt multiple stages of the clathrin-coated vesicle cycle in vivo. J. Cell Biol. *152*, 607–620.

Nielsen, P.J., and McConkey, E.H. (1980). Evidence for control of protein synthesis in HeLa cells via the elongation rate. J. Cell. Physiol. *104*, 269–281.

Oh, E., Becker, A.H., Sandikci, A., Huber, D., Chaba, R., Gloge, F., Nichols, R.J., Typas, A., Gross, C.A., Kramer, G., et al. (2011). Selective ribosome profiling reveals the cotranslational chaperone action of trigger factor in vivo. Cell *147*, 1295–1308.

Qian, S.B., Waldron, L., Choudhary, N., Klevit, R.E., Chazin, W.J., and Patterson, C. (2009). Engineering a ubiquitin ligase reveals conformational flexibility required for ubiquitin transfer. J. Biol. Chem. *284*, 26797–26802.

Qian, S.B., Zhang, X., Sun, J., Bennink, J.R., Yewdell, J.W., and Patterson, C. (2010). mTORC1 links protein quality and quantity control by sensing chaperone availability. J. Biol. Chem. *285*, 27385–27395.

Rakotondrafara, A.M., and Hentze, M.W. (2011). An efficient factor-depleted mammalian in vitro translation system. Nat. Protoc. *6*, 563–571.

Ron, D., and Walter, P. (2007). Signal integration in the endoplasmic reticulum unfolded protein response. Nat. Rev. Mol. Cell Biol. *8*, 519–529.

Saini, P., Eyler, D.E., Green, R., and Dever, T.E. (2009). Hypusine-containing protein eIF5A promotes translation elongation. Nature *459*, 118–121.

Sonenberg, N., and Hinnebusch, A.G. (2009). Regulation of translation initiation in eukaryotes: mechanisms and biological targets. Cell *136*, 731–745.

Spriggs, K.A., Bushell, M., and Willis, A.E. (2010). Translational regulation of gene expression during conditions of cell stress. Mol. Cell *40*, 228–237.

Sun, J., Conn, C.S., Han, Y., Yeung, V., and Qian, S.B. (2011). PI3K-mTORC1 attenuates stress response by inhibiting cap-independent Hsp70 translation. J. Biol. Chem. *286*, 6791–6800.

Trotter, E.W., Kao, C.M., Berenfeld, L., Botstein, D., Petsko, G.A., and Gray, J.V. (2002). Misfolded proteins are competent to mediate a subset of the responses to heat shock in Saccharomyces cerevisiae. J. Biol. Chem. *277*, 44817–44825.

Zhang, X., and Qian, S.B. (2011). Chaperone-mediated hierarchical control in targeting misfolded proteins to aggresomes. Mol. Biol. Cell *22*, 3277–3288.

CELL BIOLOGY

Nutrient Signaling in Protein Homeostasis: An Increase in Quantity at the Expense of Quality

Crystal S. Conn[1] and Shu-Bing Qian[1,2]*

The discovery that rapamycin extends the life span of diverse organisms has triggered many studies aimed at identifying the underlying molecular mechanisms. Mammalian target of rapamycin complex 1 (mTORC1) regulates cell growth and may regulate organismal aging by controlling mRNA translation. However, how inhibiting mTORC1 and decreasing protein synthesis can extend life span remains an unresolved issue. We showed that constitutively active mTORC1 signaling increased general protein synthesis but unexpectedly reduced the quality of newly synthesized polypeptides. We demonstrated that constitutively active mTORC1 decreased translation fidelity by increasing the speed of ribosomal elongation. Conversely, rapamycin treatment restored the quality of newly synthesized polypeptides mainly by slowing the rate of ribosomal elongation. We also found distinct roles for mTORC1 downstream targets in maintaining protein homeostasis. Loss of S6 kinases, but not 4E-BP family proteins, which are both involved in regulation of translation, attenuated the effects of rapamycin on the quality of newly translated proteins. Our results reveal a mechanistic connection between mTORC1 and protein quality, highlighting the central role of nutrient signaling in growth and aging.

INTRODUCTION

The mammalian target of rapamycin (mTOR) is a highly conserved serine/threonine kinase that is named for its inhibition by the drug rapamycin (*1*, *2*). mTOR assembles into two functionally and structurally distinct complexes in the cytoplasm: mTORC1 (mTOR complex 1) and mTORC2. As a major hub that integrates multiple signaling pathways, mTORC1 is a master regulator of protein synthesis that couples nutrient signaling to cell growth and proliferation (*3*, *4*). In mammalian cells, mTORC1 is positioned downstream of the tumor suppressors tuberous sclerosis complex 1 (TSC1) and TSC2. The TSC1/2 complex inhibits mTORC1 by acting as a guanosine triphosphatase (GTPase)–activating enzyme (GAP) for Ras homolog enriched in brain (Rheb), which binds to and activates mTORC1 (*5*, *6*). Cells lacking functional TSC exhibit constitutive activation of mTORC1 signaling, resulting in increased protein synthesis and cell size (*7*). The phenotypes associated with *Tsc* deficiency can be rescued by rapamycin treatment (*8*). In further support of the critical role of mTORC1 in cell growth and proliferation, dysregulation of mTORC1 has been implicated in many disease states including cancer, metabolic disorders, and aging (*9*).

The role of mTORC1 in aging has received increasing attention owing to its mechanistic connection with other pathways in longevity studies. In many model organisms, longevity is regulated by the conserved insulin and insulin-like growth factor 1 (IGF-1) signaling pathway (*10*). Reducing the activity of phosphoinositide 3-kinase (PI3K), an upstream signaling of mTORC1, promotes longevity (*11*). In addition, caloric restriction increases life span in various organisms and is proposed to function by inhibiting mTORC1 (*12*). Direct inhibition of mTORC1 signaling also increases life span (*13*–*15*), and administration of rapamycin to adult mice substantially extends life span (*16*). A consequence of mTORC1 suppression is the general attenuation of protein synthesis. Indeed, partially inhibiting the translation machinery also increases life span in various organisms (*17*–*19*). Thus, reduced mRNA translation might be a common mechanism to extend life span in multiple species under different conditions.

How can reducing protein synthesis extend life span? Protein homeostasis refers to a delicate equilibrium between synthesizing proteins, maintaining protein conformations, and removing damaged proteins from cells (*20*) and has been postulated to play a critical role in growth and aging (*21*). This balance is maintained by molecular chaperones, the ubiquitin-proteasome system, and the autophagy pathway (*22*). A robust stress response is often associated with life span extension, which supports a critical role for protein homeostasis in growth and aging. We previously reported that constitutively active mTORC1 attenuates the expression of genes encoding chaperones at the translational level during stress conditions (*23*). However, how mTORC1-controlled mRNA translation influences the quality of translational products is not fully understood.

mTORC1 stimulates protein synthesis by phosphorylating several translational regulators. Two well-characterized downstream targets are the eukaryotic initiation factor 4E binding proteins (4E-BPs) and the p70 ribosomal S6 kinases (S6Ks) (*3*, *24*). The nonphosphorylated 4E-BPs bind and sequester eIF4E, a key rate-limiting factor for cap-dependent mRNA translation initiation. mTORC1 phosphorylates 4E-BPs, thereby derepressing eIF4E and promoting formation of the translation initiation complex. mTORC1-mediated phosphorylation of S6K promotes protein synthesis through multiple substrates, including the translation initiation factor eIF4B and the elongation regulator eEF2K (*25*, *26*). Ribosome profiling analysis indicates that 4E-BPs are the master effectors of mTORC1 in controlling translation of mRNAs containing 5′ terminal oligopyrimidine tract (TOP) and TOP-like sequences (*27*, *28*). This finding raises the question regarding the role of S6Ks in mTORC1-mediated translational regulation. Notably, the phosphorylation of S6Ks is rapamycin-sensitive, whereas mTORC1-mediated phosphorylation of 4E-BPs is largely rapamycin-resistant (*29*). This finding suggests that the antiaging effects of rapamycin might be mediated by the target of S6Ks rather than 4E-BPs. Supporting this notion, deletion of S6K1 in mice leads to increased life span and resistance to age-related pathologies (*30*). However, the differential effects of mTORC1 downstream targets on mRNA translation remain poorly understood.

Here, we sought to dissect the role of mTORC1 in various aspects of protein homeostasis. We found that persistent activation of mTORC1

[1]Graduate Field of Genetics, Genomics and Development, Cornell University, Ithaca, NY 14853, USA. [2]Division of Nutritional Sciences, Cornell University, Ithaca, NY 14853, USA.
*Corresponding author. E-mail: sq38@cornell.edu

signaling led to less functional proteins. The defective ribosome products were mainly due to reduced translation fidelity as a result of increased elongation speed. Rapamycin treatment largely restored protein homeostasis in these cells. The differential effects of mTORC1 downstream targets on translation fidelity further support the critical role of elongation in the quality of translational products. Our results provide mechanistic insights into the molecular connection between nutrient signaling and protein homeostasis and may offer new opportunities for treating age-related diseases.

RESULTS

Constitutively active mTORC1 signaling reduces the stability of synthesized polypeptides

To monitor the quality of translational products, we used firefly luciferase (Fluc) as a reporter, whose activity can be measured by a luminescence-based assay with exquisite sensitivity. Fluc folds rapidly upon translation on eukaryotic ribosomes and does not require posttranslational modification for its activity (*31*). Its sensitivity to various stress conditions makes it an ideal molecule to evaluate intracellular protein homeostasis (*32*). To monitor the biosynthesis of synthesized Fluc in cells with altered mTORC1 signaling, we used a real-time luminometer that allows continuous measurement of Fluc activity in live cells (*23*). Shortly after transfection with plasmids encoding Fluc, luciferase activity progressively accumulated in a mouse embryonic fibroblast (MEF) cell line (Fig. 1A). Unexpectedly, MEFs lacking TSC2 showed less Fluc activity with about 50% reduction by 15 hours after transfection. This was not due to a difference in transfection and transcription efficiency because *Fluc* mRNA abundance was comparable between these two sets of MEFs (fig. S1). To further exclude the possibility of altered transcription, we synthesized *Fluc* mRNA and performed mRNA transfection. Consistent with the plasmid transfection, TSC2 null cells showed lower Fluc activity than wild-type cells (Fig. 1B). Thus, constitutively active mTORC1 signaling reduces the functionality of synthesized Fluc.

Because mTORC1 is believed to promote protein synthesis, it was surprising to find reduced Fluc activity in TSC2 knockout cells. Immunoblotting of whole-cell lysates revealed that the steady-state amounts of Fluc were significantly lower in TSC2 knockout cells than in wild-type MEFs (Fig. 1C), which is consistent with the reduced Fluc activity measured in live cells. We then treated the transfected cells with the proteasome inhibitor MG132 to examine whether the reduced Fluc quantity was due to increased degradation. Proteasome inhibition by MG132 had minimal effects on translation initiation factors such as eIF2α (fig. S2). In comparison to wild-type cells, TSC2 knockout cells showed increased Fluc abundance after MG132 treatment with the majority recovered in the insoluble fraction (Fig. 1C). This result suggests that a substantial proportion of synthesized Fluc is short-lived in cells with increased mTORC1 signaling.

To examine the feature of other proteins under constitutively active mTORC1 signaling, we expressed green fluorescent protein (GFP), which is relatively stable in cells. Similar to Fluc, GFP also showed decreased steady-state amounts in TSC2 knockout cells with an increased accumulation after MG132 treatment (fig. S3). Proteasome inhibition leads to an accumulation of endogenous substrates in the form of polyubiquitin conjugates (*33*). We measured the abundance of polyubiquitinated species after MG132 treatment in cells with unrestrained mTORC1 signaling. Compared to wild-type cells, TSC2 knockout cells demonstrated a substantial increase of polyubiquitin signals with MG132 treatment (Fig. 1D). Together, these results suggest that mTORC1 signaling disrupts the stability of synthesized polypeptides.

Rheb overexpression reduces the stability of synthesized polypeptides

To independently confirm that uncontrolled mTORC1 signaling contributes to the reduced stability of translational products, we transfected human embryonic kidney (HEK) 293 cells with plasmids encoding Rheb, a direct activator of mTORC1. Rheb overexpression enhanced mTORC1 signaling in a dose-dependent manner as evidenced by increased RpS6 phosphorylation (Fig. 2). Consistent with TSC2 null cells, Rheb overexpression also resulted in a decrease of Fluc steady-state amounts in transfected HEK293 cells. MG132 treatment largely rescued the loss of Fluc, indicating a higher turnover of synthesized Fluc under Rheb overexpression. These cells also showed a higher accumulation of polyubiquitinated species in the presence of MG132 (Fig. 2, bottom panel). Thus, an increase in mTORC1 activity by Rheb overexpression also reduces the stability of synthesized polypeptides.

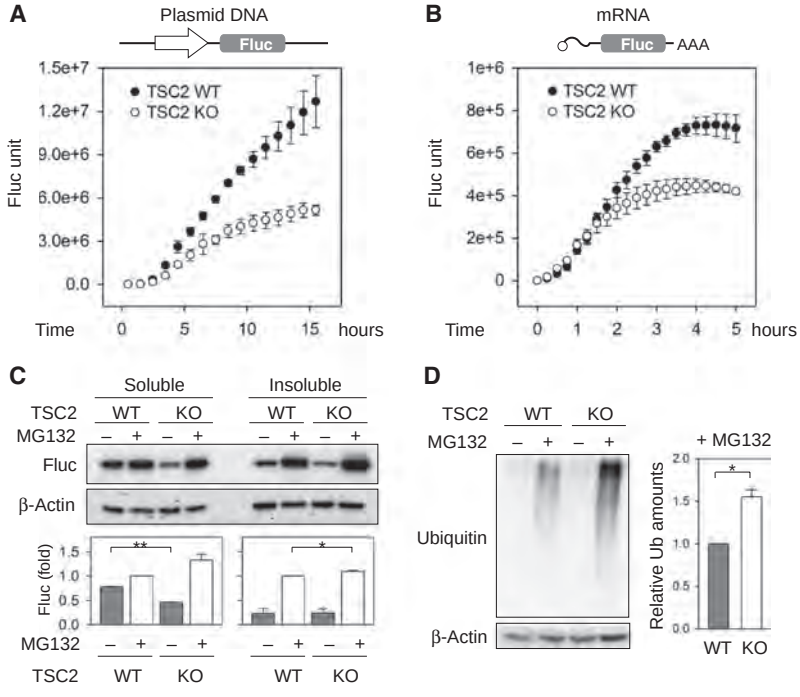

Fig. 1. Constitutively active mTORC1 reduces the stability of synthesized polypeptides. (**A**) Wild-type (WT) and TSC2 knockout (KO) cells were transfected with Fluc plasmids, and the Fluc activity was monitored continuously (means ± SEM; n = 6 independent experiments). (**B**) Similar to (A) except that the cells were transfected with *Fluc* mRNA (means ± SEM; n = 3 independent experiments). (**C**) WT and TSC2 KO cells transfected with Fluc plasmids were treated with MG132. Whole-cell lysates were separated into soluble and insoluble fractions followed by immunoblotting using antibodies as indicated. Bottom panel shows quantification of Fluc amounts (means ± SEM; n = 3 independent experiments; $^*P < 0.05$, $^{**}P < 0.01$, ratio paired t test). (**D**) MG132-treated WT and TSC2 KO cells were immunoblotted with the indicated antibodies. Right panel shows quantification (means ± SEM; n = 3 independent experiments; $^*P = 0.014$, ratio paired t test).

Suppressing mTORC1 restores the stability of synthesized polypeptides

Having found that an increase in mTORC1 signaling reduced the stability of translational products, we next asked whether suppressing mTORC1 signaling by rapamycin could restore the stability of synthesized polypeptides. Although treating wild-type cells with rapamycin slightly reduced Fluc expression, the presence of rapamycin increased the steady-state Fluc amounts in TSC2 knockout cells (Fig. 3A). This was not due to an increased translation rate in the presence of rapamycin because the abundance of synthesized Fluc under proteasome inhibition remained consistent after rapamycin treatment (Fig. 3A). The presence of rapamycin also substantially decreased the amount of polyubiquitinated species accumulated after proteasome inhibition by MG132 (Fig. 3B). Therefore, suppressing mTORC1 signaling decreases protein synthesis but increases the stability of synthesized polypeptides.

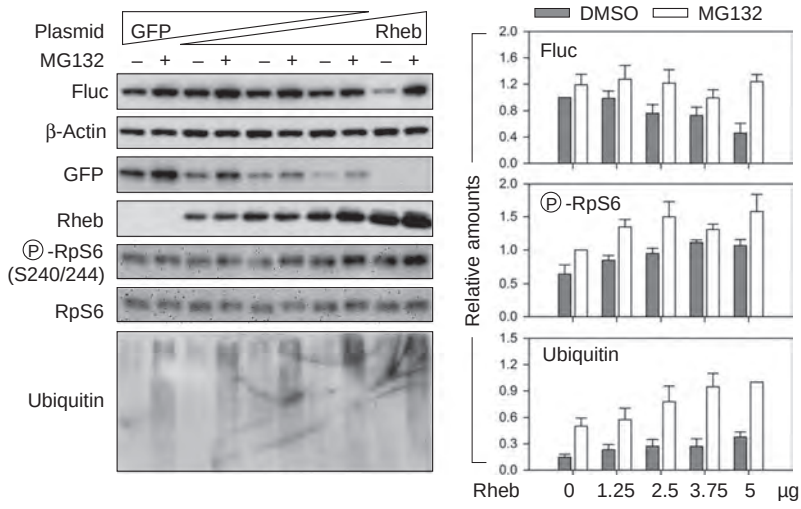

Fig. 2. Rheb overexpression reduces the stability of synthesized polypeptides. MG132-treated HEK293 cells cotransfected with plasmids encoding Fluc and Rheb, supplemented with GFP, were immunoblotted with the indicated antibodies (left panel). Fluc and polyubiquitinated species were quantified after normalizing to β-actin abundance (right panels). Phosphorylated RpS6 was normalized to total RpS6 protein abundance (means ± SEM; n = 3 independent experiments).

mTORC1 does not primarily affect chaperone and proteasome activities

The reduced stability of translational products under constitutively active mTORC1 signaling suggests a lower quality of newly synthesized polypeptides, or saturation of the protein quality control system in cells. Molecular chaperones and the ubiquitin-proteasome system are two major mechanisms that maintain intracellular protein homeostasis (*20*, *34*, *35*). We previously demonstrated that mTORC1 inhibited the cap-independent Hsp70 translation induced by heat shock stress (*23*). However, it remains unknown whether the chaperone network is adversely affected by persistent mTORC1 signaling under a nonstressed condition. To directly measure the chaperone activity in wild-type and TSC2 knockout cells, we used whole-cell lysates to refold heat-denatured Fluc. This in vitro refolding assay revealed that the chaperone activities in both cells were comparable (Fig. 4A). Furthermore, Rheb overexpression in HEK293 cells also had no appreciable effects on cellular chaperone activities (fig. S4A).

The ubiquitin-proteasome system is the main pathway for elimination of damaged proteins in eukaryotes, and its increased activity might contribute to lower steady-state protein abundance in cells with constitutively active mTORC1 signaling. To compare the proteasome activity between wild-type and TSC2 knockout cells, we used a cell-based proteasome assay in which the chymotrypsin-like activity of the proteasome can be directly measured using a luminogenic substrate (Proteasome-Glo). We observed similar chymotrypsin-like activity in both cell types (Fig. 4B). Consistently, Rheb overexpression in HEK293 cells also did not affect the proteasome activity

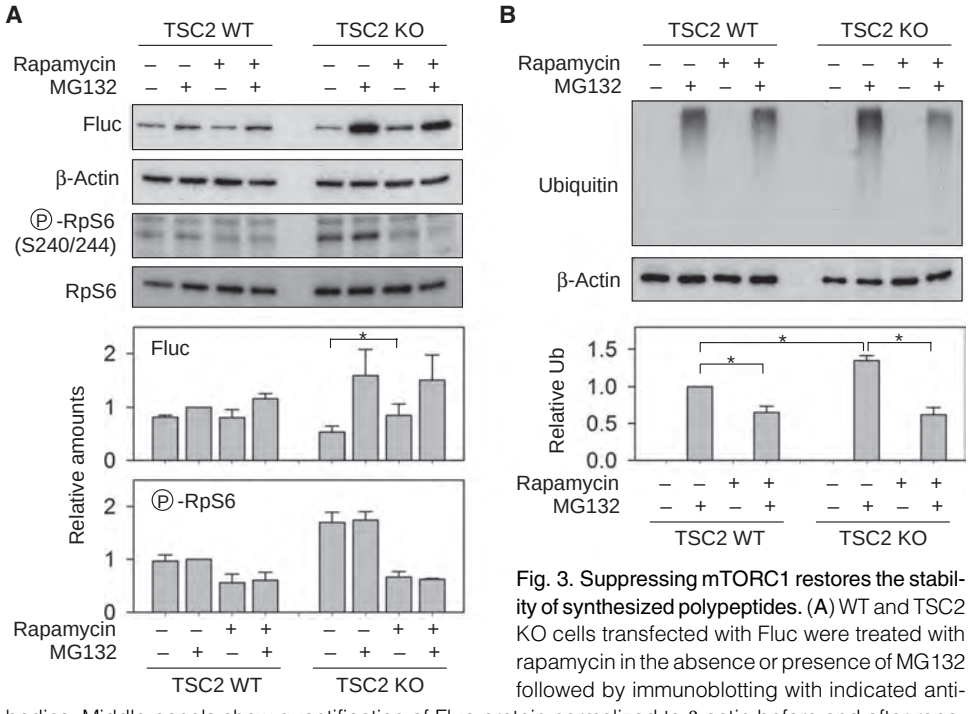

Fig. 3. Suppressing mTORC1 restores the stability of synthesized polypeptides. (**A**) WT and TSC2 KO cells transfected with Fluc were treated with rapamycin in the absence or presence of MG132 followed by immunoblotting with indicated antibodies. Middle panels show quantification of Fluc protein normalized to β-actin before and after rapamycin treatment. Lower panel is the quantification of phosphorylated RpS6 normalized to total RpS6 protein abundance (means ± SEM; n = 3 independent experiments; *P < 0.05, ratio paired t test). (**B**) Cells in (A) were immunoblotted using antibody against polyubiquitinated species. Lower panel shows quantitation of ubiquitin before and after rapamycin treatment normalized to β-actin (means ± SEM; n = 4 independent experiments; *P < 0.05, mixed model with random blots and fixed treatment using normalized values; P values are adjusted with a Bonferroni correction).

(fig. S4B). Thus, mTORC1 does not primarily affect the intracellular proteasome system.

mTORC1 decreases translation fidelity

With no apparent influence on either chaperone or proteasome function in cells, how does constitutively active mTORC1 signaling decrease the stability of synthesized proteins? Nascent chains are synthesized during elongation, and folding generally begins during translation on the ribosome (*36*, *37*). Thus, the efficiency of cotranslational folding is influenced by translation fidelity during elongation (*38*). We reasoned that dysregulated mTORC1 signaling might decrease translation fidelity and increase the generation of defective ribosomal products. To test this hypothesis, we generated two Fluc reporters to assess translational fidelity. One reporter, Fluc(Stop), has leucine at position 210 replaced with a stop codon, which leads to the synthesis of a truncated and enzymatically inactive protein product. This reporter has previously been used to assess readthrough errors occurring during translation (*39*). To evaluate the potential of misincorporation during translation, we mutated the arginine at the active-site position 218 into serine, which renders the resultant Fluc(R218S) mutant devoid of enzymatic activity. As expected, both Fluc(Stop) and Fluc(R218S) mutants showed less than 1% of the enzymatic activity of the wild-type Fluc; however, TSC2 knockout cells showed a significant increase in Fluc activity for both Fluc(Stop) and Fluc(R218S) when compared to wild-type cells (2- and 1.5-fold increase, respectively) (Fig. 4C). Again, this relative increase was not due to a difference in transfection efficiency between these two cells, because quantitative polymerase chain reaction (qPCR) revealed comparable amounts of *Fluc* mRNA (fig. S5). Consistent with the findings in TSC2 knockout cells, overexpressing Rheb in HEK293 cells also led to a higher rate of readthrough and misincorporation errors during translation of Fluc mutants (fig. S6).

Because rapamycin treatment increases the stability of synthesized proteins, we examined whether repressing mTORC1 signaling would restore translation fidelity. Indeed, rapamycin treatment decreased the functionality of Fluc mutants in both wild-type and TSC2 knockout cells (Fig. 4D). The effect of rapamycin on promoting translation fidelity in TSC2 knockout cells is an underestimate because wild-type Fluc in these cells showed increased activity in the presence of rapamycin (Fig. 4D). This is consistent with the finding that rapamycin rescues the stability of Fluc under persistent mTORC1 signaling (Fig. 3A). Therefore, repressing mTORC1 signaling increases the stability of newly synthesized polypeptides by promoting accurate mRNA translation.

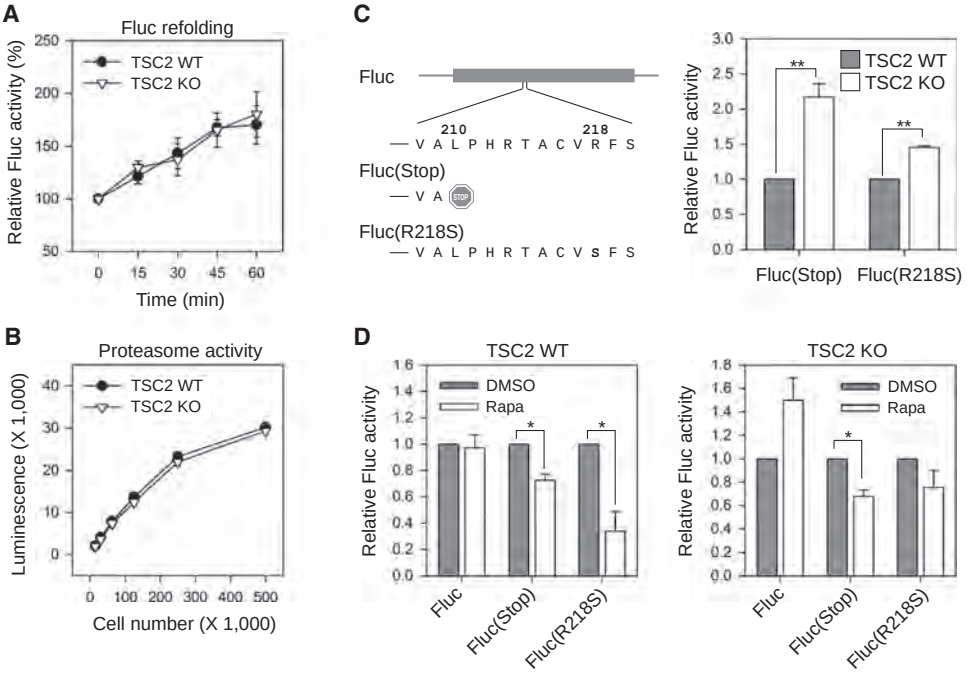

Fig. 4. mTORC1 primarily affects translation fidelity. (**A**) Heat-denatured Fluc proteins were incubated with whole-cell lysates derived from TSC2 WT and KO cells at room temperature. Fluc refolding was monitored by measuring Fluc activities at the time points indicated. Relative Fluc activity is presented (means ± SEM; $n = 3$ independent experiments). (**B**) The intracellular chymotrypsin activities in TSC2 WT and KO cells were measured by luminescent reagent (Proteasome-Glo) (means ± SEM; $n = 3$ independent experiments). (**C**) Schematic diagram of Fluc mutants Fluc(Stop) and Fluc(R218S) (left panel). TSC2 WT and KO cells were transfected with plasmids encoding Fluc mutants followed by measurement of Fluc activity. Relative Fluc activities were normalized to WT Fluc (means ± SEM; $n = 4$ independent experiments; $^{**}P < 0.01$, paired *t* test). (**D**) WT (left panel) and TSC2 KO cells (right panel) transfected with plasmids encoding Fluc mutants as in (C) were treated with rapamycin (Rapa) followed by measurement of Fluc activity. Relative Fluc activities were normalized to WT Fluc with dimethyl sulfoxide (DMSO) (means ± SEM; $n = 4$ independent experiments; $^{*}P < 0.05$, paired *t* test).

mTORC1 downstream targets exhibit distinct roles in translation fidelity

Two well-established mTORC1 downstream targets are 4E-BPs and S6Ks. Although 4E-BP family proteins are the master effectors of mTORC1 in controlling translation of TOP and TOP-like mRNAs (*27*, *28*), the phosphorylation of 4E-BPs is resistant to rapamycin treatment. Because rapamycin effectively abolishes phosphorylation of S6Ks, we suspected that rapamycin might act through S6Ks to restore translation fidelity. Indeed, enzymatic activities of transfected Fluc(Stop) and Fluc(R218S) mutants were significantly reduced in S6K1 and S6K2 double-knockout MEFs when compared to wild-type cells (Fig. 5A). This result indicates increased translation fidelity in the absence of S6Ks. In contrast, MEFs lacking both 4E-BP1 and 4E-BP2 showed comparable activity for both Fluc mutants (Fig. 5B). Considering that 4E-BPs mainly act on translation initiation, the critical role of S6Ks in translation fidelity supports the notion that ribosomal elongation may be responsible for the quality of translational products.

To substantiate the finding that rapamycin acts through S6Ks in restoring translational fidelity, we examined how rapamycin influences the translation of Fluc mutants in MEFs lacking either S6Ks or 4E-BPs. Rapamycin treatment significantly reduced the activity of transfected Fluc mutants in wild-type cells but showed no effects in S6K double-knockout cells (Fig. 5C). In contrast, the presence of rapamycin equally restored the translation fidelity in both

4E-BP wild-type and double-knockout MEFs as evidenced by the suppressed activity of Fluc mutants, in particular Fluc(Stop) (Fig. 5D). These results confirm the distinct roles of mTORC1 downstream targets in controlling the quality of translational products.

mTORC1 increases ribosome speed during translation elongation

Translation fidelity is influenced by multiple factors. For instance, defective ribosome biogenesis reduces the accuracy of amino acid incorporation (*40*). However, both TSC2 wild-type and knockout cells showed a similar ratio of 28*S* to 18*S* ribosomal RNAs (rRNAs) (fig. S7). The accuracy of codon-anticodon recognition is also susceptible to ribosome dynamics during elongation. In addition to translation initiation, mTORC1 promotes elongation through S6K-mediated eEF2K phosphorylation (*26*). We hypothesize that constitutively active mTORC1 signaling might potentially compromise the fidelity of the decoding process by increasing the speed of elongation. To evaluate the ribosome dynamics in both TSC2 wild-type and knockout cells, we performed ribosome sedimentation analysis. Consistent with an increase in cap-dependent mRNA translation, TSC2 null cells exhibited higher polysome formation than wild-type cells, and the monosome peak was correspondingly reduced (Fig. 6A). Although this feature is consistent with more efficient translation initiation in cells with increased mTORC1 signaling, the snapshot of polysome profiles does not offer insight into ribosome dynamics during elongation.

The translation inhibitor harringtonine stalls initiating ribosomes at the start codon while allowing elongating ribosomes to run off the transcript (*41*). The time required for polysome depletion correlates with the global translation elongation speed. By treating cells with harringtonine for various times, we evaluated the average elongation speed (fig. S8). Compared to wild-type cells, TSC2 knockout cells showed an earlier polysome runoff, indicating faster ribosome movement during elongation (Fig. 6B).

Because rapamycin treatment essentially restored translation fidelity in TSC2 knockout cells, we examined the effect of rapamycin on ribosome dynamics. As a specific mTORC1 inhibitor, rapamycin suppresses translation initiation. Supporting this notion, the monosome peak was increased after rapamycin treatment (Fig. 6A). Intriguingly, we observed a slight increase rather than a decrease of polysome formation in TSC2 knockout cells in the presence of rapamycin. Under this condition, the retained polysome is a strong indication of ribosome slowing down during elongation. Indeed, application of harringtonine showed delayed depletion of polysomes in the presence of rapamycin (Fig. 6C). These results support the interpretation that mTORC1 decreases translation fidelity by increasing ribosome speed.

mTORC1 controls cellular susceptibility to proteotoxic stress

mTORC1 signaling adversely affected the quality of newly synthesized proteins; therefore, we reasoned that cells with persistent mTORC1 signaling might be sensitive to proteotoxic stress. To test this possibility, we treated cells with MG132 to induce proteotoxic stress and compared the cell viability between wild-type and TSC2 knockout cells. MG132 treatment significantly reduced cell growth and caused about 10% cell death in wild-type cells (Fig. 7A). In contrast, more than 20% of cell death occurred in TSC2 knockout cells after the same treatment. Because proteotoxic stress triggers apoptosis, we analyzed molecular markers of apoptosis in these cells and detected increased caspase-3 cleavage in TSC2 knockout cells (Fig. 7B).

Adding rapamycin together with MG132 restored the cell viability of TSC2 null cells (Fig. 7, A B). Accordingly, there was a decrease in the proportion of cells undergoing apoptosis (Fig. 7B). These protective effects of rapamycin in response to proteotoxic stress might be attributed to the involvement of multiple pathways including macroautophagy (*42*). Nevertheless, our results extend the benefits of rapamycin by showing that it alleviates proteotoxic stress by increasing the quality of newly synthesized proteins.

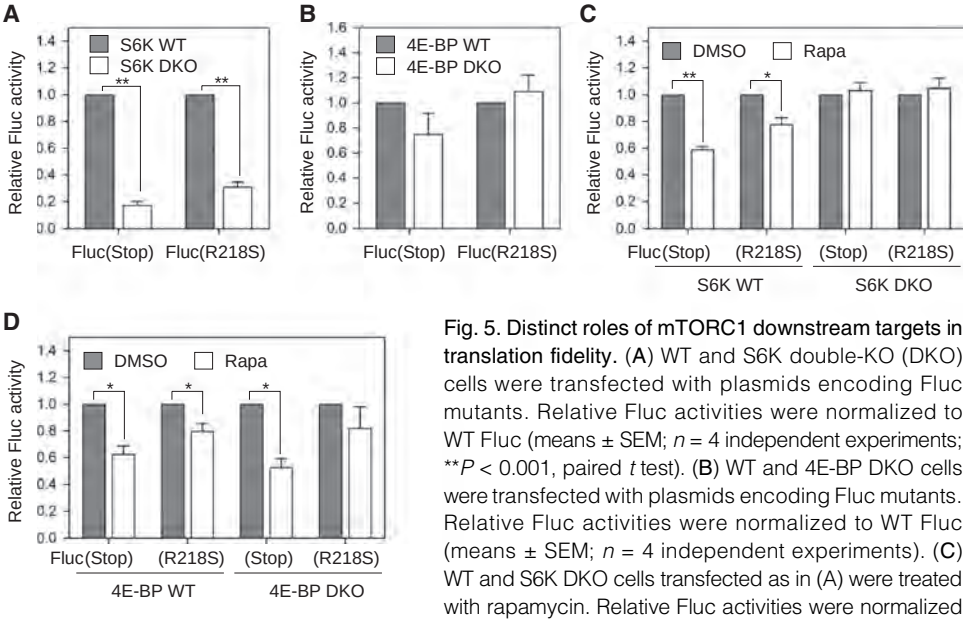

Fig. 5. Distinct roles of mTORC1 downstream targets in translation fidelity. (**A**) WT and S6K double-KO (DKO) cells were transfected with plasmids encoding Fluc mutants. Relative Fluc activities were normalized to WT Fluc (means ± SEM; $n = 4$ independent experiments; $^{**}P < 0.001$, paired t test). (**B**) WT and 4E-BP DKO cells were transfected with plasmids encoding Fluc mutants. Relative Fluc activities were normalized to WT Fluc (means ± SEM; $n = 4$ independent experiments). (**C**) WT and S6K DKO cells transfected as in (A) were treated with rapamycin. Relative Fluc activities were normalized to WT Fluc (means ± SEM; $n = 3$ independent experiments; $^{*}P < 0.05$, $^{**}P < 0.001$, paired t test). (**D**) WT and 4E-BP DKO cells transfected as in (B) were treated with rapamycin. Relative Fluc activities were normalized to WT Fluc (means ± SEM; $n = 4$ independent experiments for WT and $n = 3$ independent experiments for DKO; $^{*}P < 0.05$, $^{**}P < 0.001$, paired t test).

DISCUSSION

Studies conducted in rodents over the past 70 years have shown that life span is extended by caloric restriction (*43*). Similar to caloric restriction, mTORC1 inhibition also extends life span in various model organisms (*14*, *15*, *44*), and administration of rapamycin to adult mice is sufficient to extend life span considerably (*16*). However, how mTORC1 inhibition increases longevity in mammals remains an unresolved issue. Protein synthesis–dependent and protein synthesis–independent mechanisms have been proposed, and several models have been suggested to explain the potential benefits of reducing protein synthesis. First, a decrease of overall translational products could lower the cellular burden of erroneously synthesized polypeptides. This situation results in "spare" proteolytic and chaperone function in cells, which may contribute to the observed increase in organism stress resistance and life span (*45*).

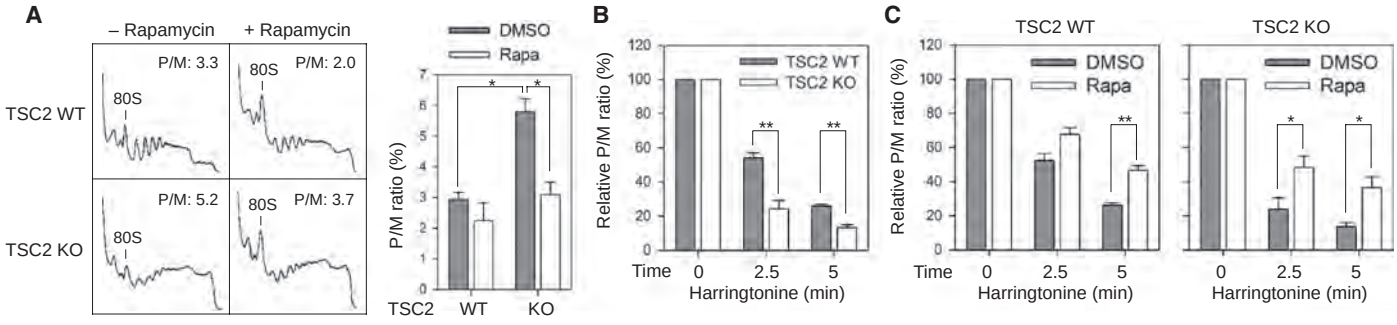

Fig. 6. mTORC1 alters ribosome dynamics during translation elongation. (**A**) Polysome profiles of WT and TSC2 KO cells in the presence of rapamycin were determined using sucrose gradient sedimentation. The P/M (polysome/monosome) ratio was calculated by measuring the areas under the polysome and 80*S* peak and further quantified in the left panel (means ± SEM; $n = 3$ independent experiments; $^{*}P < 0.05$, ratio paired *t* test). (**B**) Polysome profiling of WT and TSC2 KO cells was conducted after treatment with harringtonine for indicated times. The P/M ratio was determined and normalized to no harringtonine treatment per cell type (means ± SEM; $n = 4$ independent experiments; $^{**}P < 0.01$, paired *t* test). (**C**) WT and TSC2 KO cells were pretreated with rapamycin followed by harringtonine treatment for indicated times before polysome profiling. The P/M ratio was determined and normalized to no harringtonine treatment (means ± SEM; $n = 3$ independent experiments; $^{*}P < 0.05$, $^{**}P < 0.01$, unpaired *t* test).

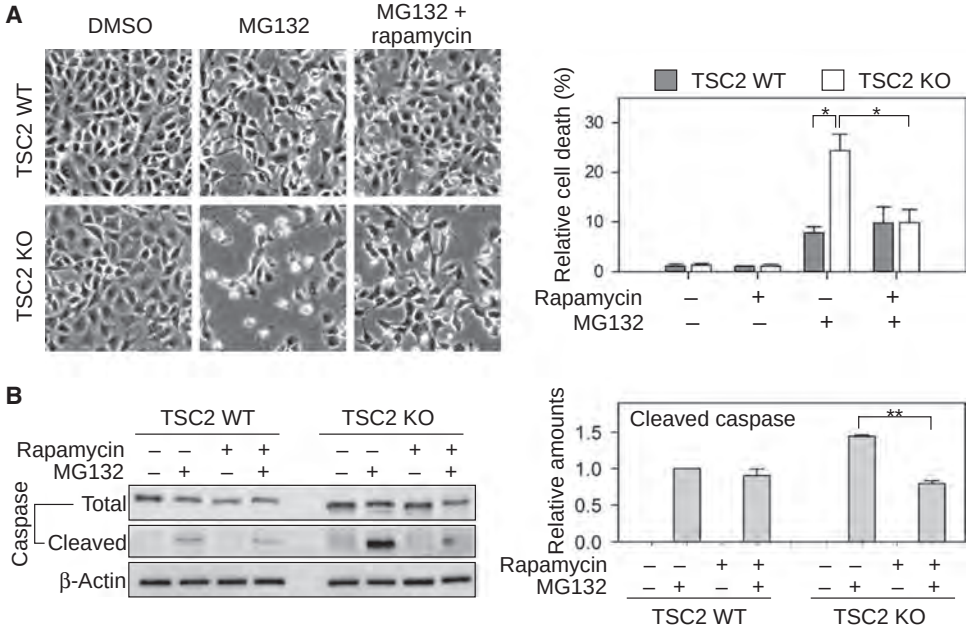

Fig. 7. mTORC1 regulates cellular susceptibility to proteotoxic stress. (**A**) WT and TSC2 KO cells were treated with MG132 in the absence or presence of rapamycin. Cell viability and morphology were assessed by phase-contrast microscope images (left panel). Images were assessed for cell viability and quantified (right panel) (means ± SEM; $n = 4$ independent experiments; $^{*}P < 0.05$, ratio paired *t* test). (**B**) Cell samples from (A) were lysed and immunoblotted using the indicated antibodies. The amount of cleaved caspase-3 relative to the total caspase-3 was quantified (right panel) (means ± SEM; $n = 3$ independent experiments; $^{**}P < 0.01$, ratio paired *t* test).

Second, global suppression of protein synthesis may allow selective translation of a subset of mRNAs that exert a protective function (*46*). Here, we report that a global decrease in mRNA translation improves the fidelity of protein synthesis. Our observations not only extend the functional connection between mTORC1 and protein homeostasis (Fig. 8) but also suggest a molecular basis for how constitutively active mTORC1 signaling favors the development of age-related pathologies by disrupting protein homeostasis.

mTORC1 regulates mRNA translation at multiple stages. The regulatory mechanisms impinging on the initiation stage have received considerable attention, but accumulating evidence points to the elongation phase as another target of translational control (*47*). We monitored ribosome dynamics in cells with altered mTORC1 signaling using the translation inhibitor harringtonine. Consistent with the positive role of mTORC1 in regulating eEF2 activity (*26*), TSC2 knockout cells exhibit faster ribosome runoff than the wild-type cells. Despite the wide belief that rapamycin suppresses general protein synthesis by acting primarily on translation initiation, we found that rapamycin does not disassemble the polysome, at least in the early stage. Thus, it is conceivable that rapamycin exerts additional impacts on elongation. Supporting this notion, rapamycin treatment reduces the elongation rate of ribosomes in both wild-type and TSC2 knockout cells.

One unanticipated finding in this study is the distinct roles of mTORC1 downstream targets in translation fidelity. It appears that S6Ks, but not 4E-BPs, influence the quality of translational products, presumably through the regulation of elongation. This is in agreement with the finding that mice lacking S6K1 showed increased life span and resistance to age-related pathologies (*30*). In contrast, deleting 4E-BPs mainly affected cell proliferation, but not cell growth (*48*). In addition, only the phosphorylation of S6Ks, but not 4E-BPs, is sensitive to rapamycin treatment (*29*). The differential effects of rapamycin on

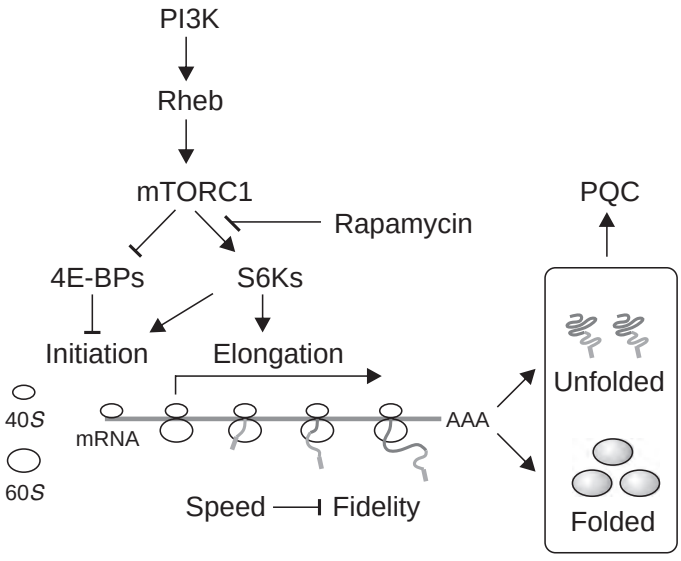

Fig. 8. Model for functional connection between mTORC1 and protein homeostasis. mTORC1 regulates protein synthesis at multiple stages through different downstream targets. Whereas 4E-BPs control the initiation step, S6Ks mainly promote the elongation stage. The altered ribosome dynamics when mTORC1 signaling is deregulated results in protein dyshomeostasis and disruption of the protein quality control (PQC) network. Rapamycin restores protein homeostasis by enhancing translation fidelity through the S6Ks.

mTORC1 downstream targets support the notion that the antiaging benefits of rapamycin occur through the elongation stage by S6Ks (Fig. 8).

How does an increased elongation rate affect translation fidelity? mRNA translation is an error-prone step in gene expression with about 1 in every 10^3 to 10^4 codons mistranslated (*49*). Amino acid incorporation is a competitive process between the cognate and the near-cognate transfer RNAs (tRNAs) for a given codon. The increased elongation rate could potentially compromise the translational fidelity by promoting misincorporation of amino acids. Reduced elongation speed, on the other hand, allows for a relatively longer dwell time of the ribosome in its search for correct tRNA pairing. It is thus conceivable that an increased translation speed, such as that under constitutively active mTOR signaling, generates more aberrant translational products. In addition, variations of elongation speed may coordinate cotranslational folding of emerging polypeptides (*37*). The local discontinuous translation (ribosome pausing) temporally separates the translation of segments of the peptide chain and actively coordinates their cotranslational folding (*50*). Supporting this notion, a study in *Escherichia coli* has demonstrated that slowing translation speed enhances protein folding efficiency (*51*). The faster translation speed may eliminate the ribosome pausing necessary for cotranslational events. Supporting this notion, we observed an inverse correlation between elongation speed and the quality of nascent polypeptides in mammalian cells.

Ribosome biogenesis is largely controlled by mTORC1 at the level of translation because ribosomal subunits are encoded by TOP mRNAs (*28*, *52*). The reduced translation fidelity under constitutively active mTORC1 signaling could create errors in synthesized ribosomal proteins, which may cause an error catastrophe due to dysfunctional translation machinery. This catastrophe would create additional errors of newly synthesized polypeptides. We cannot exclude the possibility that this may account for the reduced quality of synthesized proteins. It remains to be investigated whether cells with unrestrained mTORC1 signaling contain defective ribosome subunits.

The observations described in this study have several implications. First, the critical role of mTORC1 in ribosome dynamics and translation quality extends the molecular linkage between mTORC1 and protein homeostasis. Second, the finding that an increase in protein synthesis is accompanied by a decrease in protein quality provides a plausible mechanism for how persistent mTORC1 signaling favors the development of age-related pathologies. With the most common feature of aging being an accumulation of misfolded proteins derived from erroneous biosynthesis and postsynthetic modification, protein homeostasis is an important mediator of rapamycin in longevity.

MATERIALS AND METHODS

Cell lines and reagents

TSC2 wild-type and knockout MEFs were provided by D. J. Kwiatkowski (Harvard Medical School). 4E-BP wild-type and double-knockout MEFs were provided by N. Sonenberg (McGill University), and S6K wild-type and double-knockout MEFs by G. Thomas (University of Cincinnati). All cell lines were maintained in Dulbecco's modified Eagle's medium with 10% fetal bovine serum grown at 37°C with 5% CO_2. Cycloheximide, rapamycin, and MG132 were purchased from Sigma, and harringtonine from LKT Laboratories. Dual-Luciferase Assay System, Luciferase Assay System, and Proteasome-Glo kit were purchased from Promega. D-Luciferin was purchased from Registech. Antibodies against phosphorylated and total S6 and caspase-3 were purchased from Cell Signaling Technology; β-actin from Sigma-Aldrich; myc from Santa Cruz; and polyubiquitin from Assay Designs. Anti-Fluc was purchased from Novus Biologicals.

Plasmids and transfection

The *Fluc* gene was directly removed from pGL3 vector (Promega) with Hind III and Xba I sites and then cloned into pcDNA3.1 (Invitrogen). Fluc mutants for fidelity assays were created from pGL3 vector with PCR Mutagenesis Kit (Agilent Technologies) with the following primers: Fluc(Stop), 5′-GGTCTGCCTAAAGGTGTCGCTTAGCCTCATAGAACTGCC-3′; Fluc(R218S), 5′-GCCTCATAGAACTGCCTGCGTGTCTTTCTCGCATGCCAGAGATCC-3′. Plasmids encoding Rheb-myc were provided by K.-L. Guan (University of California, San Diego). Transfection was performed with Lipofectamine 2000 (Invitrogen) according to the manufacturer's instructions.

mRNA in vitro transcription

mRNA with a m^7G-cap was synthesized with the mMessage mMachine T7 Ultra Kit (Ambion), followed by purification with the MEGAclear Kit (Ambion), according to the manufacturer's instructions. mRNA transfections were performed with Lipofectamine 2000 (Invitrogen) according to the manufacturer's instructions.

Luciferase assay

For real-time measurement of Fluc activity, cells were plated on 35-mm dishes and transfected with plasmid or mRNA containing the *Fluc* gene. Immediately after transfection, 1 mM luciferase substrate D-luciferin was added into the culture medium, and the Fluc activity was recorded at 37°C with 5% CO_2 using Kronos Dio Luminometer (ATTO). For luciferase assay with cell lysates, Fluc activity was measured with a luciferase reporter assay (Promega) on a Synergy HT Multi-detection Microplate Reader (BioTek Instruments). For the fidelity assay, Fluc activity from Fluc mutants was normalized to Fluc activity derived from pGL3.

In vitro refolding assay

QuantiLum Recombinant Fluc (Promega) was diluted in lysis buffer at a concentration of 50 μg/ml and then split into two individual Eppendorf tubes. One tube was placed at 42°C for 15 min to denature Fluc, whereas the other was kept at room temperature. The denatured or nondenatured Fluc protein was then added to cell lysates for a final concentration of 16.5 μg/ml. Refolding was conducted at room temperature, and the Fluc activity was monitored every 15 min with the Promega Luciferase Assay System. Fluc activity in lysis buffer alone was measured in parallel to exclude spontaneous refolding of denatured Fluc. The nondenatured Fluc activity was used to normalize the denatured Fluc activity after cell lysate–mediated refolding.

Immunoblotting

Cells were lysed on ice in tris-buffered saline (TBS) buffer [50 mM tris-HCl (pH 7.5), 150 mM NaCl, 1 mM EDTA] containing protease inhibitor cocktail tablet (Roche) and 2% Triton X-100. After incubating on ice for 30 min with interval vortexing, the lysates were centrifuged for 5 min at 12,500 rpm, and an aliquot was removed for quantification by Bradford assay (Bio-Rad). Samples were adjusted to 1 μg/μl and heated for 5 min in SDS–polyacrylamide gel electrophoresis (SDS-PAGE) sample buffer [50 mM tris-HCl (pH 6.8), 100 mM dithiothreitol (DTT), 2% SDS, 0.1% bromophenol blue, 10% glycerol]. For fractionation analysis, the Triton X-100–soluble and Triton X-100–insoluble fractions were dissolved individually in SDS-PAGE sample buffer. Proteins were resolved on SDS-PAGE and transferred to Immobilon-P membranes (Millipore). Membranes were blocked for 30 min in TBS containing 5% blotting milk, followed by incubation with primary antibodies overnight. After several washes with TBS containing 0.1% Tween 20, the membrane was incubated with horseradish peroxidase–coupled secondary antibodies. Immunoblots were developed with enhanced chemiluminescence (ECL Plus, GE Healthcare). Individual Western experiments were quantified with ImageJ software and normalized to either β-actin or total protein of phosphorylated target as a loading control.

Reverse transcription PCR and qPCR

Total RNA was extracted from whole-cell lysates with TRIzol reagent (Invitrogen) according to the manufacturer's instructions. RNA quality was validated by NanoVue Spectrophotometer (GE Healthcare) and run on an agarose gel for integrity examination. Reverse transcription was performed with SuperScript III kit (Invitrogen) followed by PCR. The primers for the Fluc gene are 5′-ATTTATCGGAGTTGCAGTTGCGCC-3′ (forward) and 5′-CCAGCAGCGCACTTTGAATCTTGT-3′ (reverse), and the primers for 18*S* are 5′-CTTGGATGTGGTAGCCGTTT-3′ (forward) and 5′-TATGGTTCCTTTGGCGCTC-3′ (reverse). For qPCR, reverse transcription was performed with High Capacity cDNA Reverse Transcription Kit (Applied Biosystems). qPCR was then conducted with Power SYBR Green PCR Master Mix (Applied Biosystems) according to the manufacturer's protocols. PCR was performed on a LightCycler 480 Real-Time PCR System (Roche Applied Science) with three technical replicates per sample per run. The primers for the Fluc gene are 5′-ATCCGGAAGCGACCAACGCC-3′ (forward) and 5′-GTCGGGAAGACCTGCCACGC -3′ (reverse), and the primers for β-actin are 5′-TTGCTGACAGGATGCAGAAG-3′ (forward) and 5′-ACTCCTGCTTGCTGATCCACAT-3′ (reverse).

Polysome profiling

A sucrose solution was prepared in polysome buffer [10 mM Hepes (pH 7.4), 100 mM KCl, 5 mM $MgCl_2$, cycloheximide (100 μg/ml), 5 mM DTT]. A 15 to 45% sucrose density gradient was prepared in SW41 ultracentrifuge tubes (Fisher) with a Gradient Master (BioComp Instruments). Cells were treated with cycloheximide (100 μg/ml) for 3 min at 37°C in culture media followed by lysis in ice-cold polysome buffer containing 2% Triton X-100. Lysate was centrifuged for 10 min at 12,500 rpm, and 500 μl of supernatant was loaded onto sucrose gradient and centrifuged for 100 min at 38,000*g* at 4°C in a SW40 rotor. Gradients were fractioned at 0.75 ml/min with an automated fractionation system (ISCO), which continually monitors absorbance values at 254 nm. For rescue experiments, rapamycin was used at 20 nM for 3 hours before the addition of cycloheximide. For the ribosome runoff assay, cells were pretreated with harringtonine (1 μg/ml) with or without 20 nM rapamycin for up to 5 min before the addition of cycloheximide.

Proteotoxic stress and viability assay

TSC2 wild-type and knockout MEFs were treated with 10 μM MG132 overnight with or without 10 nM rapamycin. Multiple fields were selected for examination by a Nikon Eclipse Ti-S inverted microscope. Cells were then collected and counted with trypan blue staining. Four counts were made per sample and averaged for viability assay.

Statistics

For each analysis, raw values were used when possible or raw values were normalized to an internal control from at least three biologically independent experiments. The data are expressed as means ± SEM. For each comparison, the relevant comparisons were chosen on the basis of the assay. A Bonferroni correction was used to adjust the *P* values for multiple comparisons within Fig. 3B. Statistical significance is denoted by $*P < 0.05$ and $**P < 0.01$. Microsoft Excel, GraphPad Prism 6, and JMP software were used for statistical analyses.

SUPPLEMENTARY MATERIALS

www.sciencesignaling.org/cgi/content/full/6/271/ra24/DC1

Fig. S1. Quantification of Fluc mRNA abundance in wild-type and TSC2 knockout cells.
Fig. S2. Phosphorylation status of eIF2α in wild-type and TSC2 knockout cells.
Fig. S3. Features of GFP in wild-type and TSC2 knockout cells.
Fig. S4. Chaperone and proteasome activity in cells expressing Rheb.
Fig. S5. Quantification of mRNA abundance of Fluc mutants in wild-type and TSC2 knockout cells.
Fig. S6. Translation fidelity in cells expressing Rheb.
Fig. S7. Ratio of 28*S* to 18*S* rRNAs in wild-type and TSC2 knockout cells.
Fig. S8. Measurement of ribosome dynamics during translation elongation.

REFERENCES AND NOTES

1. S. Wullschleger, R. Loewith, M. N. Hall, TOR signaling in growth and metabolism. *Cell* **124**, 471–484 (2006).
2. M. Laplante, D. M. Sabatini, mTOR signaling in growth control and disease. *Cell* **149**, 274–293 (2012).
3. X. M. Ma, J. Blenis, Molecular mechanisms of mTOR-mediated translational control. *Nat. Rev. Mol. Cell Biol.* **10**, 307–318 (2009).
4. N. Sonenberg, A. G. Hinnebusch, Regulation of translation initiation in eukaryotes: Mechanisms and biological targets. *Cell* **136**, 731–745 (2009).
5. K. Inoki, K. L. Guan, Complexity of the TOR signaling network. *Trends Cell Biol.* **16**, 206–212 (2006).
6. J. Huang, B. D. Manning, The TSC1–TSC2 complex: A molecular switchboard controlling cell growth. *Biochem. J.* **412**, 179–190 (2008).
7. D. J. Kwiatkowski, B. D. Manning, Tuberous sclerosis: A GAP at the crossroads of multiple signaling pathways. *Hum. Mol. Genet.* **14**, R251–R258 (2005).
8. J. Goto, D. M. Talos, P. Klein, W. Qin, Y. I. Chekaluk, S. Anderl, I. A. Malinowska, A. Di Nardo, R. T. Bronson, J. A. Chan, H. V. Vinters, S. G. Kernie, F. E. Jensen, M. Sahin, D. J. Kwiatkowski, Regulable neural progenitor-specific *Tsc1* loss yields giant cells with organellar dysfunction in a model of tuberous sclerosis complex. *Proc. Natl. Acad. Sci. U.S.A.* **108**, E1070–E1079 (2011).
9. R. Zoncu, A. Efeyan, D. M. Sabatini, mTOR: From growth signal integration to cancer, diabetes and ageing. *Nat. Rev. Mol. Cell Biol.* **12**, 21–35 (2011).
10. C. Kenyon, The plasticity of aging: Insights from long-lived mutants. *Cell* **120**, 449–460 (2005).

11. E. Cohen, J. F. Paulsson, P. Blinder, T. Burstyn-Cohen, D. Du, G. Estepa, A. Adame, H. M. Pham, M. Holzenberger, J. W. Kelly, E. Masliah, A. Dillin, Reduced IGF-1 signaling delays age-associated proteotoxicity in mice. *Cell* **139**, 1157–1169 (2009).
12. L. Fontana, The scientific basis of caloric restriction leading to longer life. *Curr. Opin. Gastroenterol.* **25**, 144–150 (2009).
13. P. Kapahi, D. Chen, A. N. Rogers, S. D. Katewa, P. W. Li, E. L. Thomas, L. Kockel, With TOR, less is more: A key role for the conserved nutrient-sensing TOR pathway in aging. *Cell Metab.* **11**, 453–465 (2010).
14. P. Kapahi, B. M. Zid, T. Harper, D. Koslover, V. Sapin, S. Benzer, Regulation of lifespan in *Drosophila* by modulation of genes in the TOR signaling pathway. *Curr. Biol.* **14**, 885–890 (2004).
15. M. Kaeberlein, R. W. Powers III, K. K. Steffen, E. A. Westman, D. Hu, N. Dang, E. O. Kerr, K. T. Kirkland, S. Fields, B. K. Kennedy, Regulation of yeast replicative life span by TOR and Sch9 in response to nutrients. *Science* **310**, 1193–1196 (2005).
16. D. E. Harrison, R. Strong, Z. D. Sharp, J. F. Nelson, C. M. Astle, K. Flurkey, N. L. Nadon, J. E. Wilkinson, K. Frenkel, C. S. Carter, M. Pahor, M. A. Javors, E. Fernandez, R. A. Miller, Rapamycin fed late in life extends lifespan in genetically heterogeneous mice. *Nature* **460**, 392–395 (2009).
17. K. Z. Pan, J. E. Palter, A. N. Rogers, A. Olsen, D. Chen, G. J. Lithgow, P. Kapahi, Inhibition of mRNA translation extends lifespan in *Caenorhabditis elegans*. *Aging Cell* **6**, 111–119 (2007).
18. M. Hansen, S. Taubert, D. Crawford, N. Libina, S. J. Lee, C. Kenyon, Lifespan extension by conditions that inhibit translation in *Caenorhabditis elegans*. *Aging Cell* **6**, 95–110 (2007).
19. P. Syntichaki, K. Troulinaki, N. Tavernarakis, eIF4E function in somatic cells modulates ageing in *Caenorhabditis elegans*. *Nature* **445**, 922–926 (2007).
20. W. E. Balch, R. I. Morimoto, A. Dillin, J. W. Kelly, Adapting proteostasis for disease intervention. *Science* **319**, 916–919 (2008).
21. R. I. Morimoto, Proteotoxic stress and inducible chaperone networks in neurodegenerative disease and aging. *Genes Dev.* **22**, 1427–1438 (2008).
22. B. Bukau, J. Weissman, A. Horwich, Molecular chaperones and protein quality control. *Cell* **125**, 443–451 (2006).
23. J. Sun, C. S. Conn, Y. Han, V. Yeung, S. B. Qian, PI3K-mTORC1 attenuates stress response by inhibiting cap-independent Hsp70 translation. *J. Biol. Chem.* **286**, 6791–6800 (2011).
24. R. J. Jackson, C. U. Hellen, T. V. Pestova, The mechanism of eukaryotic translation initiation and principles of its regulation. *Nat. Rev. Mol. Cell Biol.* **11**, 113–127 (2010).
25. S. G. Dann, A. Selvaraj, G. Thomas, mTOR Complex1–S6K1 signaling: At the crossroads of obesity, diabetes and cancer. *Trends Mol. Med.* **13**, 252–259 (2007).
26. C. G. Proud, mTOR signalling in health and disease. *Biochem. Soc. Trans.* **39**, 431–436 (2011).
27. A. C. Hsieh, Y. Liu, M. P. Edlind, N. T. Ingolia, M. R. Janes, A. Sher, E. Y. Shi, C. R. Stumpf, C. Christensen, M. J. Bonham, S. Wang, P. Ren, M. Martin, K. Jessen, M. E. Feldman, J. S. Weissman, K. M. Shokat, C. Rommel, D. Ruggero, The translational landscape of mTOR signalling steers cancer initiation and metastasis. *Nature* **485**, 55–61 (2012).
28. C. C. Thoreen, L. Chantranupong, H. R. Keys, T. Wang, N. S. Gray, D. M. Sabatini, A unifying model for mTORC1-mediated regulation of mRNA translation. *Nature* **485**, 109–113 (2012).
29. A. Y. Choo, S. O. Yoon, S. G. Kim, P. P. Roux, J. Blenis, Rapamycin differentially inhibits S6Ks and 4E-BP1 to mediate cell-type-specific repression of mRNA translation. *Proc. Natl. Acad. Sci. U.S.A.* **105**, 17414–17419 (2008).
30. C. Selman, J. M. Tullet, D. Wieser, E. Irvine, S. J. Lingard, A. I. Choudhury, M. Claret, H. Al-Qassab, D. Carmignac, F. Ramadani, A. Woods, I. C. Robinson, E. Schuster, R. L. Batterham, S. C. Kozma, G. Thomas, D. Carling, K. Okkenhaug, J. M. Thornton, L. Partridge, D. Gems, D. J. Withers, Ribosomal protein S6 kinase 1 signaling regulates mammalian life span. *Science* **326**, 140–144 (2009).
31. J. Frydman, H. Erdjument-Bromage, P. Tempst, F. U. Hartl, Co-translational domain folding as the structural basis for the rapid de novo folding of firefly luciferase. *Nat. Struct. Biol.* **6**, 697–705 (1999).
32. R. Gupta, P. Kasturi, A. Bracher, C. Loew, M. Zheng, A. Villella, D. Garza, F. U. Hartl, S. Raychaudhuri, Firefly luciferase mutants as sensors of proteome stress. *Nat. Methods* **8**, 879–884 (2011).
33. S. B. Qian, D. E. Ott, U. Schubert, J. R. Bennink, J. W. Yewdell, Fusion proteins with COOH-terminal ubiquitin are stable and maintain dual functionality in vivo. *J. Biol. Chem.* **277**, 38818–38826 (2002).
34. F. U. Hartl, A. Bracher, M. Hayer-Hartl, Molecular chaperones in protein folding and proteostasis. *Nature* **475**, 324–332 (2011).
35. M. Y. Sherman, A. L. Goldberg, Cellular defenses against unfolded proteins: A cell biologist thinks about neurodegenerative diseases. *Neuron* **29**, 15–32 (2001).
36. A. N. Fedorov, T. O. Baldwin, Cotranslational protein folding. *J. Biol. Chem.* **272**, 32715–32718 (1997).
37. A. A. Komar, A pause for thought along the co-translational folding pathway. *Trends Biochem. Sci.* **34**, 16–24 (2009).
38. J. R. Buchan, I. Stansfield, Halting a cellular production line: Responses to ribosomal pausing during translation. *Biol. Cell* **99**, 475–487 (2007).
39. M. Rakwalska, S. Rospert, The ribosome-bound chaperones RAC and Ssb1/2p are required for accurate translation in *Saccharomyces cerevisiae*. *Mol. Cell. Biol.* **24**, 9186–9197 (2004).
40. S. Belin, A. Beghin, E. Solano-Gonzàlez, L. Bezin, S. Brunet-Manquat, J. Textoris, A. C. Prats, H. C. Mertani, C. Dumontet, J. J. Diaz, Dysregulation of ribosome biogenesis and translational capacity is associated with tumor progression of human breast cancer cells. *PLoS One* **4**, e7147 (2009).
41. N. T. Ingolia, L. F. Lareau, J. S. Weissman, Ribosome profiling of mouse embryonic stem cells reveals the complexity and dynamics of mammalian proteomes. *Cell* **147**, 789–802 (2011).
42. X. Zhou, T. Ikenoue, X. Chen, L. Li, K. Inoki, K. L. Guan, Rheb controls misfolded protein metabolism by inhibiting aggresome formation and autophagy. *Proc. Natl. Acad. Sci. U.S.A.* **106**, 8923–8928 (2009).
43. C. M. McCay, M. F. Crowell, L. A. Maynard, The effect of retarded growth upon the length of life span and upon the ultimate body size. 1935. *Nutrition* **5**, 155–171 (1989).
44. R. W. Powers III, M. Kaeberlein, S. D. Caldwell, B. K. Kennedy, S. Fields, Extension of chronological life span in yeast by decreased TOR pathway signaling. *Genes Dev.* **20**, 174–184 (2006).
45. A. R. Hipkiss, On why decreasing protein synthesis can increase lifespan. *Mech. Ageing Dev.* **128**, 412–414 (2007).
46. B. M. Zid, A. N. Rogers, S. D. Katewa, M. A. Vargas, M. C. Kolipinski, T. A. Lu, S. Benzer, P. Kapahi, 4E-BP extends lifespan upon dietary restriction by enhancing mitochondrial activity in *Drosophila*. *Cell* **139**, 149–160 (2009).
47. C. G. Proud, mTORC1 signalling and mRNA translation. *Biochem. Soc. Trans.* **37**, 227–231 (2009).
48. R. J. Dowling, I. Topisirovic, T. Alain, M. Bidinosti, B. D. Fonseca, E. Petroulakis, X. Wang, O. Larsson, A. Selvaraj, Y. Liu, S. C. Kozma, G. Thomas, N. Sonenberg, mTORC1-mediated cell proliferation, but not cell growth, controlled by the 4E-BPs. *Science* **328**, 1172–1176 (2010).
49. H. Gingold, Y. Pilpel, Determinants of translation efficiency and accuracy. *Mol. Syst. Biol.* **7**, 481 (2011).
50. G. Zhang, M. Hubalewska, Z. Ignatova, Transient ribosomal attenuation coordinates protein synthesis and co-translational folding. *Nat. Struct. Mol. Biol.* **16**, 274–280 (2009).
51. E. Siller, D. C. DeZwaan, J. F. Anderson, B. C. Freeman, J. M. Barral, Slowing bacterial translation speed enhances eukaryotic protein folding efficiency. *J. Mol. Biol.* **396**, 1310–1318 (2010).
52. T. L. Hamilton, M. Stoneley, K. A. Spriggs, M. Bushell, TOPs and their regulation. *Biochem. Soc. Trans.* **34**, 12–16 (2006).

Acknowledgments: We thank Qian laboratory members for helpful discussion of the manuscript and E. Ferrie for technical assistance. We are grateful to D. Kwiatkowski (Harvard), G. Thomas (University of Cincinnati), and N. Sonenberg (McGill University) for providing MEF cell lines and K.-L. Guan (University of California, San Diego) for Rheb plasmids. We also thank the Stover and Qi laboratories at Cornell for equipment accessibility. **Funding:** This work was supported by grants to S.-B.Q. from the NIH (1 DP2 OD006449-01), the Ellison Medical Foundation (AG-NS-0605-09), and the Department of Defense Exploration-Hypothesis Development Award (W81XWH-11-1-0236). C.S.C. was partially supported by an NIH training grant for Cornell University Genetics, Genomics and Development Graduate Program (T32GM00761). **Author contributions:** C.S.C. and S.-B.Q. conceived and designed the project; C.S.C. performed the experiments; and C.S.C. and S.-B.Q. wrote the manuscript. **Competing interests:** The authors declare that they have no competing interests.

Submitted 20 August 2012
Accepted 14 March 2013
Final Publication 16 April 2013
10.1126/scisignal.2003520
Citation: C. S. Conn, S.-B. Qian, Nutrient signaling in protein homeostasis: An increase in quantity at the expense of quality. *Sci. Signal.* **6**, ra24 (2013).